ABSTRACT

THERMAL AND MORPHOLOGICAL ANALYSIS OF COLLAGEN-PLLA ELECTROSPUN BLENDS

by
Angana Banerjee

Electrospinning of bovine Type I collagen and Poly (L-lactic acid) produces blended nanofiber scaffolds that may have application in tissue engineering, wound dressing and drug delivery.

The goal of this research work was to produce and characterize blended nanofibers of a protein, collagen, and a synthetic polymer, poly (L-lactic acid). This study focuses on the in-depth analysis of the appearance of the structural relaxation occurring at the glass transition temperature of PLLA in the collagen-PLLA blended electrospun mats. It is speculated that occurrence of this thermal event is more prominent in PLLA with high molecular weight due to the presence of entanglements. It has also been demonstrated that electrospinning leads to the formation of an aligned microstructure of the chains but not a crystalline arrangement. In addition, morphological characterization of the collagen-PLLA nanofiber mats were performed using scanning electron microscope and transmission electron microscope in order to understand the structural features of the PLLA-collagen electrospun blended filaments. A hypothesis has been developed on the solid state structure of the electrospun PLLA-collagen filament blends and also on the formation of sheath-core morphology in blended nanofibers.

THERMAL AND MORPHOLOGICAL ANALYSIS OF COLLAGEN-PLLA ELECTROSPUN BLENDS

by
Angana Banerjee

A Thesis
Submitted to the Faculty of
New Jersey Institute of Technology
in Partial Fulfillment of the Requirements for the Degree of
Master of Science in Biomedical Engineering

Department of Biomedical Engineering

May 2008

APPROVAL PAGE

THERMAL AND MORPHOLOGICAL ANALYSIS OF COLLAGEN-PLLA ELECTROSPUN BLENDS

Angana Banerjee

4/25/08

Dr. Treena L Arinzeh, Thesis Co-advisor and Committee Chair — Date
Associate Professor of Biomedical Engineering, NJIT

4/25/08

Dr. George Collins, Thesis Co-advisor and Committee Chair — Date
Research Professor of Biomedical Engineering, NJIT

4/25/08

Dr. William C Hunter, Committee Member — Date
Chair of Biomedical Engineering, NJIT

4/25/08

Dr. Michael Jaffe, Committee Member — Date
Research Professor of Biomedical Engineering, NJIT

BIOGRAPHICAL SKETCH

Author: Angana Banerjee

Degree: Master of Science

Date: May 2008

Undergraduate and Graduate Education:

- Master of Science in Biomedical Engineering,
  New Jersey Institute of Technology, Newark USA 2008

- Bachelor of Engineering in Biotechnology
  Visveswaraiah Technology University
  R.V.College of Engineering, Bangalore. India 2006

Major: Biomedical Engineering

Presentations and Publications:

Poster presentation of thesis titled "Thermal and Morphological Analysis of Collagen-PLLA Electrospun Blends" at the Fifth Annual New Jersey Biomedical Engineering Showcase, held at Rutgers University in March 2008.

Poster presentation of thesis titled "Thermal and Morphological Analysis of Collagen-PLLA Electrospun Blends" at Fourth Annual Provost's Student Research Showcase held at NJIT in April 2008 as one of the best research works in the University.

Manuscript in preparation: *"Observations of Thermal Behavior of Electrospun Blends of Collagen and PLLA"*, G.Collins, S.Wang, A.Banerjee, B.Matarlo, M.Jaffe, Z.Ophir

Dedicated to the memory of my beloved grandparents, my wonderful and caring parents,

my dear sister and my closest friends and relatives

for their unconditional love and support.

"If we knew what it was we were doing, it would not be called research, would it?"

-Albert Einstein

ACKNOWLEDGEMENT

My thesis is an outcome of the efforts, help, co-operation, guidance and encouragement of many people whom I wish to acknowledge.

It gives me immense pleasure to express my deep sense of gratitude to my thesis advisor, Dr. George Collins for giving me his invaluable guidance, attention, constant support and encouragement. His enthusiasm and passion for polymer chemistry along with his great ability to explain things lucidly, helped me develop deep interest in polymer science and decide a career path in biomaterials.

I wish to express my sincere thanks to Dr. Treena Arinzeh for providing me with suggestions and valuable inputs and also for being on my committee.

I would like to extend my heartfelt thanks to Dr. Michael Jaffe and Dr. William Hunter for being a part of my committee.

I am grateful to Dr. Xueyan Zhang and Dr. Markus F. Meyenhofer for their invaluable support in electron microscopy experiments.

My sincere thanks to Sherry Wang and Yuki Imura for training me in electrospinning and also for their constant encouragement and valuable inputs. My special thanks to Dr. Zohar Ophir and Kimberly Griswold for their sincere advice and help. I am thankful to Pinar Nebol and Joe Pickton for their support and for making the laboratory work, an enjoyable experience.

Last, but not the least, I am deeply grateful to my parents and my sister for encouraging me to pursue my dream.

TABLE OF CONTENTS

Chapter		Page
1	INTRODUCTION	1
2	BACKGROUND AND SIGNIFICANCE	4
	2.1 Electrospinning	4
	2.1.1 History of Electrospinning	4
	2.1.2 Process of Electrospinning	6
	2.1.3 Applications of Electrospun Fibers	8
	2.1.4 Shortcomings of the Process of Electrospinning in Producing Aligned Fibers	9
	2.2 Collagen	10
	2.2.1 Composition of the Extracellular Matrix	10
	2.2.2 Structure and Stability of Collagen Molecules	11
	2.2.3 Biosynthesis and Assembly of Collagen Fibers	13
	2.2.4 Electrospun Collagen Nanofibers and Tissue Engineering Aspects	15
	2.3 Poly (L-Lactic Acid)	17
	2.3.1 Lactic Acid-based Polymers	17
	2.3.2 Solubility of PLLA	18
	2.3.3 Mechanical Properties of PLLA	19
	2.3.4 Thermal Stability and Hydrolysis of PLLA	19
	2.3.5 Crystallization Rate of PLLA	20
	2.3.6 Double Melting in PLLA	22
	2.3.7 Glass Transition and Structural Relaxation of PLLA	23
	2.3.8 Characteristic Ratio of PLLA	25

TABLE OF CONTENTS
(Continued)

Chapter	Page
2.4 Electrospinning by Blending Polymers	26
3 EXPERIMENTAL	28
3.1 Materials	28
3.1.1 Bovine Collagen Tendon Derivation and Purification	28
3.1.2 Solution Preparation	30
3.1.3 Addition of Water to TFA and Increasing Degradation Time	31
3.1.4 Time Based Degradation of Collagen-PLLA	31
3.1.5 Dispersion of Collagen-PLLA	31
3.1.6 PLLA Extraction	32
3.1.7 Aging Experiments	32
3.1.8 Cast Films	33
3.2 Methods	33
3.2.1 Electrospinning Set-up	33
3.2.2 Differential Scanning Calorimetry	34
3.2.3 Thermogravimetric Analysis	36
3.2.4 Scanning Electron Microscope	36
3.2.5 Transmission Electron Microscope	39
4 RESULTS	40
4.1 Thermal Analysis	40
4.1.1 Aging	40

TABLE OF CONTENTS
(Continued)

Chapter		Page
	4.1.2 Cast Films	51
	4.1.3 Degradation	52
	4.1.4 DSC of the Electrospun Mats After 45-60 Days	53
	4.1.5 Thermogravimetric Analysis	54
	4.1.6 Dispersion of Collagen and PLLA	55
4.2	Morphological Analysis	56
5	DISCUSSION	66
6	CONCLUSION	79
7	FUTURE WORK	81
APPENDIX A	DSC THERMOGRAMS OF 5% ELECTROSPUN MAT, ELECTROSPUN AND NON- ELECTROSPUN COLLAGEN, 10% ELECTROSPUN MAT	82
APPENDIX B	POSITION AND MAGNITUDE OF CRYSTALLIZATION, MELTING, GLASS TRANSITION TEMPERATURES FOR PLLA PELLETS, AGED PLLA PELLETS, AGED PLLA PELLETS AFTER A HEAT-COOL CYCLE, ELECTROSPUN PLLA AND AGED ELECTROSPUN PLLA, 1%, 3%, 5% AND 8% ELECTROSPUN BLENDED MATS, AGED MATS AND CAST FILMS	84
APPENDIX C	DSC THERMOGRAMS OF CAST FILMS AND TIME BASED DEGRADATION EXPERIMENTS	94
APPENDIX D	DSC THERMOGRAMS OF EXPERIMENTS DEGRADING PLLA AND COLLAGEN IN SOLUTION	99
APPENDIX E	TGA RESULTS OF ELECTROSPUN MATS	109
APPENDIX F	SEM IMAGES OF COLLAGEN AND PLLA NANOFIBERS	113

TABLE OF CONTENTS
(Continued)

Chapter		Page
APPENDIX G	DIAMETERS OF ELECTROSPUN COLLAGEN-PLLA NANOFIBERS BEFORE AND AFTER EXTRACTION OF PLLA	114
APPENDIX H	ENERGY DISPERSIVE X-RAY SPECTROSCOPY (EDS) RESULTS	116
REFERENCES		118

LIST OF TABLES

Table		Page
3.1	Solution Composition	30
B.1	Position of Cold Crystallization Peak of PLLA Pellets and Electrospun Mats	84
B.2	Cold Crystallization Magnitude of PLLA Pellets and Electrospun Mats	85
B.3	Position of Enthalpy Recovery Peak of PLLA Pellets and Electrospun Mats	85
B.4	Position of Glass Transition of PLLA Pellets and Electrospun Mats	86
B.5	Position of Melting Peak of PLLA Pellets and Electrospun Mats	86
B.6	Melting Peak Magnitude of PLLA Pellets and Electrospun Mats	87
B.7	Position of Cold Crystallization Peak of Blended Electrospun Mats	87
B.8	Cold Crystallization Magnitude of Blended Electrospun Mats	88
B.9	Position of Enthalpy Recovery of Peak Blended Electrospun Mats	88
B.10	Position of Glass Transition of Blended Electrospun Mats	89
B.11	Position of Melting Peak of Blended Electrospun Mats	89
B.12	Melting Peak Magnitude of Blended Electrospun Mats	90
B.13	Position of Cold Crystallization Peak of Aged Blended Electrospun Mats	90
B.14	Cold Crystallization Magnitude of Aged Blended Electrospun Mats	91
B.15	Position of Enthalpy Recovery Peak of Aged Blended Electrospun Mats	91
B.16	Position of Glass Transition of Aged Blended Electrospun Mats	92
B.17	Position of Melting Peak of Aged Blended Electrospun Mats	92
B.18	Melting Peak Magnitude of Aged Blended Electrospun Mats	93

LIST OF TABLES
(Continued)

Table		Page
G.1	Diameters of 8% Collagen-PLLA Nanofibers Before and After Extraction.....	114
G.2	Diameters of 5% Collagen-PLLA Nanofibers Before and After extraction.....	114
G.3	Diameters of 5% Collagen-PLLA Nanofibers Before and After Extraction.....	115
H.1	EDS Results for 5% Electrospun Blend.....	116
H.2	EDS Results for Electrospun Collagen.....	117

LIST OF FIGURES

Figure		Page
1.1	Human hair compared to nanofibers	1
2.1	Illustration of the formation of Taylor cone from the needle tip	5
2.2	Electrospinning set-up	7
2.3	Illustrates the major events that take place during the biosynthesis of fibrous collagens	13
2.4	Structural features of collagen ranging from amino acid sequence, tropocollagen molecules and collagen fibrils to collagen fibers	14
2.5	Electron micrograph of collagen fibrils	15
2.6	Ring opening polymerization of lactide to poly(lactide)	17
2.7	Solubility of lactic acid based polymers in common organic solvents	18
2.8	Kinetic analysis of common polymeric growth rate curve	21
2.9	DSC thermograms of melt-crystallized samples being heated	22
2.10	Illustrates structural relaxation of PLLA	24
2.11	TEM images of electrospun polybutadiene/polycarbonate nanofibers	27
3.1	Schematic of the electrospinning set-up	33
3.2	Example of a DSC thermogram	35
3.3	Schematic demonstrating the working of SEM	37
3.4	Schematic demonstrating the scattering of electrons	38
4.1	DSC of second heat cycle of PLLA pellet	41
4.2	DSC of second heat cycle of aged PLLA pellet	41
4.3	DSC of aged PLLA pellet after heat-cool cycle	42
4.4	DSC of electrospun PLLA mat	43

LIST OF FIGURES
(Continued)

Figure		Page
4.5	DSC of first heat cycle of overnight aged electrospun PLLA mat.....	43
4.6	DSC of first heat cycle of electrospun PLLA mat 60 days after electrospinning.....	44
4.7	DSC of first heat cycle of electrospun 1% collagen-PLLA mat.....	46
4.8	DSC of first heat cycle of overnight aged electrospun 1% collagen-PLLA mat.....	47
4.9	DSC of first heat cycle of electrospun 3% collagen-PLLA mat.....	47
4.10	DSC of first heat cycle of overnight aged electrospun 3% collagen-PLLA mat.....	48
4.11	DSC of first heat cycle of electrospun 5% collagen-PLLA mat.....	48
4.12	DSC of first heat cycle of overnight aged electrospun 5% collagen-PLLA mat.....	49
4.13	DSC of first heat cycle of electrospun 7% collagen-PLLA mat.....	49
4.14	DSC of first heat cycle of overnight aged electrospun 7% collagen-PLLA mat.....	50
4.15	DSC of first heat cycle of electrospun 8% collagen-PLLA mat.....	50
4.16	DSC of first heat cycle of overnight aged electrospun 8% collagen-PLLA mat.....	51
4.17	Overlay of first heat cycle of DSC thermogram of 1% electrospun mat, a day after electrospinning, after aging at 40°c and repeating the scan after 45 days.....	54
4.18	DSC thermogram of collagen-PLLA dispersion.....	55
4.19	SEM image of 1% collagen-PLLA electrospun blend.....	58
4.20	SEM image of 1% collagen-PLLA electrospun blend after extraction of PLLA with methylene chloride.....	59

LIST OF FIGURES
(Continued)

Figure		Page
4.21	SEM image of 5% collagen-PLLA electrospun blend.....	59
4.22	SEM image of 5% collagen-PLLA electrospun blend after extraction of PLLA with methylene chloride.....	60
4.23	SEM image of 8% collagen-PLLA electrospun blend.....	60
4.24	SEM image of 8% collagen-PLLA electrospun blend after extraction of PLLA with methylene chloride.....	61
4.25	SEM image of 10% collagen-PLLA electrospun blend.....	61
4.26	SEM image of 10% collagen-PLLA electrospun blend after extraction of PLLA with methylene chloride.....	62
4.27	TEM image of a 5% electrospun collagen-PLLA nanofiber.....	63
4.28	TEM image of a 5% electrospun collagen-PLLA nanofiber.....	63
4.29	SEM image of collagen-PLLA dispersion mat.....	64
4.30	SEM image of PLLA extracted dispersion mat.....	65
5.1	Polymer chains in an oriented and crystalline state.....	68
5.2	Illustrates the polymer chains before and after electrospinning.....	71
5.3	Effects of higher and lower molecular weight between entanglements.....	74
5.4	Illustration of sheath-core morphology of collagen-PLLA nanofiber blends....	76

LIST OF FIGURES
(Continued)

Figure		Page
A.1	DSC of 5% collagen-PLLA electrospun mats.....	82
A.2	DSC thermogram of non-electrospun collagen.....	82
A.3	DSC thermogram of electrospun collagen in TFA.....	83
A.4	DSC thermogram of first heat cycle of electrospun 10% collagen-PLLA mat...	83
C.1	DSC of first heat cycle of 1% collagen-PLLA cast film.....	94
C.2	DSC of first heat cycle of 3% collagen-PLLA cast film.....	95
C.3	DSC of first heat cycle of 5% collagen-PLLA cast film.....	95
C.4	DSC of first heat cycle of 8% collagen-PLLA cast film.....	96
C.5	DSC of first heat cycle of 5% electrospun blend after 10 hours in solution.....	96
C.6	DSC of first heat cycle of 5% electrospun blend after 14 hours in solution.....	97
C.7	DSC of first heat cycle of 5% electrospun blend after 18 hours in solution.....	97
C.8	DSC of first heat cycle of 5% electrospun blend after 34 hours in solution.....	98
C.9	DSC of first heat cycle of 5% electrospun blend after 54 hours in solution.....	98
D.1	DSC of 5% electrospun collagen-PLLA mat when PLLA was added 4 hours after the addition of collagen to TFA.....	99
D.2	DSC of 5% electrospun collagen-PLLA mat when PLLA was added 4 hours after the addition of collagen to TFA. 10 microliters of water was added to TFA.....	100
D.3	DSC of 5% electrospun collagen-PLLA mat when PLLA was added 10 hours after the addition of collagen to TFA.....	100
D.4	DSC of 5% electrospun collagen-PLLA mat when PLLA was added 10 hours after the addition of collagen to TFA. 10 microliters of water was added to TFA.....	101

LIST OF FIGURES
(Continued)

Figure		Page
D.5	DSC of 5% electrospun collagen-PLLA mat when PLLA was added 20 hours after the addition of collagen to TFA	101
D.6	DSC of 5% electrospun collagen-PLLA mat when PLLA was added 10 hours after the addition of collagen to TFA. 10 microliters of water was added to TFA	102
D.7	DSC of 5% electrospun collagen-PLLA mat when collagen was added four hours after the addition of PLLA to TFA	102
D.8	DSC of 5% electrospun collagen-PLLA mat when collagen was added four hours after the addition of PLLA to TFA. 10 microliters of water was added to TFA	103
D.9	DSC of 5% electrospun collagen-PLLA mat when collagen was added 10 hours after the addition of PLLA to TFA	103
D.10	DSC of 5% electrospun collagen-PLLA mat when collagen was added 10 hours after the addition of PLLA to TFA. 10 microliters of water was added to TFA	104
D.11	DSC of 5% electrospun collagen-PLLA mat when collagen was added 20 hours after the addition of PLLA to TFA	104
D.12	DSC of 5% electrospun collagen-PLLA mat when collagen was added 20 hours after the addition of PLLA to TFA. 10 microliters of water was added to TFA	105
D.13	DSC of 5% electrospun collagen-PLLA mat when collagen was added 40 hours after the addition of PLLA to TFA. 10 microliters of water was added to TFA	105
D.14	DSC of first heat cycle of 1% electrospun collagen-PLLA mat after 45 to 60 days of electrospinning	106
D.15	DSC of first heat cycle of 5% electrospun collagen-PLLA mat after 45 to 60 days of electrospinning	106
D.16	DSC of first heat cycle of 7% electrospun collagen-PLLA mat after 45 to 60 days of electrospinning	107

LIST OF FIGURES
(Continued)

Figure		Page
D.17	DSC of first heat cycle of 8% electrospun collagen-PLLA mat after 45 to 60 days of electrospinning	107
D.18	DSC of first heat cycle of 10% electrospun collagen-PLLA mat after 45 to 60 days of electrospinning	108
E.1	TGA analysis of electrospun PLLA mat	109
E.2	TGA analysis of electrospun collagen mat	109
E.3	TGA analysis of 1% electrospun collagen-PLLA mat	110
E.4	TGA analysis of 5% electrospun collagen-PLLA mat	110
E.5	TGA analysis of 7% electrospun collagen-PLLA mat	111
E.6	TGA analysis of 8% electrospun collagen-PLLA mat	111
E.7	TGA composition calibration curve	112
F.1	PLLA nanofibers visualized under the SEM	113
F.2	Collagen nanofibers visualized under the SEM	113

CHAPTER 1

INTRODUCTION

Nanofibers can be produced from different materials ranging from metals, ceramics to polymers. With diameters ranging from micrometers to nanometers, these fibers have a very high surface area to volume ratio, low density and small pore size.

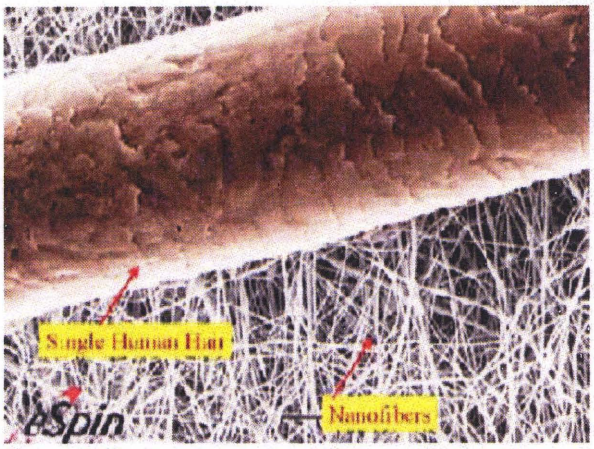

Figure 1.1 Human hair compared to nanofibers [2].

A strand of human hair which is about 50-150μm and polymeric nanofibers that are between 100-500nm have been compared in Figure 1.1 [1, 2, 3]. Biodegradable nanofibers are important in drug delivery, wound healing and tissue regeneration [1]. Larger surface area and small pore sizes, allow the nanofibers to play an important role in filtering submicron particles from water or air in filtering applications [3]. Nanofibers are also widely used in medical applications. As a drug delivery device, the carbon fiber hollow nano tubes are capable of carrying drugs into blood cells owing to their small size. Such fibers can also be used to carry medicines to internal tissues of the body. Anti-adhesion materials using cellulose nanofibers are already available for commercial

use. The use of nanofibers in making bandages or sutures which eventually get dissolved in the body are of significance as it may be able to reduce infection rate and blood loss [3].

It is valuable to note that the non-woven meshes produced by electrospinning have an architecture that closely mimics the extra cellular matrix [4]. Another interesting feature is that, even though the pore sizes of the nanofiber meshes are much smaller than the normal cells, results indicate that the meshes allow the infiltration of cells, instead of inhibiting cell migration [5]. It has also been suggested that the architecture of the nanofibers allow the cells to expand the pores by pushing them and thus, enter into the matrix. Previous research has shown that synthetic materials do not possess cell recognition signal [6]. As a consequence, scaffold which is made from proteins found in the extra cellular matrix, like collagen would surely allow better migration of cells into the nanofiber scaffold. For tissue engineering purposes, in order to make the scaffold more stable and biocompatible, it may be modified by different treatments and processes like polymer blending, multi-layering, cross linking, co-electrospinning and various other types of surface modifications [5].

The possibility of enhancing mechanical properties like stiffness and tensile strength along with the flexibility in modifying surface functionalities allows the fibers to be more amenable for biomedical applications [7]. Each application may require the development of a specific property in these fibers. Such properties may be related to a specific morphology, biocompatibility or even chemical nature of the fibers. Thus it is of critical importance to understand the process of production of these fibers by electrospinning.

Electrospinning has emerged as one of the most successful methods to produce nanofibers. The flexibility and the ease of the electrospinning process is what make this

technique so versatile [8]. Even though, nanofibers can be fabricated using techniques like phase separation, drawing, template synthesis etc, each of these method has their own limitation in producing the desired size and quantity of the fibers [7]. The interaction of the scaffold with the cells and subsequent tissue formation has been shown to be dependent on fiber size. Electrospinning is able to produce fibers of varying diameters and thus, is considered an ideal technique for scaffold design and tissue engineering [5].

Objective of this Research:

The primary objective of this research work was to produce and characterize blended nanofibers of a protein, collagen, and a synthetic polymer, poly (L-lactic acid). The nanofiber blends are produced by electrospinning from solutions containing both the components. One aspect of this research was to perform an in-depth analysis of the thermal behavior of the collagen-PLLA electrospun mat. In particular, it has been previously observed that there is the unusual appearance of a structural relaxation occurring at the glass transition of PLLA in electrospun blend mats. Another aspect was the morphological characterization of the collagen-PLLA nanofiber filaments and to develop a hypothesis on the solid state structure of the PLLA and collagen filament blends after they are electrospun. This morphological analysis has been performed using scanning electron microscope and transmission electron microscope. Thermal characterization was performed using the differential scanning calorimetry and thermo gravimetric analysis.

CHAPTER 2

BACKGROUND AND SIGNIFICANCE

2.1 Electrospinning

The technique of electrospinning has gained a lot of attention in the last decade not only due to its versatility in producing continuous fibers with diameters ranging from sub-microns down to nanometers, but also because of its flexibility, low cost and ease of production [1,9]. Electrospinning is the process of spinning fibers with the aid of electrostatic forces [10]. Electrospinning has the potential to fabricate continuous nanofibers from a wide range of materials, majority being polymers, composites, semiconductors and ceramics [8]. The most important consideration for the fiber industries is the amount of fiber production. Compared to the industrial process of fiber spinning, electrospinning is a very slow process. Industrial dry spinning technique has a yarn take-up rate of 200–1500 m min^{-1} as opposed to 30 m min^{-1} for yarn produced by electrospinning [8].

2.1.1 History of Electrospinning

The behavior of water under the influence of electro-statistics was studied in the early 1700s [11]. During the late 1800s, the phenomenon of excitation of a dielectric liquid due to the influence of an electric charge was explained using electrodynamics [12].

In early 1900s, Cooley and Morton invented the technique of electrospinning for the production of artificial fibers [8]. In 1934, Formhals patented his first electrospinning set up which was used to produce filaments using electric charges. The production of artificial threads had been in use for a long time but it had not gained a lot of importance

until Formals' invention because of problems in fiber drying and method of collection of fibers. The set up comprised a movable thread collecting device and in his first patent, Formhals reported the production of cellulose acetate fibers using acetone as the solvent. But, there were certain problems with drying the fibers due to less distance between the spinning and fiber collector. In a later set up, this difficulty was overcome by allowing more distance between the feeding nozzle and the collecting device. In 1940 Formhals patented a method that led to the production of composite fibers from multiple polymers by electrostatically spinning the fibers on a moving base [10].

In 1960s, Sir Geoffrey Ingram Taylor studied the formation of the polymer jet, which led to a better understanding of the method by which the polymer solution streams out of the needle. Taylor studied the shape of the polymer droplet which is produced at the tip of the needle when an electric field is applied and showed that it takes the shape of a cone and the jets eventually eject from the vertices of the cone. Subsequent researchers referred to this as the "Taylor cone" as illustrated in Figure 2.1.

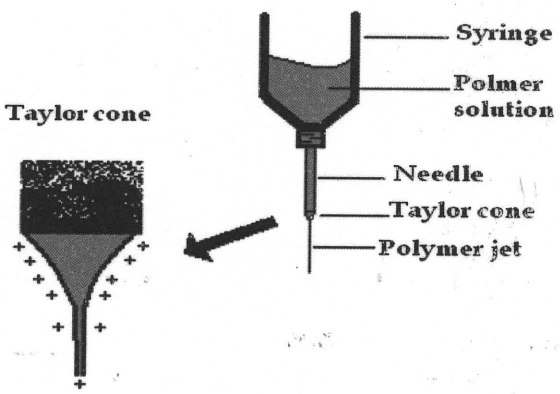

Figure 2.1 Illustration of the formation of Taylor cone from the needle tip [13].

In addition, Taylor examined various viscous fluids and determined that an angle of 49.3 degrees is needed to balance the surface tension of the polymer with the applied

electrostatic forces. Literature also mentions that the conical shape of the jet is important because it helps to understand the onset of the extensional velocity gradients in the fiber formation [10].

Subsequently, the focus of research shifted to understanding the structural features of the nanofibers. Relationship between the morphology of the fibers and the process parameters during production of the nanofibers have been studied by using electron microscopy, wide-angle X-ray diffraction (WAXD) and differential scanning calorimetry (DSC) [10].

More research in this area showed that there is a dependence of fiber diameter on the viscosity of the solution. It has been shown that the diameter of the polymer jet reached a minimum value after an initial increase in the electric field and then the diameter grew larger with increase in the applied field. In 1987, experimental conditions were studied in which highly conductive fluids were seen to produce unstable streams when exposed to increasing voltages. Such conditions made the fluid stream to whip around in different directions once it left the needle. It was also observed that unstable jets produced fibers with a much broader diameter distribution [10].

2.1.2 Process of Electrospinning

The process of electrospinning requires a high voltage electric field created between the needle or capillary tube and the collection device as illustrated in Figure 2.2. The polymer solution is loaded in a syringe. A single fluid jet will be ejected from the Taylor cone and drawn towards the collection device only when the electric field is able to overcome the surface tension and viscoelastic forces of the solution. As the ejected fluid leaves the needle, it is subjected to forces which cause it to stretch immensely. During its travel; the

polymer jet will partially or fully vitrify by solvent evaporation into a coherent filament [16]. The fibers get collected onto the collector and they do possess electric charge [14, 15, 17 and 18]. In this way, continuous fibers are laid to form a non-woven fabric. The description of the process surely suggests that the following parameters play a very important role: solution viscosity, surface tension and controlled variables include hydrostatic pressure in the capillary, electric potential at the tip of the needle, the distance between the needle tip and the collection device and ambient parameters include temperature, humidity, and air velocity in the electrospinning chamber [9].

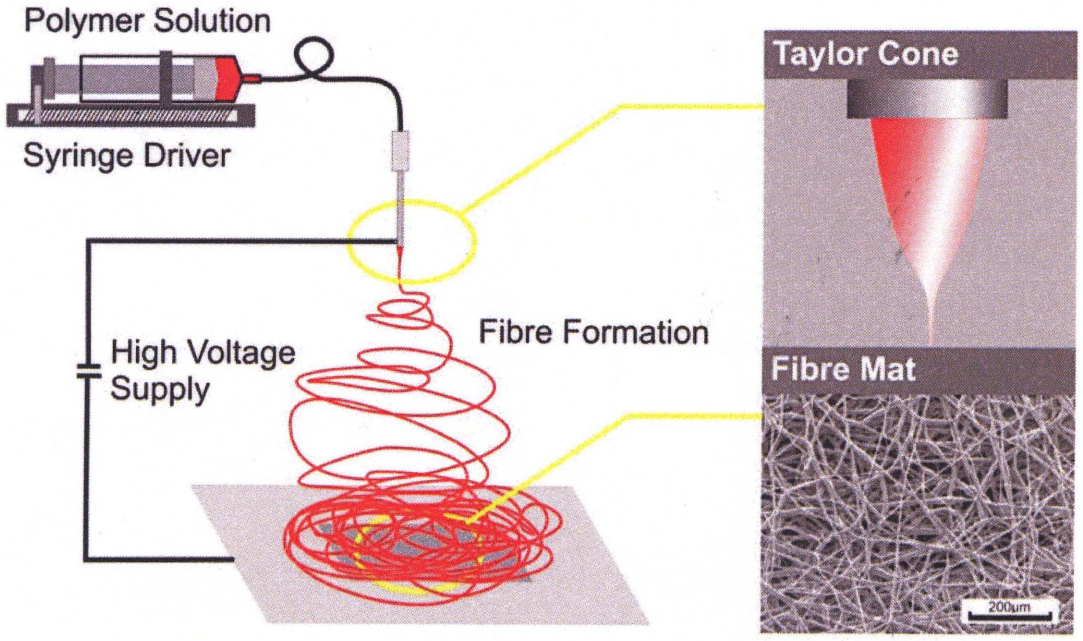

Figure 2.2 Electrospinning set up [47].

2.1.3 Applications of Electrospun Fibers

The potential of the electrospun nanofibers in the field of tissue engineering and healthcare is extremely promising. The nanofiber scaffolds produced by electrospinning may be both synthetic and natural polymers. They are important as biodegradable and biocompatible medical implant devices, in wound dressings impregnated with drugs, medical diagnostics, as protective fabrics against environmental hazards and infectious agents in hospitals and also in cosmetics and dental applications.

Tissue/organ repair and tissue regeneration are new approaches to treatment and cure replacing the need for donor tissues and organ transplantation. In this type of treatment, a scaffold is needed such that, it can be fabricated from either natural or synthetic polymers by different processing techniques. It is of crucial importance that the biocompatibility of the scaffold be tested by culturing organ specific cells on it and then monitoring the cell growth and proliferation. Nanofiber scaffolds are very well suited for the purpose of tissue engineering because they can be engineered in order to fill anatomical defects and provide growth factors and drugs. They can also be fabricated and designed to enhance mechanical properties and thus, support cell growth, cell motility, proliferation and cell differentiation.

Another useful feature of these nanofibers is that they are able to mimic the extra cellular matrix of tissues and organs. The extra cellular matrix (ECM) has complex functions. It not only provides support and anchorage for cells, segregating tissues from one another but also regulates intercellular communication. ECM consists of fibrous proteins like collagen and fibronectin, glycoproteins, proteoglycan and other growth factors and bio-active molecules which help in cell growth. Studies based on cell-scaffold

interactions have clearly shown that cells adhere and proliferate well when cultured on polymer nanofibers [1, 21].

Electrospun nanofibers are also used for applications in sensor technology due to their large surface area. More surface area is desired in order to absorb more of a gas analyte molecule and change the sensor's conductivity by a significant amount. For detection of toxic gases like ammonia, electrospinning is used to produce nanoparticles and nanofibers of semi-conducting oxides which are used as gas sensing elements [22].

For defense purposes, electrospun nanofibers are used in making protective clothing, which is based on full barrier protection like hazardous materials (HAZMAT) suits. Also, permeable adsorptive protective over-garments are known to be used by US military. However, weight and moisture retention are some of the problems associated with these suits and thus, they cannot be put on for a long time [1].

2.1.4 Shortcomings of the Process of Electrospinning in Producing Aligned Fibers

Even though there has been a lot of research and development to introduce various designs and modifications of the electrospinning process, there are still many areas which require more understanding and refinement. This process of fiber production is quite complex and various process parameters simultaneously influence the spinning capability of a certain material. The concept of production of aligned nanofibers is still not clear and even though, several set ups have been designed to achieve fiber alignment, there are still difficulties in getting such fibers over an area of considerable thickness. Previous research has shown that aligned nanofibers are able to induce cell elongation and proliferation in the direction of the fiber alignment. Thus, even though extensive studies

have been made, all aspects of how the electrospinning technology works are not fully understood [8,14].

2.2 Collagen

The word collagen has been derived from the Greek word for glue, *kolla*, which means "glue producer" and refers to the ancient process of boiling the skin and sinews of horses to produce glue [23]. About 4000 years ago, collagen adhesive was used by Egyptians. Native Americans used it in bows about 1,500 years ago [24]. Type I collagen is the most abundantly found protein in human beings [25]. In connective tissues, collagen is present as chains in a native triple helical structure, and as a result of its excellent tensile strength, it is an important component of ligaments and tendons. Collagen is largely responsible for elasticity of the skin and degradation of collagen leads to wrinkles on the skin with aging. Interestingly, collagen is also present in the cornea of our eyes in a crystalline form. For cosmetic surgery purposes, if injected beneath the skin as filler, collagen helps to plump up lines and wrinkles and adds fullness to sunken areas of the face, cheeks or lips [23]. Different types of abnormalities in the structural formation of collagen molecules can lead to various human disease conditions like scurvy.

2.2.1 Composition of the Extracellular Matrix

Our body is made up of tissues which not only host cells but a large part of their volume is taken up by extracellular space composed of macromolecules which in turn constitutes the extracellular matrix. The matrix is composed of a variety of proteins, the majority being collagen and also, polysaccharides which are released locally and then assembled into an organized meshwork. Other proteins that constitute the ECM include elastin,

fibronectin, laminin, entactin and they provide structural and biological support to several tissues and organs including bone, skin, muscle, tendon, blood vessels, and cartilage. Proteoglycans also form a part of this matrix and various growth factors and cytokines are required for their synthesis [26].

2.2.2 Structure and Stability of Collagen Molecules

There are about 16 types of collagen but type I, II, III are the most commonly found ones in the animal kingdom. Collagen type I consists of three coiled subunits: two α1(I) and one α2(I) chains which forms fibrils of 50 nm diameter. Collagen type II comprises three identical α1(II) chains which form fibrils of less than 80 nm in diameter. Collagen type III fibrils are made of three α1(III) chains resulting in a wide range of fibril diameters, from 30 to 130 nm [5, 27].

The triple helical structure of collagen is largely composed of the amino acids glycine, proline and the oxidized form of proline, hydroxyproline. These three compounds form the repeating motif in its structure, X–Y–Gly, where Gly represents glycine and X and Y mostly represent proline (Pro) or 4(*R*)-hydroxyproline (Hyp) [28]. Hydrogen bonds link the peptide bond NH of a glycine molecule with a peptide carbonyl (C=O) group in the next polypeptide. This helps in holding the three chains together. Each of the polypeptide chains is able to fold into a helix maintaining geometry such that they can form a triple stranded helix [26]. The molecular weight of collagen has been determined to be 285,000, which clearly indicates the presence of crosslinks between molecules or physical associations [20].

Proline and hydroxyproline make up about 25% of the residues in a collagen molecule. Thus, the stability of collagen is dependent upon the properties of these

molecules. Collagen without the hydroxyl groups having proline in place of hydroxyproline is able to form triple helices, but these helical structures are unable to maintain their stability at room temperature [29].

Previous research by Berg et al. in 1983 states that the hydroxyl group on the pyrrolidine ring of the hydroxyproline residues enhances the thermal stability of the triple helical structure of collagen. It is also stated that the hydrogen bonds mediated by water molecules help to maintain this stability. Evidence of such water bridges were obtained by X-ray diffraction analysis of crystalline collagen. They showed that two water molecules helped to connect a hydroxyproline side chain of one strand to a carbonyl on the main chain of another strand. In 1998, another group of researchers mentioned that the entropic cost of building and maintaining such water bridges would be extremely high. If it was true, then the bridges would actually immobilize more than 500 water molecules per triple helical structure. Also, research has shown that triple helices of $(ProProGly)_{10}$ and $(ProHypGly)_{10}$ maintain stability when put in methanol or propane-1,2-diol and the hydroxyproline residues are able to maintain stability even in such anhydrous conditions [28, 29].

Research on the inductive effect of the hydroxyl group of hydroxyproline was distinctly noticed in the structure and properties of molecules that mimic collagen. In order to understand the differences between the effect of hydrogen bonding and inductive effects, $(ProFlpGly)_{10}$ was synthesized, where Flp represents 4(*R*)-fluoroproline. Fluoroproline was chosen not only because fluorine is the most electronegative element but also because it does not form hydrogen bonds. With the results obtained after addition of fluoroproline, support against the water-bridge model became quite strong. Thus, a

new model to explain the stability of collagen came into being. It was found that the thermal stability of $(ProFlpGly)_{10}$ triple helices surpassed that of any known collagen of same size. It was concluded that the inductive effects probably helped to maintain the collagen stability by allowing trans conformation of the hydroxypropyl peptide bond. A fluorine atom is able to exert a greater inductive effect than a hydroxyl group, and thus, fluoroproline residues contribute much more to the stability of collagen than the hydroxyproline residues. Hence, chemical modification of the hydroxyproline hydroxyl group with an electron withdrawing substituent could increase the stability of natural collagen, with the promise of producing new biomaterials [28].

2.2.3 Biosynthesis and Assembly of Collagen Fibers

Collagen precursors are called procollagens. Such long, growing peptide chains are transferred into the lumen of the endoplasmic reticulum(ER) where a series of reactions occur.

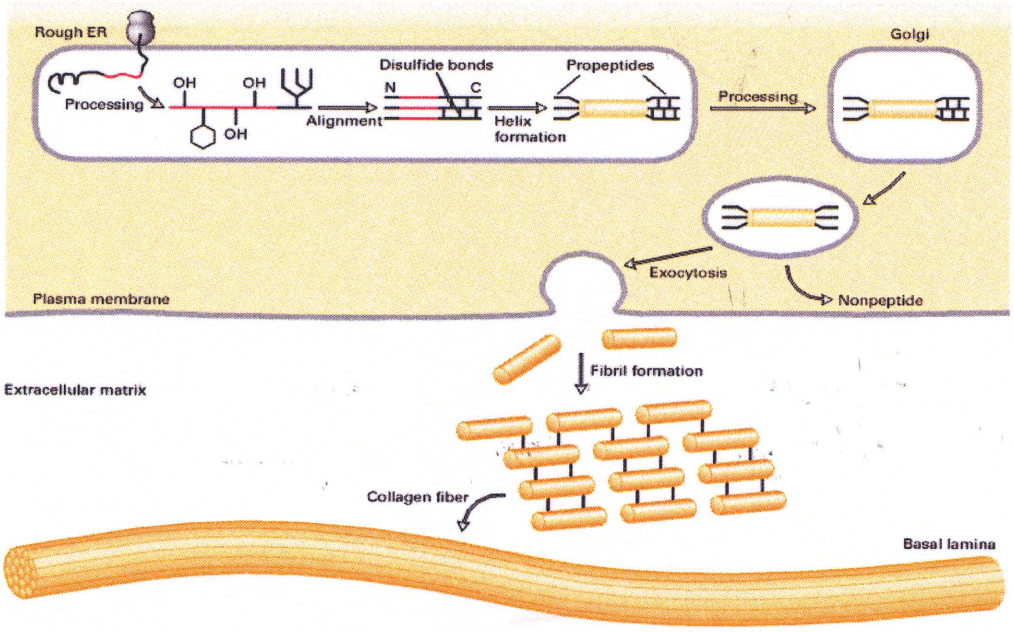

Figure 2.3 Illustrates the major events that take place during the biosynthesis of fibrous collagens [26].

Beginning with the glycosylation of procollagen in the ER and Golgi complex, galactose and glucose are added to hydroxylysine residues and oligosaccharides become a part of the asparagine residues in the C-terminal, called propeptide. At this time, both the C and N terminals possess propeptides. Also, a few of the proline and lysine residues undergo hydroxylation by the hydroxylases. Finally, the intra-chain disulfide bonds located between the N- and C-terminal propeptide sequences help the three chains to be aligned before they form the triple helix. As Figure 2.3 indicates, the procollagen is secreted into the extra cellular space after the completion of processing and assembly. This is followed by the process of exocytosis, the procollagen peptidases along with extra cellular enzymes remove the N and C terminal propeptides. This triple stranded helical structure of the protein is called tropocollagen. The tropocollagen molecules polymerize into normal fibrils in the extracellular space. Figure 2.4 illustrates the structural features of collagen. Certain aldehydes immediately form covalent cross-links between two triple-helical molecules and thus stabilize the collagen molecules [26].

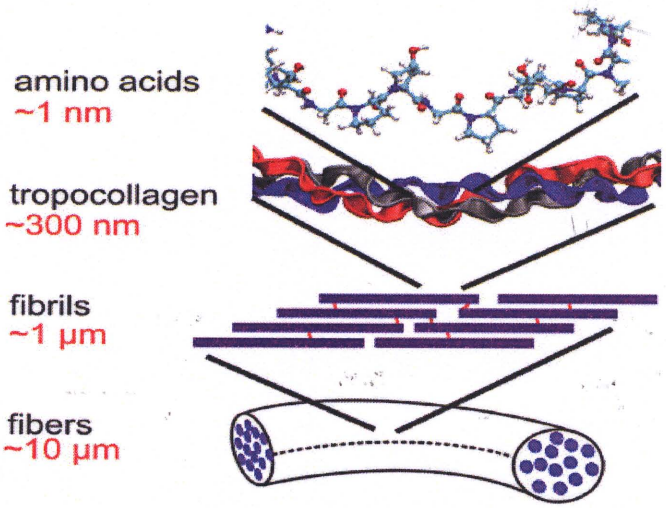

Figure 2.4 Illustration indicates the structural features of collagen ranging from amino acid sequence, tropocollagen molecules and collagen fibrils to collagen fibers [30].

2.2.4 Electrospun Collagen Nanofiber and Tissue Engineering Aspects

Electrospun collagen nanofibers not only have significant importance in the field of tissue engineering but they are also crucial from a biophysical point of view. Research demonstrates that these fibers are able to transmit forces, dissipate energy, prevent premature mechanical failure and also transfers biological signals to adjacent cells that regulate functional responses. The goal of a tissue engineer would be to develop three-dimensional scaffolds of appropriate biological and biomechanical properties, such that it closely resembles the natural ECM and allows cell adhesion, differentiation and proliferation. Collagen has high affinity for water, low antigenicity, very good cell compatibility and also helps in tissue regeneration. The other interesting features that make collagen, the most obvious choice for scaffold material is that, it is biodegradable, bioresorbable and also provides sufficient nutrient supply, appropriate viscoelasticity and strength [5].

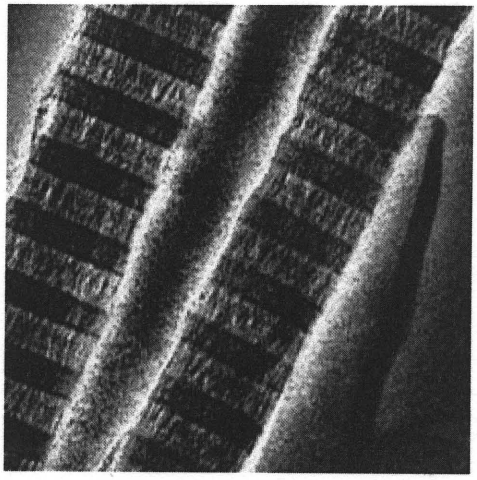

Figure 2.5 An electron micrograph of collagen fibrils [31].

Transmission Electron Microscope study of the electrospun type I calfskin collagen nanofibers, exhibited the 67 nm banding pattern which is typical of native collagen [32]. Figure 2.5 illustrates the TEM image of collagen fibrils. It has also been shown that fiber size is of great importance for proper attachment and interaction of the cells with the scaffold. The variety of possible diameters of the nanofibers that can be obtained by electrospinning surely makes it an ideal technique to design scaffolds for tissue engineering. Synthetic materials, even though they may possess superior mechanical properties, lack the signals required for cell recognition. Thus scaffolds which are produced from naturally occurring proteins in the ECM, like collagen, allow much better infiltration of the cells into the scaffold. The architecture of the electrospun fibers allow the cells to adjust according to the pore size and grow into the nanofiber matrix [5].

In order to achieve specific properties, scaffold materials can be modified by the methods of polymer blending, co-electrospinning, multi-layering and also cross linking or coating the scaffold which helps to enhance its stability and biocompatibility. Poly(L-lactic acid)-*co*-poly(ε-caprolactone) nanofiber mesh when coated with collagen was able to improve endothelialization and preserved the phenotype of human coronary artery endothelial cells, as observed by increased spreading, cell viability, attachment and phenotypic maintenance [5, 33, 34]. A study performed by another group of researchers [28], showed that a combination of collagen-glycosaminoglycan nanofiber scaffold produced from natural ECM components could mimic the characteristics of the extracellular matrix and thus, is an evidence of the promising role that it can play in tissue engineering applications.

2.3 Poly (l-lactic acid)

Poly(L-lactic acid) or PLLA is a widely used biodegradable and biocompatible polyester. Major applications in the field of biomedical engineering includes wound closure, prosthetic implants, controlled drug delivery systems and also in the production of three-dimensional scaffolds for tissue engineering. It is also used in textiles and the packaging industry. Pure polylactic acid (PLA) is a semi-crystalline polymer with a glass transition temperature in the range of 50-65°C and melting point of about 180°C [36].

2.3.1 Lactic Acid Based Polymers

Lactic acid (2-hydroxypropanoic acid) is one of the smallest optically active molecules which can exist in either L (+) or D (-) stereoisomer form. L-Lactic acid is the stereoform present in mammalian systems and literature states that both the D and the L stereoisomers are found in bacterial systems. Polymers derived from lactic acid by polycondensation are referred to as poly(lactic) acid and the polymers derived from lactide by ring open polymerization are called poly(lactide) as illustrated in Figure 2.6. Both poly(lactic) acid and poly(lactide) are generally referred as PLA [36].

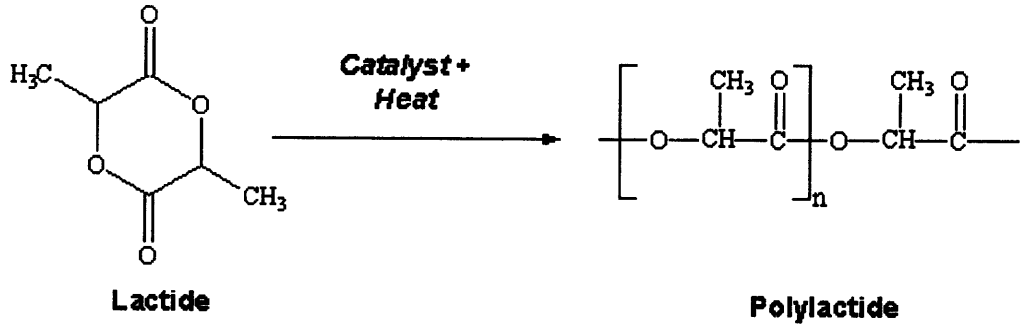

Figure 2.6 Illustrates ring opening polymerization of lactide to poly(lactide) [37].

As already mentioned, due to the chiral nature of lactic acid, polylactide exists as poly-L-lactide (PLLA) and poly-D-lactide (PDLA). Polymerization of a mixture of both the L and D lactides leads to the synthesis of poly-DL-lactide (PDLLA) which is amorphous [37]. Research indicates that PLLA forms stereocomplex crystallites with poly(D-lactic acid), (PDLA), from solution or during crystallization from the melt, which helps to increase the mechanical performance, thermal stability, and hydrolysis-resistance of poly(lactic) acid based materials [36,37].

2.3.2 Solubility of PLLA

The degree of crystallinity and the molar mass are important factors that contribute to the differences in solubility of PLLA. Some solvents commonly used to dissolve PLLA are chlorinated or fluorinated organic solvents, dioxane, dioxolane and furane. Figure 2.7 lists the solubility of PLLA in common organic solvents [36].

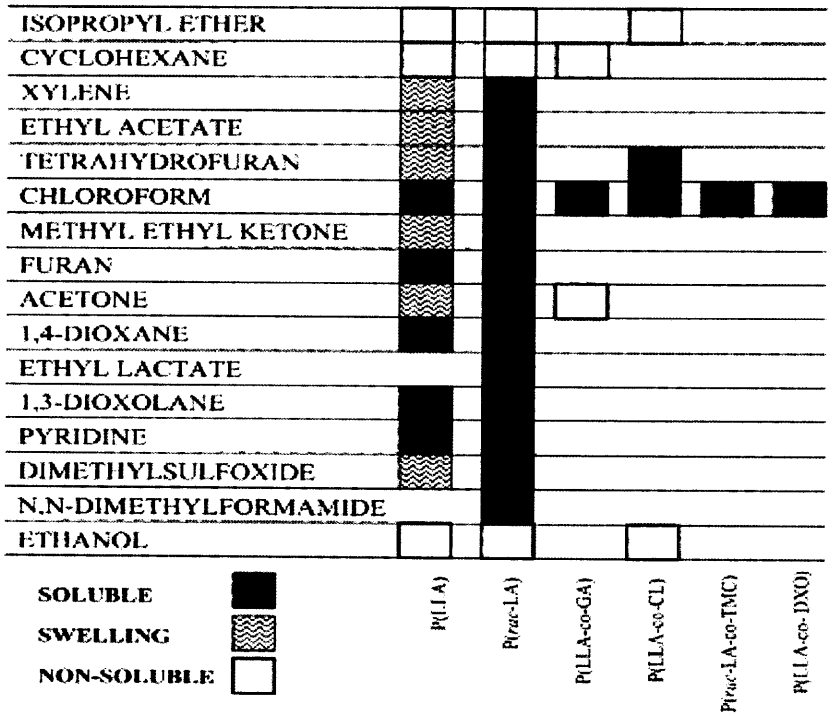

Figure 2.7 Solubility of lactic acid based polymers in common organic solvents [36].

2.3.3 Mechanical Properties of PLLA

The uniqueness in the mechanical properties of the lactic acid based polymers allows them to vary from soft plastics to stiff materials with higher mechanical strength. Semicrystalline poly(lactide) is used more often, as opposed to amorphous poly(lactide) when higher mechanical strength is required. Research has shown that the tensile strength and modulus of PLLA enhances by a factor of 2 when the molar mass is increased from 50 to 100 K Da. Increase of the molar mass to about 300 K Da showed differences in degrees of crystallinity. Research performed on mechanical properties of polymers having the same molar mass but produced by different polymerization process showed no difference. These results have been observed in PLA produced by polycondensation and ring opening polymerization. In addition, fiber spinning can be used to manipulate tensile strength and modulus of PLLA and its blends [36].

2.3.4 Thermal Stability and Hydrolysis of PLLA

In general, the thermal stability of the lactic acid based polymers decreases with increase in temperature [36]. Research has shown that the kinetics for the thermal degradation of poly(lactide) is of first order [38]. It has also been reported that as a result of isothermal heating, the carbonyl carbon-oxygen linkage is possibly the most common one to be split [39]. Rheological measurements on semicrystalline PLLA have demonstrated that the thermal degradation of PLLA is enhanced with increase in moisture content and if proper drying conditions are maintained, degradation is reduced [36].

Hydrolysis of polymers leads to molecular fragmentation which can be regarded as reverse polymerization. Amongst the different reactions involved in the thermal degradation of lactic acid based polymers, zipper like depolymerization appears to be the

most significant in PLLA [36]. In semicrystalline PLLA, the first stage of the hydrolytic degradation takes place in the amorphous regions where the molecules get hydrolyzed. The undegraded remnants thus, have more space and mobility, which lead to reorganizations in the polymer chains and an increase in the crystallinity of the polymer [40]. Differences in stability of the polymer are mainly because of the differences in polymer purity, molar mass and distribution and crystallinity.

The rate of poly-L-lactide degradation may be increased by plasticization with triethyl citrate, but this produced a less crystalline, more flexible material. Time required for poly-L-lactide implants to be absorbed is relatively long and depends on polymer quality, processing conditions, implant site, and physical dimensions of the implant. The biological resorption time of some of these homopolymers can vary from a few months to many years [36]. PLLA has been documented to take as much as 5-7 years to get absorbed when used in orthopedics. PDLA is known to have a much faster absorption rate [37].

2.3.5 Crystallization Rate of PLLA

The solid state morphology and degree of crystallinity highly affects the physical and mechanical properties of stereoregular isotactic polymers like PLLA. PLLA is also known to have a very low rate of crystallization, which helps to produce PLLA polymers with various degrees of crystallinity. The crystalline lamellar organization in the polymer structure plays an important role in the degradation mechanism of PLLA. Thus, it is of significant importance to understand the degree of crystallization and the internal microstructure of the solid.

Analysis of crystallization kinetics by many research groups has shown that there is a maximum increase in the rate of crystallization around 100°C with noticeable discontinuity in phase change kinetics at 120°C. Various explanations have been put forward by researchers which include a transition in regime II-III growth of spherulites or to a variation in the rates of isothermal thickening and secondary nucleation. The kinetic analysis of growth rate curve showing regime transitions is illustrated in Figure 2.8 along with a description below the illustration.

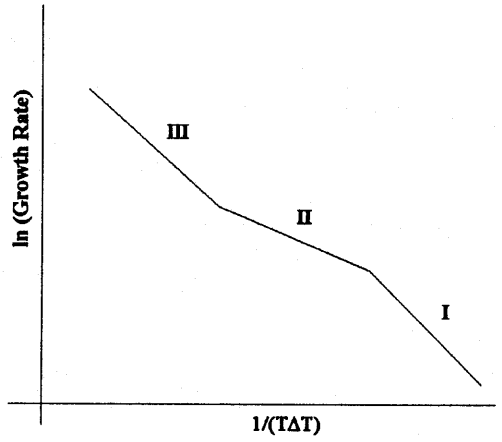

Figure 2.8 Kinetic analysis of common polymeric growth rate curve [41].
Considering *i*, to be the rate at which the nuclei form and the spreading rate, *g*,

Regime I - Mononucleation: $i << g$,

Regime II - Polynucleation: $i \approx g$

Regime III - The 'nucleation rate' is so high that lateral spreading is not required. $i > g$

Some authors have hypothesized solidification into a different crystal structure. Maria Di Lorenzo [42] has shown that the sudden increase in crystallization rate of PLLA below 120°C is the effect of increase in the growth rate of the spherulites. It has also been mentioned that this change is not associated to changes in nucleation rate or to morphological differences in the appearance of PLLA spherulites. The sudden variation

in the rate of phase transition may be due to crystal growth in a different structural modification which is favored by temperatures below 120°C. PLLA is a polymorph polymer which is able to solidify in three crystal modifications represented as α, β and γ. Researchers also hypothesize that initially, a different crystal structure develops which eventually, gets transformed into the more stable α form.

2.3.6 Double Melting in PLLA

Yasuniwa et al [35] studied the influence of crystallization rate on the melting behavior of PLLA and showed the appearance of double melting peaks at slow rates of heating samples prepared with slow cooling rates. Figures 2.9A and 2.9B illustrates the nature of the thermograms of PLLA obtained at various heating rates.

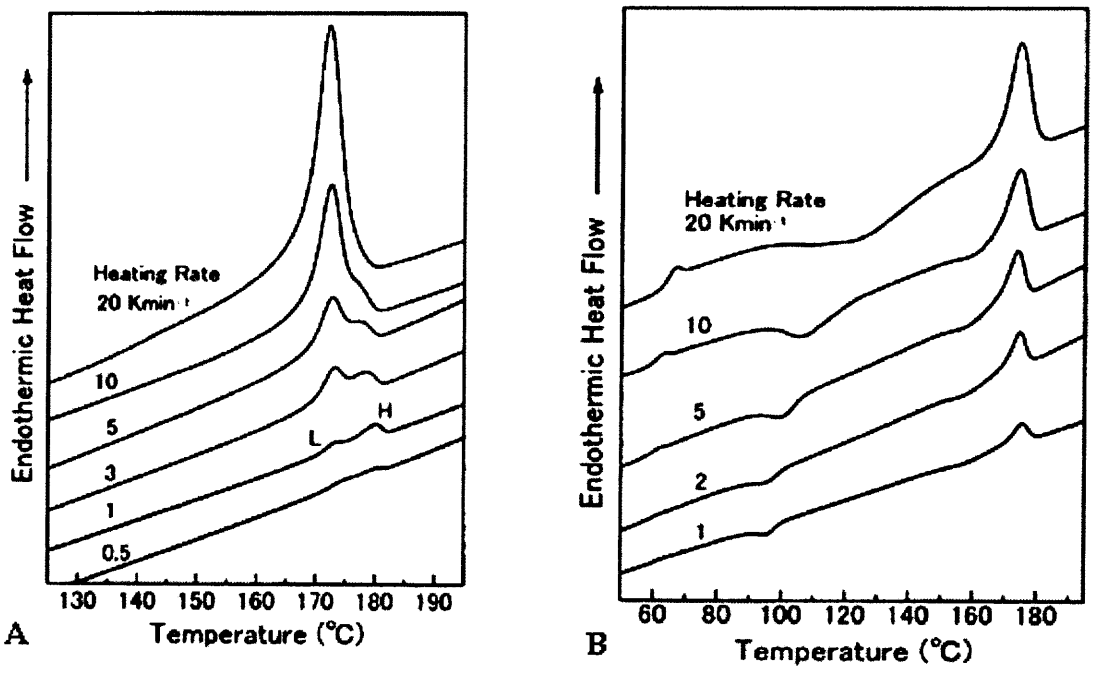

Figure 2.9 DSC thermograms of melt-crystallized samples being heated. The cooling rate was 1 $Kmin^{-1}$ (Figure A) and 10 $Kmin^{-1}$ (Figure B), and the heating rates are as indicated on the curves [35].

The double melting behavior of PLLA has been explained by many researchers with the help of a melt-recrystallization model. In the differential scanning calorimetry (DSC) scan, two endothermic peaks appear at different temperatures. This model emphasizes that the low temperature and high temperature peaks in the curve occur as a consequence of melting of some of the original crystals and due to the melting of crystals which are formed through a recrystallization process during the heating scan, respectively. It has also been mentioned that, as the process of recrystallization takes place slowly, it is suppressed at a high heating rate. Thus the process begins with the melting of the original crystals, followed by their recrystallization and finally, the melting of these recrystallized crystals. It is also suggested in the melt-recrystallization model that the smaller and imperfect crystals undergo melt-recrystallization and form more stable crystals [35].

2.3.7 Glass Transition and Structural Relaxation of PLLA

The intrinsic low rate of crystallization of PLLA allows it to produce polymers with different degrees of crystallinity depending on crystallization conditions. Literature states that even in the most favorable cases, it is hard to achieve crystallinity degree of more than 60% in PLLA [43]. Thus, it suggests that the amorphous fraction of the polymer plays an important role in determining the final properties of the polymer.

Another important phenomenon specific to the amorphous fraction of the polymer, is the presence of a sharp endothermic peak that can be observed at temperatures below its glass transition temperature (Tg) which would be an indication of structural relaxation. During this process of structural relaxation, the non equilibrium glassy state tends to relax towards thermodynamic equilibrium and thus, the physical and

mechanical characteristics of the polymer alter with time [36, 43]. This is of crucial importance in biomedical applications as the Tg of PLLA is in the range of 50-65°C which is not distant from the physiological temperature (37°C). So, the amorphous fraction of any PLA based polymer will remain in the glassy state and the system will slowly approach equilibrium at this temperature. Thus, physical aging can lead to changes in the physical properties of PLLA with time from the moment it is implanted, besides the pure chemical effect of the degradation by hydrolysis of the polymer chains [43]. Figure 2.10 illustrates the sharp endothermic peak at the Tg of PLLA which indicates occurrence of structural relaxation.

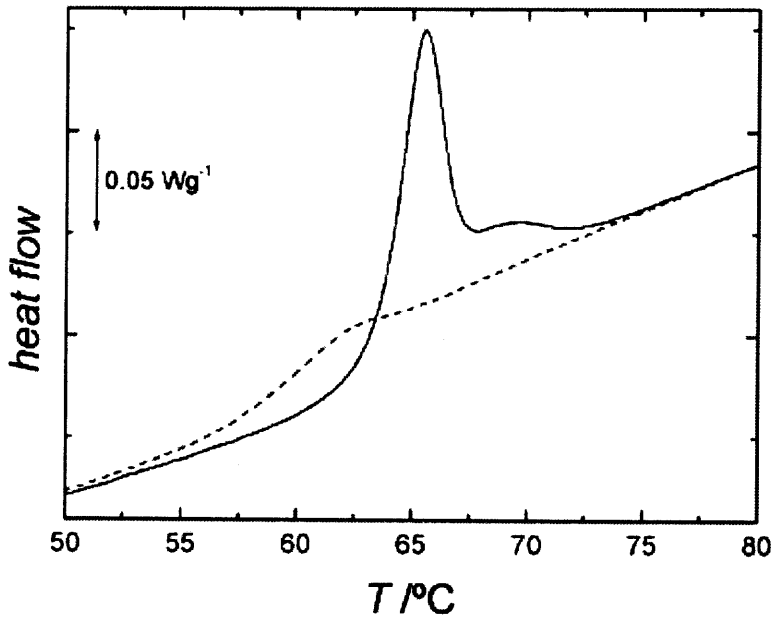

Figure 2.10 Illustrates structural relaxation of PLLA [43].

Researchers [43] studied the glass transition dynamics by aging the polymer for a long time below its glass transition temperature. They concluded the observation of two well distinguished endothermic peaks at the Tg of the polymer when the inter spherulitic and intra spherulitic amorphous phases were present in the polymer. It has been

mentioned that the two peaks correspond to Tg of a bulk like process (at lower temperature) and a broad process assigned to Tg of a confined mobile amorphous phase.

2.3.8 Characteristic Ratio of PLLA

The characteristic ratio is a measure of the intrinsic flexibility of the polymer chains [44]. While research was more focused on producing amorphous non crystallizable polylactides as an alternative to using highly crystalline PLLA, it was observed that amorphous polylactides were brittle under tension. In many cases, it was shown that the mode of fracture of amorphous polymers was controlled by the molecular weight between entanglements and the characteristic ratio. Flexible polymers with low characteristic ratio were observed as highly entangled and showed ductile fracture. This is explained by the fact that intrinsically flexible polymers are much more entangled in the melt (and in the glassy state) than stiff polymers with high values of characteristic ratio. The characteristic ratio for PLLA was determined to be 2.0(±)0.2 and the ductility for a freely jointed chain with tetrahedral bonds showed a characteristic ratio of 2. Such low values suggested ductile fracture behavior of amorphous PLLA [45].

Interestingly, the molecular weight between entanglements in the PLLA melt is close to 10×10^3. This value corresponds to a high characteristic ratio of 12, which suggests that the entangled polymer chains are stiffer. It was observed for amorphous PLLA, that polymers with such high characteristic ratio would fracture in a brittle fashion. PLLA which is produced by crystallizing it slowly from the melt is found to be more impact resistant. This also implies that the presence of crystalline domains has an enormous effect on the ductility of the specimen. Copolymers of L- and D-lactide are comparatively more flexible, with a characteristic ratio of 9.1 but they show brittle

behavior in mechanical testing [45]. Thus, the characteristic ratio and molecular weight between entanglements in the polymer chains share an inverse relationship.

2.4 Electrospinning by Blending Polymers

Electrospun nanofibers produced by blending two or more polymers may have great potential applications in the field of tissue engineering as it allows the addition of various growth factors and other proteins depending on the cell requirements. Recently, the concept of core-sheath morphology in the blended nanofibers has gained a lot of importance. One of the major applications would be to allow the core of the nanofiber to carry out a specific function while the sheath can be tailored to provide some other mechanical or chemical properties [46].

Core sheath structure in blended nanofibers:

Electrospinning a combination of two polymers like Polybutadiene/polystyrene, poly(methylmethacrylate)/polystyrene, polybutadiene/polycarbonate, polyaniline/ polycarbonate, polybutadiene/polycarbonate, and poly(methylmethacrylate)/ polycarbonate blends led to the formation of blended nanofibers with a core-sheath morphology in their internal structure. Example of such a morphology is illustrated in Figure 2.11.

Literature mentions that the formation of the core sheath structures depended greatly on thermodynamic and kinetic factors. It is possible to obtain a good phase separation by large solubility difference between the two polymers. But, it is of significant importance to understand the role of the kinetic factors involved [43]. During the process of electrospinning, when the polymer jet streams through the needle, the

process of rapid solvent evaporation favors polymers with low solubility to come out of solution faster when compared to the highly soluble polymer.

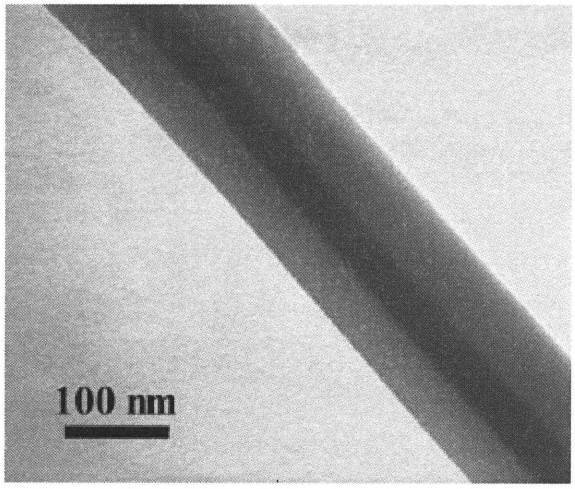

Figure 2.11 TEM images of electrospun polybutadiene/polycarbonate nanofibers at 25/75 weight % ratio after staining by OsO_4 or RuO_4 [46].

Literature also suggests that rheological factors seem to have an effect on the internal morphology of the blended nanofibers. Researchers observed that the polymer solution with a higher viscosity always formed the core while the solution with a lower viscosity formed the outer sheath of the nanofiber [46].

CHAPTER 3

EXPERIMENTAL

3.1 Materials

3.1.1 Bovine Collagen Tendon Derivation and Purification

1000g of raw bovine tendon were loaded into a plastic sleeve and kept in the freezer before further processing. D.I. water was added to the sleeve to fill in the voids. The plastic sleeve was then removed, sliced and the thin slices were ground using a grinder. 41.25 grams of KH_2PO_4 was added to 8.4 liters of distilled water to produce potassium phosphate monobasic solution (buffer solution). In order to maintain the pH to about 6.15±0.15, 1.77g of NaOH was added to the solution. The ground tendons were then placed in the solution. For enzyme treatment of the tendons, they were soaked in Ficin for 1 hour. Ficin is a proteolytic enzyme that helps to hydrolyze the proteins. The enzyme treatment bath comprised 10 grams of Ficin dissolved in the previously prepared buffer solution and heated to 37°C.

In order to prevent further denaturation of the tendon, enzyme deactivation was necessary. The tendons were hand washed and squeezed to remove the Ficin solution. They were placed in the deactivation bath for 1hour. This bath was prepared by adding 84 grams of NH_4NO_3 and 10 grams of $NaClO_2$. It was important to maintain the pH of the solution between 6 and 7. To eliminate the enzyme deactivation solution, three batches of distilled water of 600ml, 600ml and 400ml, respectively were used to wash the tendons after one hour. Each batch of washing was at least for 15 minutes.

In order to further cleanse the tendons of impurities, alkali treatment was performed. The alkali treatment bath was prepared by adding 1400 grams of anhydrous sodium sulfate and 350 grams of sodium hydroxide to 6.8 liters of distilled water. The temperature of the bath was maintained at 25°C for 42 hours.

The next step was to deactivate the alkali treatment and it required three baths of sodium sulfate washes. The first bath contained 200 grams of Anhydrous Sodium Sulfate in 3 liters DI water, followed by washing for 15 minutes with gloved hands. Second and third bath contained 300 grams of Anhydrous Sodium Sulfate in 3 liters of DI water, followed by washing with gloved hands for 15 minutes each.

The alkali deactivation step was followed by acid treatment by preparing acid bath with a pH of 4.6 by adding H_2SO_4 into water. The pH of the bath was kept close to 4.6 while washing the tendons. The pH was monitored with the help of a pH meter. The process was repeated twice. The tendons were soaked in 100% isopropanol for 2 hours at 60°C, followed by a second bath of 100% isopropanol for 1 hour at 60°C. Treatment with isopropanol was performed to dry the tendons by eliminating excess solution from the tendons.

After the treatment with isopropanol, the tendons were taken out, hand squeezed and teased into fine fibers. The teased fibers were then placed in oven which was maintained at 45°C for overnight drying. The tendon that was harvested by this process was 99% Type I bovine tendon collagen. The harvested collagen was stored in air tight containers at room temperature.

3.1.2 Solution Preparation

Materials:

1. Trifluoro acetic acid (TFA) – purchased from Sigma Aldrich, 99% [M_w 114.02]
2. Type I collagen
3. Poly (L-lactic acid) – purchased from Purasorb® in the year 2000
4. Methylene Chloride – from Sigma Aldrich

PLLA and collagen in trifluoro acetic acid solution was prepared by keeping the amount of solids constant at 3g and the amount of TFA at 10ml. The different concentrations prepared are described in Table 3.1.

Table 3.1 Solution Composition

% of collagen in TFA (wt/wt)	% of collagen in solids	Collagen (g)	PLLA (g)	TFA (ml)
1	6	0.2	2.8	10
3	20	0.6	2.4	10
5	33	1.0	2.0	10
7	43	1.3	1.7	10
8	50	1.5	1.5	10
10	66	2.0	1.0	10

After adding the constituents in the desired ratio, the solution was left to stir for about 12 – 14 hours before electrospinning. This was the minimum time required to dissolve the collagen and PLLA completely in TFA. Experiments were also performed by

adding 3g of collagen to 10ml of TFA for the production of pure collagen nanofibers and similarly 3g of PLLA to 10ml of TFA for the production of pure PLLA nanofibers. The dissolution time of collagen in TFA was greater than the dissolution time for PLLA in TFA by an hour approximately. After electrospinning, all mats were stored at room temperature.

3.1.3 Degradation Experiments

In order to evaluate the solution degradability of PLLA, PLLA was allowed to stir in TFA for 4, 10 and 20 hours longer than collagen maintaining a 5% by weight concentration of collagen. 10 micro liters of water was added to one set of solution at the zero-th hour in order to understand the facilitate hydrolytic degradation of the components. The solution was stirred for 15 hours after addition of collagen before they were electrospun. Similar experiments were performed by allowing collagen to remain in TFA for 4, 10 and 20 hours longer before the addition of PLLA at the 5weight % concentration.

3.1.4 Time Based Degradation of Collagen-PLLA

In order to evaluate the degradation of collagen-PLLA in TFA as time progresses, a solution of 5% by weight of collagen was prepared and stirred for 10hours. The solution was electrospun at the end of 10, 14, 18, 34, 58, 72 hours to analyze the degradation profile of the solution.

3.1.5 Dispersion of Collagen-PLLA

In order to evaluate electrospinning from a heterogeneous fluid, dispersion of collagen in TFA and PLLA in methylene chloride was produced. The dispersion was prepared by

adding 0.1g of collagen to 1ml of TFA in the first step. The collagen seemed to form a gel in the beginning but after about 4.5 hours, it dissolved. This step was followed by the addition of 3ml methylene chloride at the end of 4.5 hours. The dispersion was stirred for about 2 hours before 0.25g of PLLA was added to it. While adding methylene chloride to TFA, a ratio of 1:3 was maintained. The dispersion was stirred for about 15 hours before electrospinning.

3.1.6 PLLA Extraction

PLLA was extracted from the collagen-PLLA electrospun mat using methylene chloride. Initial experiments were done by cutting a 2cm x 2cm electrospun mat and placing it on an SEM stub. About 2ml of methylene chloride was added to another small beaker and the stub was immersed in the beaker containing the solvent. Care was taken such that the mat remained on the stub and did not slip away into the beaker. The stub was immersed for about 1 hour and it was followed by overnight vacuum drying. Alternatively, instead of putting the mats on SEM stubs, the mat was put on glass slides and then peeled off carefully after vacuum drying and finally, placed on the SEM stubs to view under the microscope.

3.1.7 Aging Experiments

Aging experiments were carried out on the electrospun mats by putting them in a vacuum oven at 40°C overnight. The glass transition temperature of PLLA is between 50-65°C and thus, the mats are held at a temperature below Tg to allow the structural relaxation process to take place.

3.1.8 Cast Films

In order to understand the changes that may take place in the fibers during electrospinning, cast films were also prepared on glass slides with the same solutions. Films of 1%, 5%, and 8% collagen-PLLA blends were prepared. A few drops of the solution was put on the glass slide and then drawn with another glass slide in order to form a uniformly deposited layer. The slide with the solution was kept overnight in the vacuum oven for drying.

3.2 Methods

3.2.1 Electrospinning Set Up

The components of the electrospinning set up comprised the following:

1. a syringe pump – Cole-Parmer single syringe infusion pump
2. a 30KV power supply – Gamma High Voltage Power supply
3. 10ml plastic syringe – BD Luer lok syringe
4. a stainless steel ground plate – 12 inches by 9.5 inches
5. 20 gauge stainless steel needle

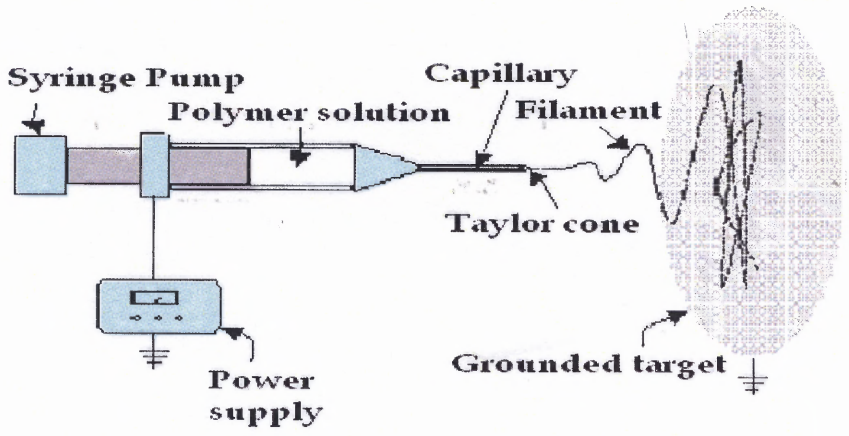

Figure 3.1 Schematic of the electrospinning set up [20].

As illustrated in Figure 3.1 the syringe is mounted such that the needle is pointed at the center of the ground plate. The distance from the tip of the needle to the ground plate is about 25cm. The syringe pump comprises a syringe filled with water which serves as the hydraulic between the syringe pump and the piston of the delivery syringe. The stainless steel ground plate is used to collect the polymer fibers. The high voltage power supply is connected to the syringe needle through an alligator clip (positive end). The negative end is attached to the stainless steel plate. The ground wire is connected back to the power supply and thus, completes the grounding of the metal plate.

3.2.2 Differential Scanning Calorimetry

The Differential Scanning Calorimeter (TA Instruments Q100) is used to analyze the temperature dependent behavior of the electrospun mats. The TA Universal Analysis software program is used for this analysis. Standard aluminum pans are used to contain the samples and dry nitrogen is used as the purge gas. The instrument works basically by heating up both the sample pan (containing the electrospun mat) and the reference (empty pan) at a programmed rate in a thermally insulated chamber. This is followed by monitoring the temperature difference between the sample and the reference pan and finally, converting it to heat flow. As heating progresses, the sample may undergo physical transformation like melting, freezing or even subtle changes like glass transition. The amount of heat absorbed or liberated depends on whether the reaction is exothermic or endothermic. By noting the difference in heat flow between the sample pan and the reference pan, differential scanning calorimeter is able to measure the amount of heat absorbed or released during phase transitions and any thermally labile physical changes.

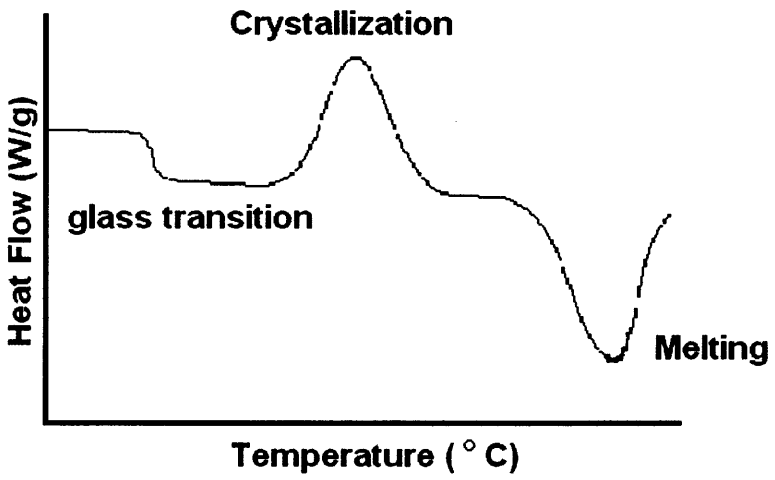

Figure 3.2 Example of a DSC thermogram [48].

The DSC thermogram in Figure 3.2 illustrates the temperature dependent behavior for typical polyester. With the increase in temperature, the thermogram demonstrates the appearance of glass transition in the polymer, followed by crystallization and finally melting of the crystals.

The DSC was programmed such that all samples were to undergo a heat-cool-heat cycle. For PLLA pellets, the high temperature was kept at 240°C and low temperature of 0°C. The heating rate and the cooling rate were kept at 10°C/min. For collagen mats and the PLLA collagen blended mats, the high temperature changed to 210°C to avoid denaturation of collagen around 230°C.

DSC is abundantly used in pharmaceutical and polymer industries. Various applications of DSC include determination and study of crystallization temperature, melting temperature, heat of melting, glass transition, curing processes of polymers, liquid crystals, purity levels of samples, oxidation reactions and also other chemical reactions [48].

3.2.3 Thermogravimetric Analysis

Thermogravimetric Analysis or TGA is another thermo-analytical technique which helps to determine changes in weight of the sample (electrospun mat) as a function of change in temperature. The sample is heated at a controlled rate and as the temperature changes, the weight of the sample is monitored. The TA Universal Analysis software program is used for analysis of the result. It is easier to use a derivative weight loss curve to be able to identify precisely, at which temperature, the rate of weight loss is highest [20, 48].

TGA is extensively used in research work to determine characteristics of polymers, their degradation temperatures, moisture content of materials, the extent of inorganic and organic components in materials, decomposition points of explosives, and solvent residues [48].

3.2.4 Scanning Electron Microscope

The scanning electron microscope (LEO 1530 VP FE-SEM) has been used for morphological analysis of the electrospun nanofibers. Mean diameters of the fibers were measured from 20 randomly chosen fibers in SEM images.

Compared to conventional light microscopy, the SEM creates magnified images by using electrons in place of light waves. It works by focusing a high energy beam of electrons on the surface of the sample and detects signals from the interaction of the incident electrons with the sample surface [49]. The type of signal varies and may include secondary electrons, backscattered electrons and X rays. The SEM is capable of showing very high magnification three dimensional images which is beyond the scope of a light microscope. The SEM images are produced without the effect of light waves and are thus, rendered black and white.The main advantage of the SEM is its great depth of field,

which as a result, allows a greater part of a specimen to be in focus for a longer time and the availability of magnifications to very high levels. Figure 3.3 illustrates the basic operation of an SEM.

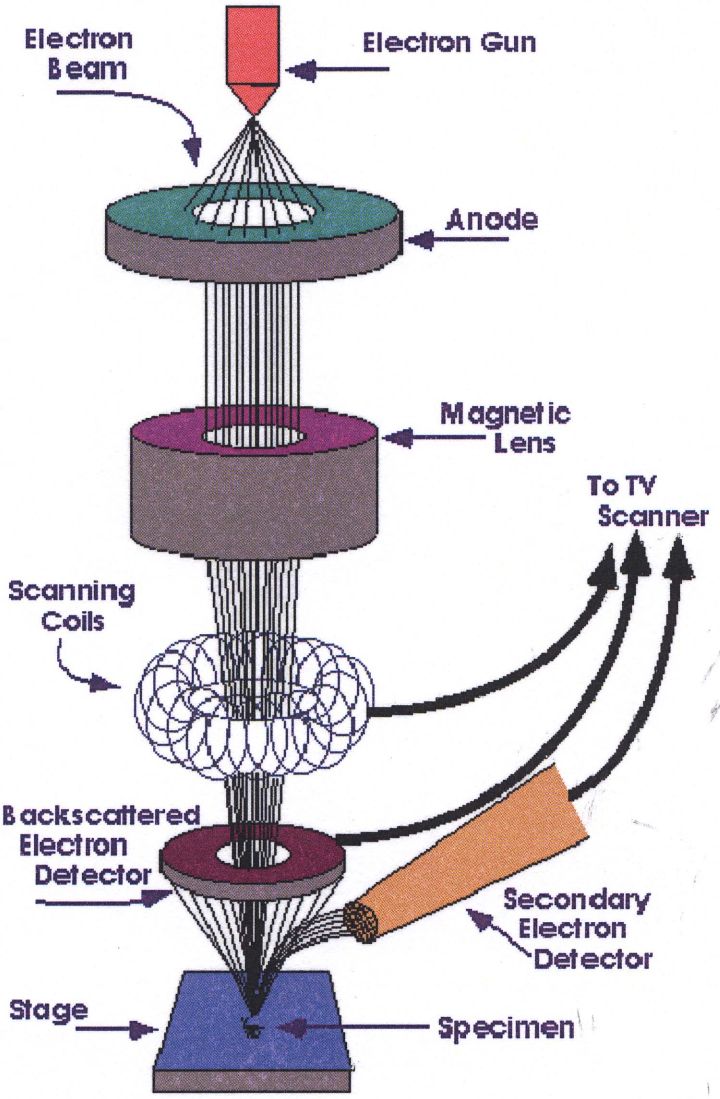

Figure 3.3 Schematic demonstrating the working of SEM [50].

As Figure 3.3 suggests, the beam of electrons which are emitted from the electron gun, follow a vertical path through the microscope, which is held within high vacuum. The electron beam is condensed by the first condenser lens that is used to form

the beam as well as limit the amount of current in the beam. The second condenser lens now helps to form the electrons into a thin, coherent beam which is usually controlled by the fine probe current knob [20]. A set of coils then scan or sweep the beam in a raster, dwelling on specific points for a period of time which depends on the scan speed as provided by the user (usually in the microsecond range). The final lens which is the objective focuses the scanning beam on the desired area of the specimen. Once the incident beam hits the surface of the sample, electrons and X-rays are emitted from the sample as shown in Figure 3.4 [50]. Detectors collect these X-rays, backscattered electrons, and secondary electrons and convert them into a signal that is sent to a screen similar to a television screen. This produces the final image.

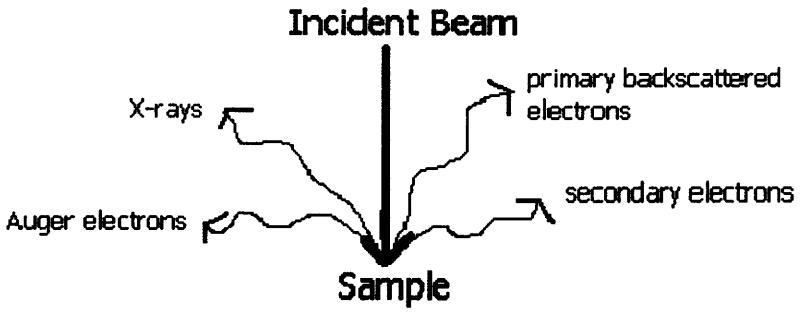

Figure 3.4 Schematic demonstrating the scattering of electrons [50].

The sample preparation forms an important part of the SEM experiment. It is important that the samples be dried and thus, made free of any solvent or liquid. The sample should be strictly free of water as it would vaporize in the vacuum. So, the samples were dried overnight in vacuum oven before they were observed under the SEM. Care should be taken that the sample is able to withstand the high vacuum that is maintained inside the chamber. For the fibers to be able to conduct electricity, the electrospun mats are coated with a thin layer of Carbon. In some experiments, gold

coating has also been used. The sputter coater in gold coating uses an electric field and argon gas.

3.2.5 Transmission Electron Microscope

The transmission electron microscopy (TEM) was used to observe the internal morphology of the collagen-PLLA nanofibers. This microscopy technique utilizes a beam of electrons which is transmitted through an ultra thin nanofiber. This instrument works by forming an image with the help of the electrons transmitted through the specimen, which is then magnified and focused by an objective lens. The image appears on an imaging screen. The samples were viewed and digitally recorded with a JEOL 1010 TEM operating at 70 KV. The samples were carefully prepared by electrospinning the collagen-PLLA blend (5% by weight of collagen) only for 10-15 seconds onto the standard 3mm diameter, 200 mesh copper grids. The TEM grids were carefully mounted on top of a stainless steel blade which was taped to a stainless steel plate. The plate was then placed inside the electrospinning chamber. After 10 seconds, the voltage was turned off and the grids were carefully collected and observed under the light microscope to check for deposition of nanofibers. The TEM is widely used material science as well as biological sciences. The specimen must be very thin and able to withstand the high vacuum present inside the instrument. For biological specimens, the maximum specimen thickness is roughly 1 micrometer.

CHAPTER 4

RESULTS

4.1 Thermal Analysis

4.1.1 Aging

The thermal analysis using DSC was carried out on collagen-PLLA electrospun mats of 1%, 3%, 5%, 7%, 8% and 10% by weight of collagen in TFA. The main aim was to understand the development of the unusually sharp endothermic peak at the Tg of PLLA in the blended nanofiber mats (Appendix A, Figure A.1), as observed in the research by S.Wang [20].

In order to analyze the thermal behavior of the blends, it was important to understand the DSC thermogram of electrospun pure collagen and electrospun pure PLLA individually. The DSC thermogram of non-electrospun collagen and electrospun collagen are illustrated in Appendix A, Figures A.2 and A.3. In order to evaluate the structural relaxation in the blends, it was important to compare the thermal behavior of PLLA pellets, electrospun PLLA and collagen-PLLA blended electrospun mats in the same temperature range. Thus, the blended mats were analyzed using DSC, a day after they were electrospun, after aging them at 40°C overnight and also, repeating the scan 45-60 days after electrospinning.

Observation of the DSC thermograms for PLLA pellets and the aged PLLA pellets (Figures 4.1 and 4.2), suggests no evidence of structural relaxation near the glass transition temperature of PLLA. The process of aging the pellets at 40°C overnight caused no considerable change in the thermal behavior of the pellets. The glass transition

temperature, cold crystallization temperature and the melting temperature of the original pellets and the aged pellets were almost the same. The absence of structural relaxation in the aged pellets clearly indicates that there is no apparent densification taking place in these pellets over time.

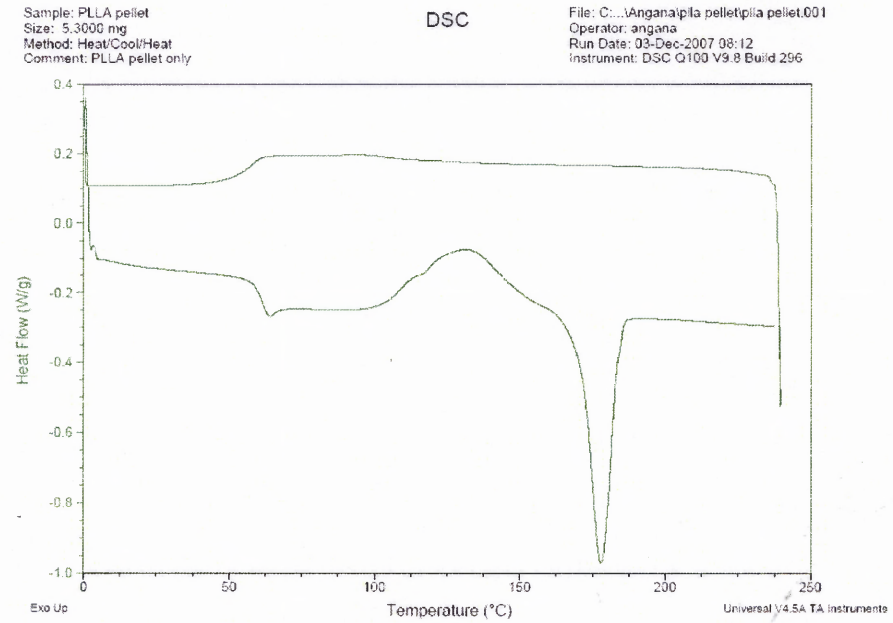

Figure 4.1 DSC of second heat cycle of PLLA pellet.

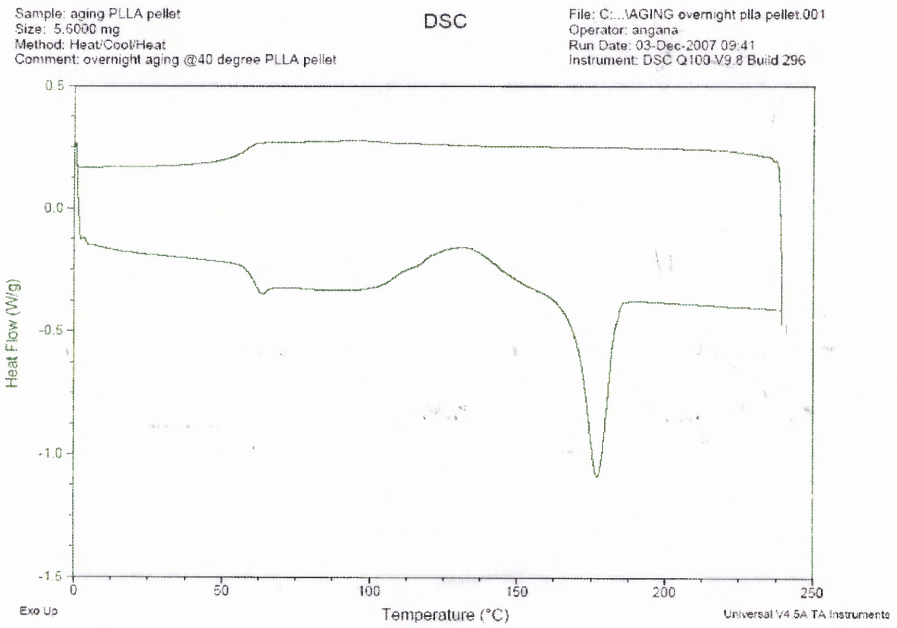

Figure 4.2 DSC of second heat cycle of aged PLLA pellet.

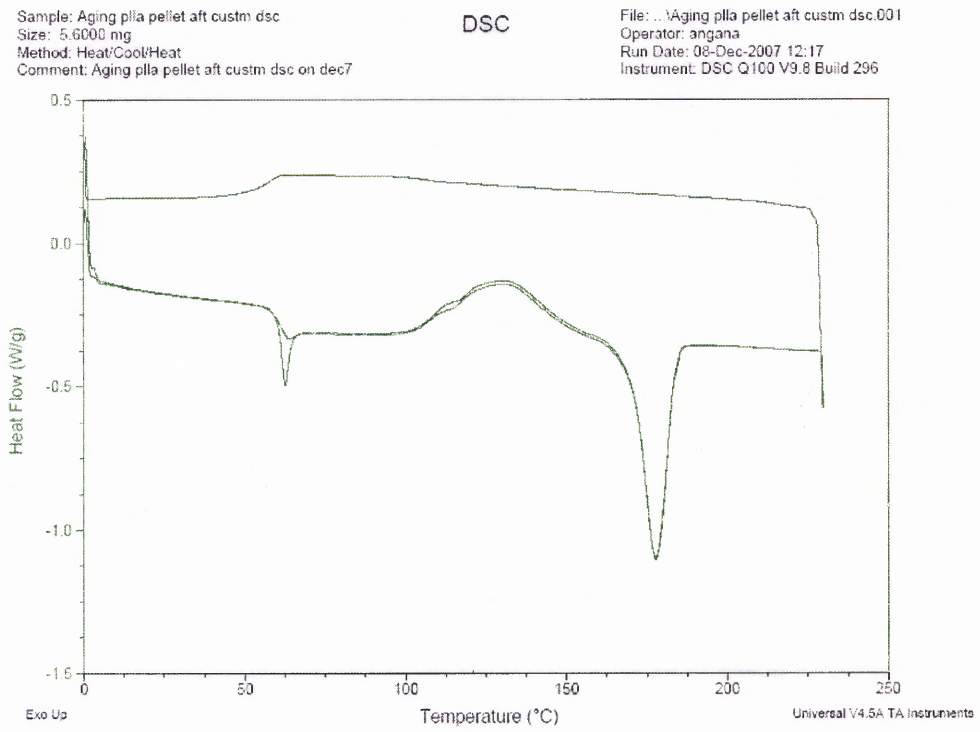

Figure 4.3 DSC of aged PLLA pellet after heat-cool cycle.

Figure 4.3 illustrates the appearance of structural relaxation at the Tg of PLLA when the pellets were subjected to aging at 40°C after a heat-cool cycle in the DSC scan. After the heat-cool cycle, the DSC of the pellets did not show any crystallization peak and thus, the pellet was more like an aged amorphous film. Further, the thermogram also indicates that, during the heating and subsequent cooling of the crystals, the polymer chains did not have sufficient time to attain a thermodynamically stable configuration. As a consequence, during the aging period below the Tg of PLLA, the polymer chains start to proceed towards a more relaxed and thermodynamically favorable state, leading to the development of the sharp endothermic peak. The appearance of the endothermic peak also indicates the increase in final enthalpy of the system.

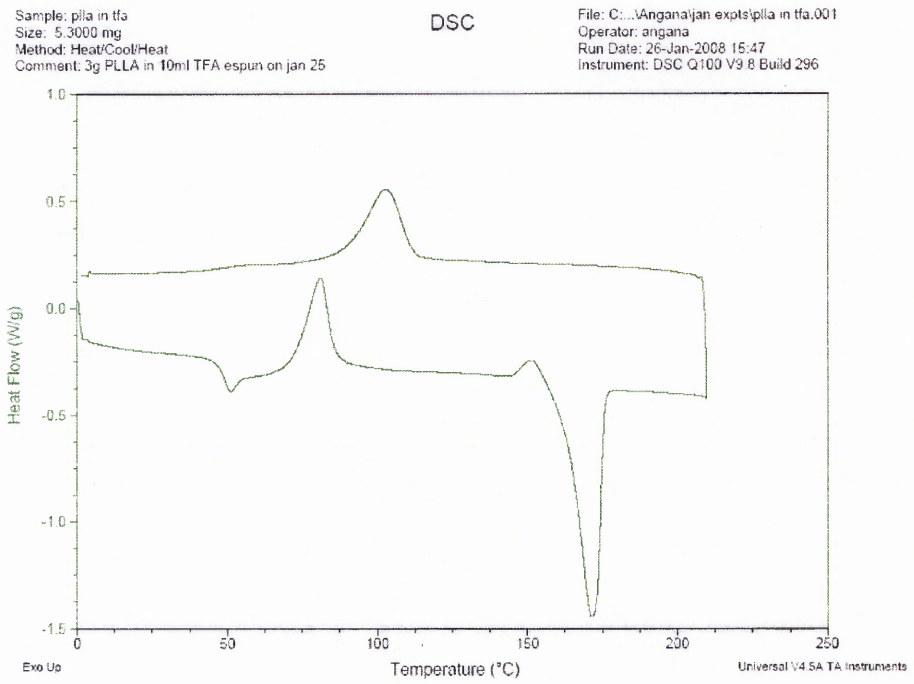

Figure 4.4 DSC of electrospun PLLA mat.

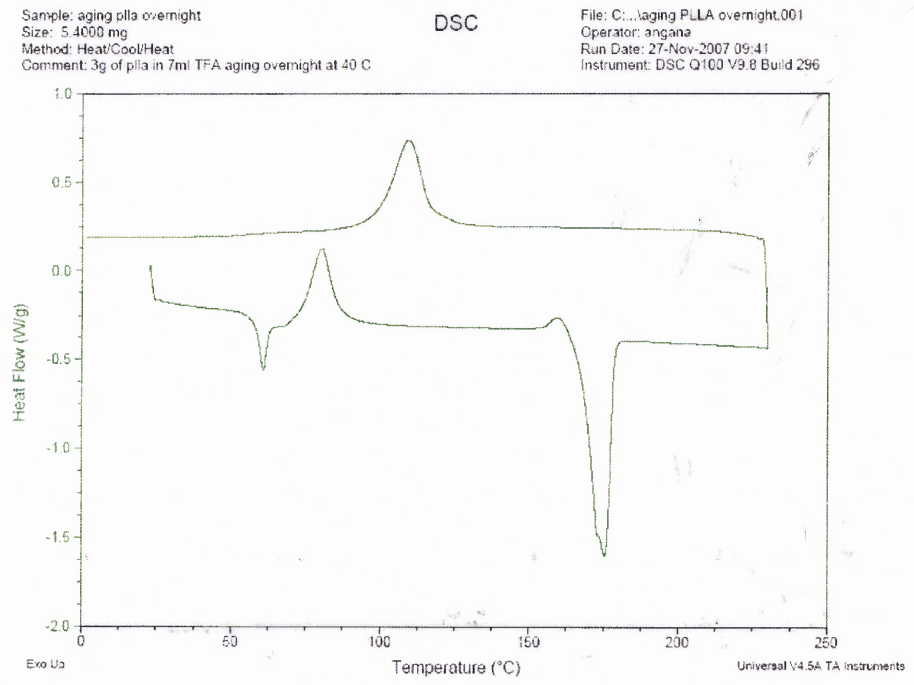

Figure 4.5 DSC of first heat cycle of overnight aged electrospun PLLA mat.

Figure 4.4 illustrates the DSC thermogram of electrospun PLLA. On comparison with the thermal behavior of PLLA pellets, the electrospun PLLA mat indicates a small enthalpy recovery peak and also, the appearance of a very sharp cold crystallization peak. The cold crystallization peak has shifted from 130°C in the pellets to about 60°C in the electrospun fibers. The reason for this may be that the molecules are already arranged in a way that facilitates crystallization. The high elongational flow in electrospinning may be facilitating the formation of extended chain structures in the polymer. In the electrospun PLLA mat which was aged at 40°C overnight, the appearance of a sharp endothermic peak (Figure 4.5) indicates the occurrence of structural relaxation in the polymer. Repeating the DSC scan on the original electrospun mat after a period of 60 days at room temperature led to the formation of a much sharper endothermic peak as illustrated in Figure 4.6. This suggests that the polymer chains underwent aging at room temperature (approximately 25°C) after they were electrospun.

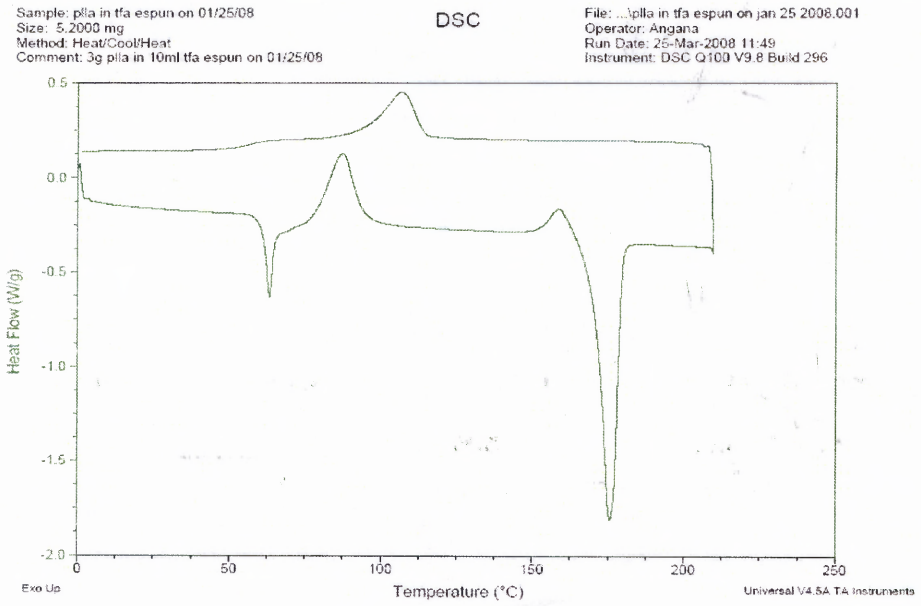

Figure 4.6 DSC of first heat cycle of electrospun PLLA mat 60 days after electrospinning.

The position and magnitude of the cold crystallization peak as well as melting peak, position of the glass transition, position of structural relaxation peak for PLLA pellets, aged PLLA pellets, aged PLLA pellets after a heat-cool cycle, electrospun PLLA and aged electrospun PLLA are given in Appendix B, Tables B.1 to B.6.

Figure 4.7 illustrates the DSC thermogram of 1% electrospun collagen-PLLA mat and Figure 4.8 illustrates the DSC thermogram of aged 1% electrospun collagen-PLLA mat. On comparison of the two, it can be clearly noted that a sharp structural relaxation peak occurs only in the case of the aged mat. Similar results have been observed (Figures 4.9, 4.10, 4.11 and 4.12) when the composition of the mats was 3% and 5% by weight of collagen. It is important to note that, at higher concentrations of collagen that is, 7% and 8% by weight of collagen, the appearance of the structural relaxation peak, is hindered. Thus increase in the amount of collagen content in the blend may not contribute to the development of the enthalpy relaxation. The DSC thermograms of 7% and 8% electrospun mats before and after aging are illustrated in Figures 4.13, 4.14, 4.15 and 4.16. It is also important to note that, the cold crystallization peak increases to a higher value with increase in concentration of collagen in the solution. The value of the cold crystallization peak increases from 80°C in original 1% electrospun mat to 89°C in original 10% electrospun mat. On comparison of the cold crystallization peaks before and after aging, it is observed that the value of the crystallization peak increases after aging the mat. For 1% mat, the cold crystallization peak shifted from 80°C to 84°C. Similarly for 3%, 5%, 7% and 8% electrospun mats, the cold crystallization peak shifted from 85°C , 87°C , 84°C and 89°C, respectively, to 90°C , 89°C , 97°C and 102°C, respectively in

the aged electrospun mats. DSC thermogram for 10% electrospun mat is given in Appendix A, Figure A.4.

The position and magnitude of the cold crystallization peak as well as melting peak, position of the glass transition, position of structural relaxation peak for 1%, 3%, 5%, 7%, and 8% collagen-PLLA electrospun mats and aged mats are mentioned in Appendix B, Tables B.7 to B.18. Tables B.7 to B.12 are the details for blended electrospun mats and Tables B.12-B.18 are for aged blended electrospun mats.

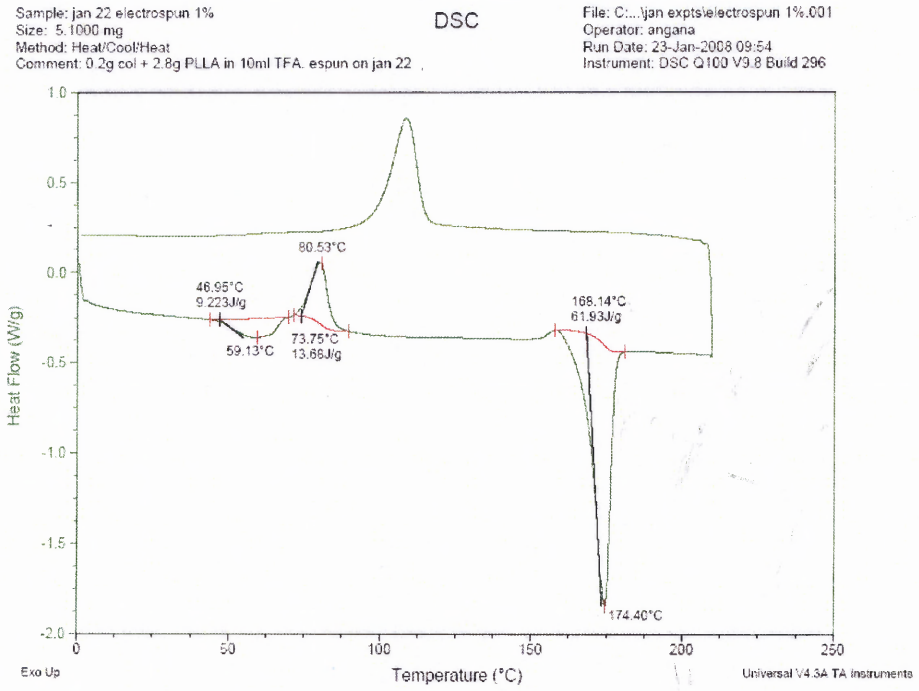

Figure 4.7 DSC of first heat cycle of electrospun 1% collagen-PLLA mat.

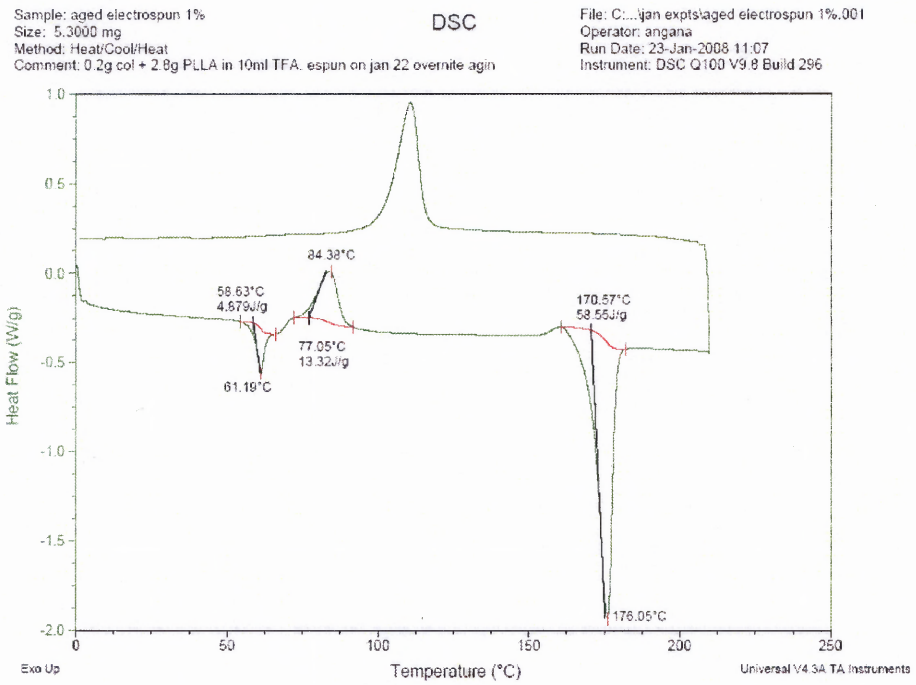

Figure 4.8 DSC of first heat cycle of overnight aged electrospun 1% collagen-PLLA mat.

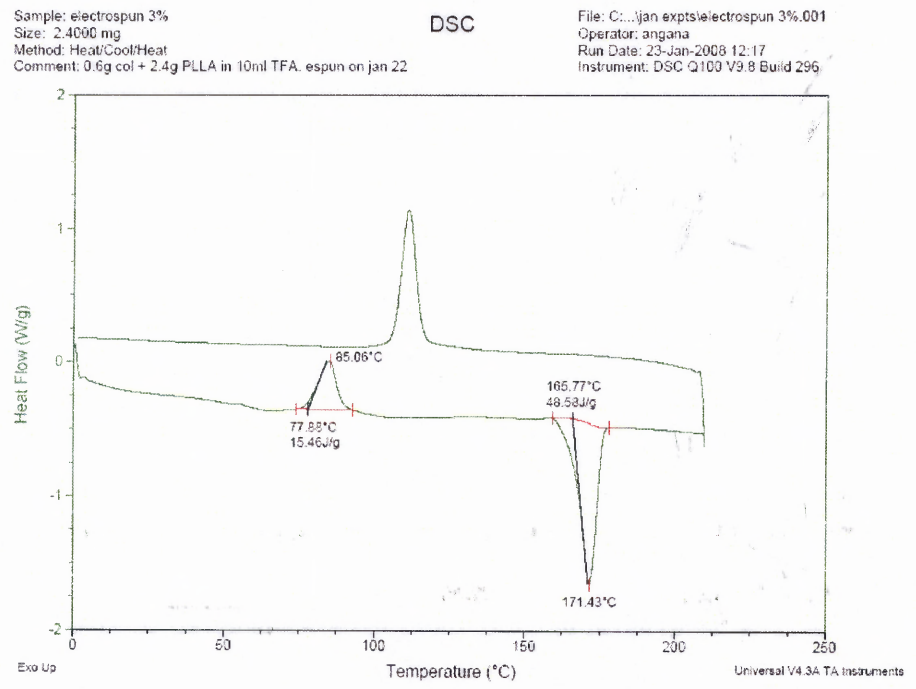

Figure 4.9 DSC of first heat cycle of electrospun 3% collagen-PLLA mat.

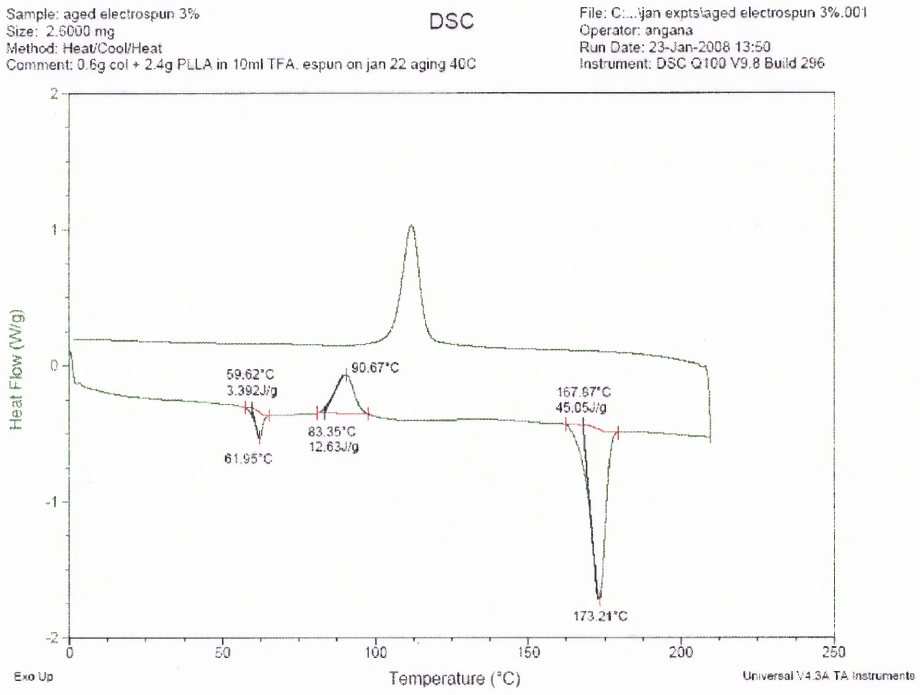

Figure 4.10 DSC of first heat cycle of overnight aged electrospun 3% collagen-PLLA mat.

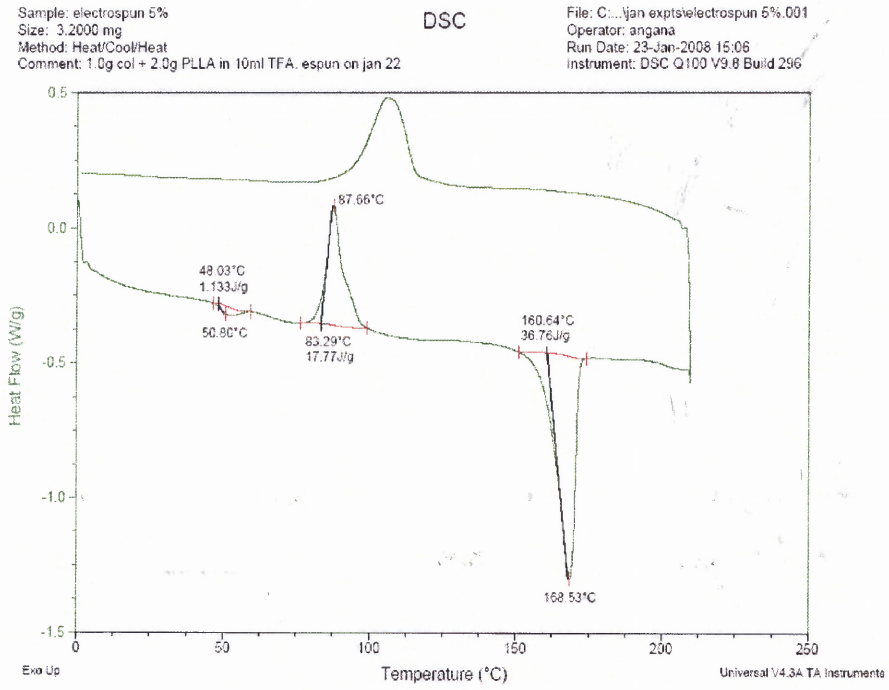

Figure 4.11 DSC of first heat cycle of electrospun 5% collagen-PLLA mat.

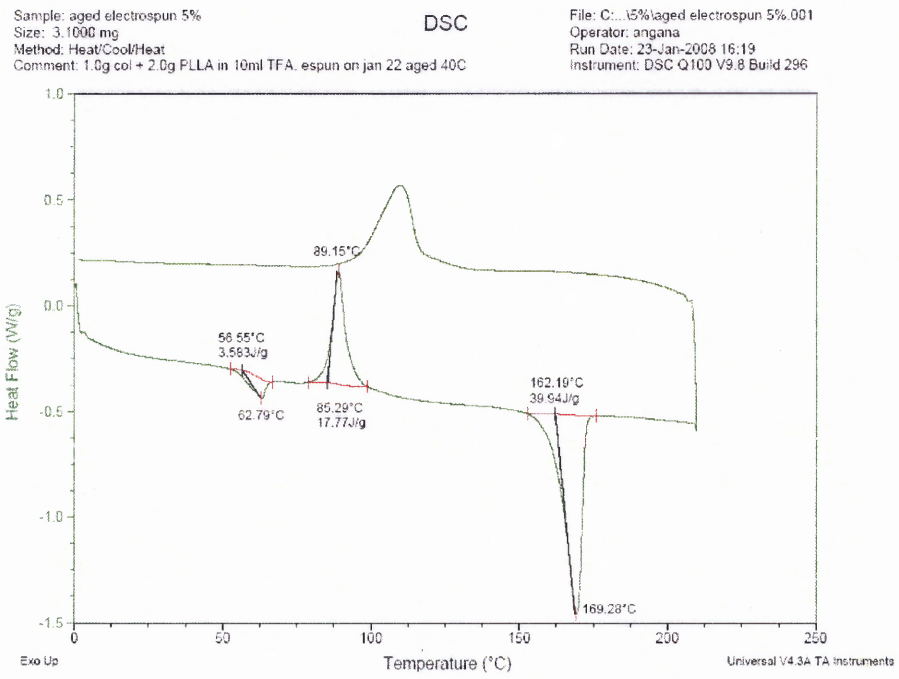

Figure 4.12 DSC of first heat cycle of overnight aged electrospun 5% collagen-PLLA mat.

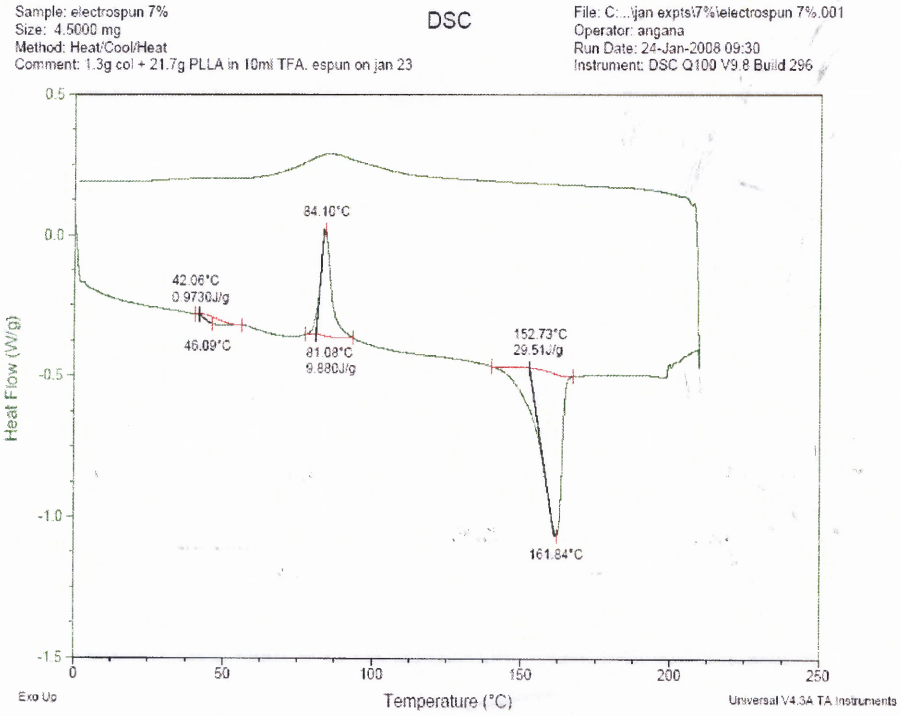

Figure 4.13 DSC of first heat cycle of electrospun 7% collagen-PLLA mat.

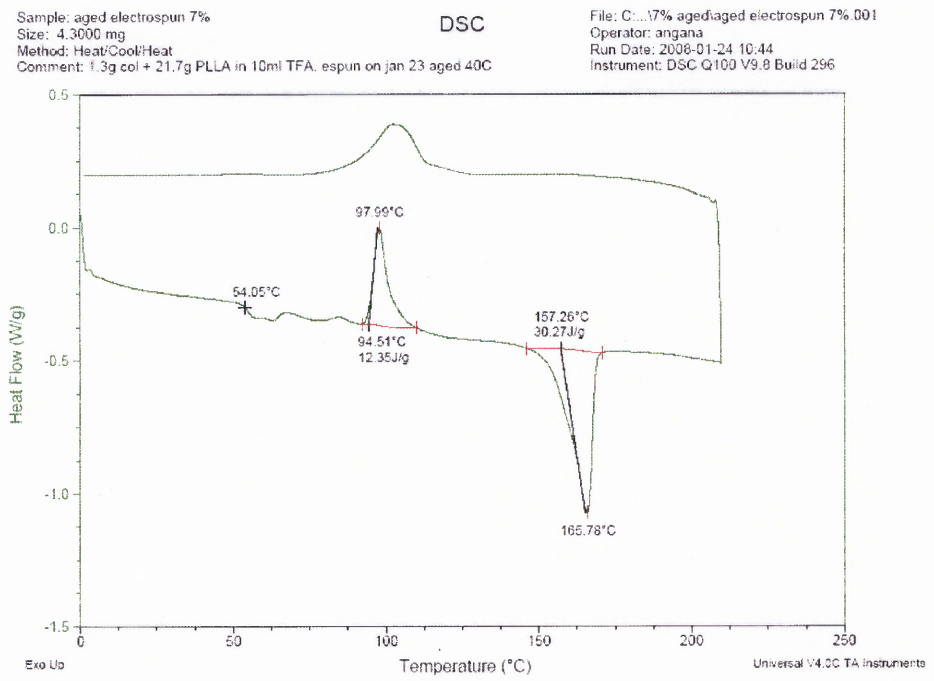

Figure 4.14 DSC of first heat cycle of overnight aged electrospun 7% collagen-PLLA mat.

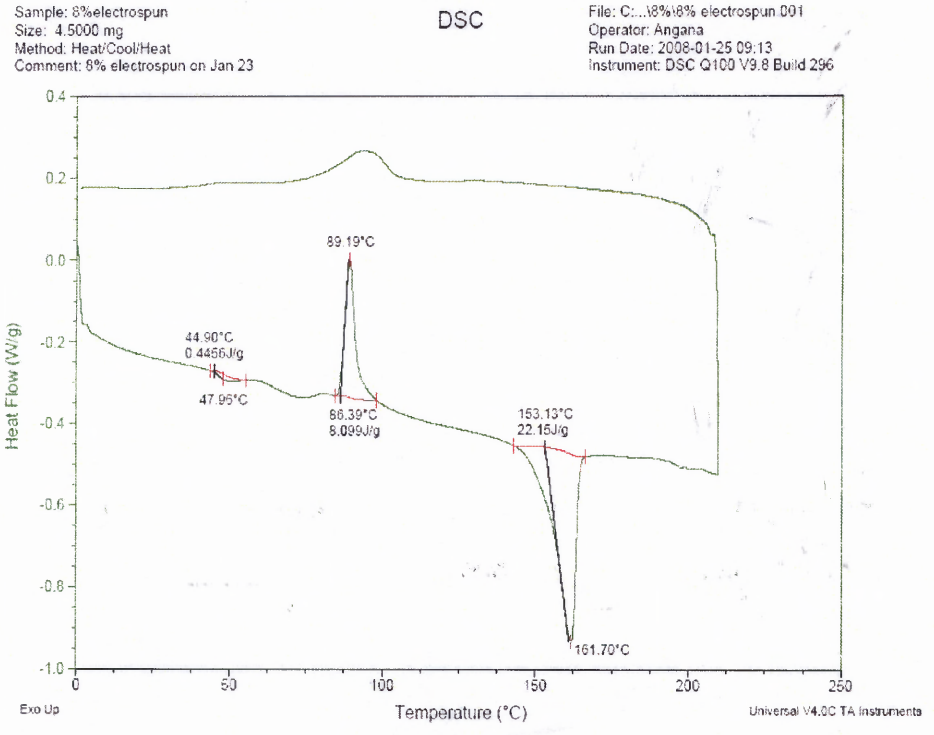

Figure 4.15 DSC of first heat cycle of electrospun 8% collagen-PLLA mat.

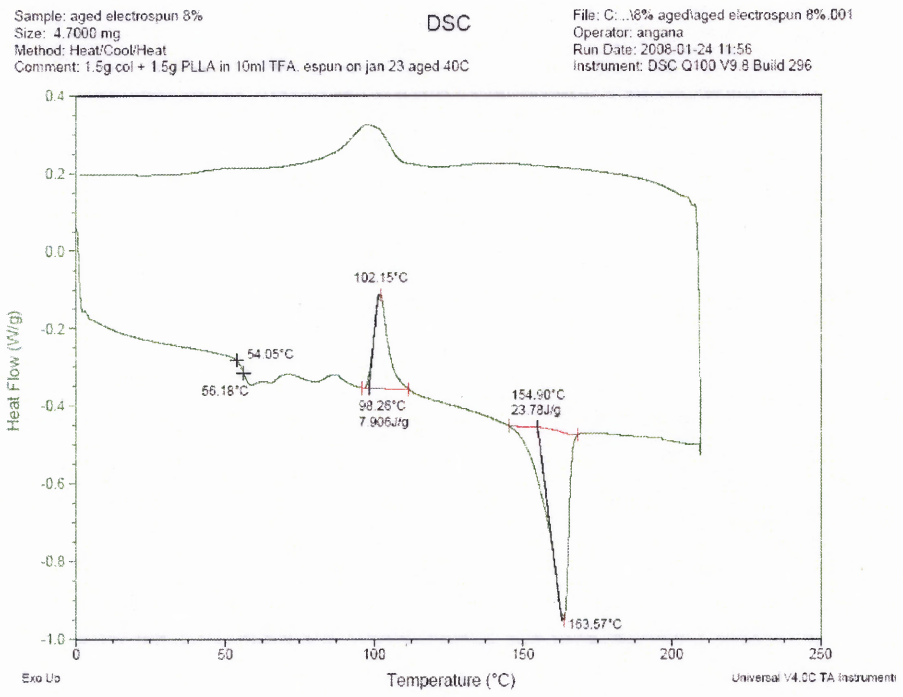

Figure 4.16 DSC of first heat cycle of overnight aged electrospun 8% collagen-PLLA mat.

4.1.2 Cast Films

The structural relaxation peak typically develops over long periods of time. The observation in these experiments is that when the polymer blends are electrospun, this property is manifested within a very short time scale. In order to understand the contribution of electrospinning in the formation of enthalpy recovery peak, thermal analysis of cast films of 1%, 3%, 5% and 8% by weight of collagen were performed. The DSC thermograms of the cast films are illustrated in the Appendix in Figures C.1-C.4. The cast films indicated no structural relaxation peaks and thus, it is demonstrated that it must be the conditions in the electrospinning process which led to the development of the endothermic peak at such short time scales.

4.1.3 Degradation

TFA is a highly corrosive solvent and it was noted that there was a considerable change in the viscosity of the solutions within 2 to 3 days after their preparation. This indicated that the TFA may be degrading the collagen and the PLLA over time. Thus, an experiment was conducted to evaluate the change in the thermal behavior of the collagen-PLLA blend over time. Such a time based degradation profile was performed for a 5% solution of collagen-PLLA. The DSC thermograms are illustrated in Figures C.5-C.9. The minimum time for the PLLA and collagen to completely dissolve is about 10 hours and DSC thermograms of electrospun mats made after stirring for 10, 14, 17 and 34 hours indicated no significant change at the glass transition temperature. At the end of 54 hours, the DSC thermograms indicated the presence of negligibly small endothermic peak at the Tg of PLLA. At the end of 72 hours, electrospinning was attempted but the viscosity of the solution was too low and led to spraying. Very few fibers were formed and they could not be recovered from the collection plate.

In order to evaluate the solution degradability of collagen, 2 sets of solutions were prepared where collagen was allowed to stir in TFA for 4, 10 and 20 hours longer than PLLA by maintaining a 5% by weight concentration of collagen. In addition to this, 10 micro liters of water was added to one set of solution at the zero-th hour in order to understand the effect of water on the electrospun blends. The DSC thermograms are illustrated in the Appendix Figures D.1-D.6.

The DSC results did not indicate any significant change in the thermal behavior. Thus, this experiment underlined the fact that, the degradation of collagen is not responsible for the appearance of the enthalpy recovery peak.

Similar experiments were done by degrading PLLA in solution by allowing it to stir in TFA for 4, 10 and 20 hours longer than collagen. The 5% composition was maintained and also 10 microliters of water was added to one set of solution in order to understand the effect of water on the blends. The DSC thermograms are illustrated in the Appendix Figures D.7-D.12.

The presence of a small endothermic peak was observed in the thermogram of the solution where collagen was added 20 hours after PLLA. This solution also contained 10 microliters of water. As a consequence, it was thought that may be, the degradation of collagen causes the appearance of the endothermic peak. In order to evaluate this hypothesis, another solution was prepared by putting PLLA about 40 hours earlier than collagen and also by adding 10 microliters of water. But, this did not result in the formation of any distinguishable structural relaxation peak (Figure D.13).

4.1.4 DSC of the Electrospun Mats after 45-60 Days

In order to evaluate whether there is any change in the thermal behavior of the electrospun mats with time, DSC scans were repeated on the original electrospun mats of compositions 1%, 5%, 7% and 8% by weight of collagen. Interestingly, it was observed that all the mats showed a sharper endothermic peak, indicating that the mats were aging even at room temperature. This also suggests that, by this process of structural relaxation, the polymer chains in the electrospun mats are trying to attain their thermodynamically most favorable configuration. The DSC thermograms for the 1%, 5%, 7%, 8% and 10% mats about 45-60 days after electrospinning are illustrated in Appendix D, Figures D.14, D.15, D.16 and D.18, respectively. An overlay of the DSC thermograms for the 1% mat is demonstrated in Figure 4.17. The green solid line indicates the DSC scan of the mat, a

day after it was electrospun. The red solid line indicates the DSC scan of the electrospun mat which was aged overnight at 40°C on the same day of electrospinning. The blue solid line indicates the DSC scan of the mat after 45 days of electrospinning.

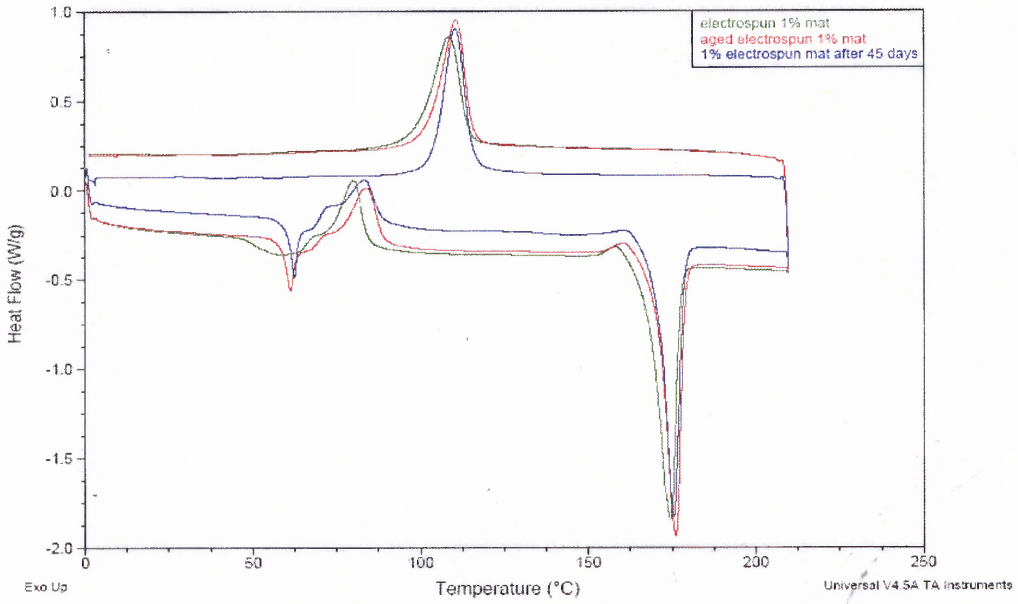

Figure 4.17 Overlay of first heat cycle of DSC thermogram of 1% electrospun mat, a day after electrospinning, after aging at 40°C and repeating the scan after 45days.

4.1.5 Thermogravimetric Analysis (TGA)

Thermogravimetric Analysis was performed to determine the changes in weight of the electrospun mat as a function of change in temperature. The TGA analysis was performed in order to ensure the presence of collagen in the electrospun mats. Various compositions of the electrospun mat (1%, 5%, 7%, 8%, and 10%) were compared with TGA of 100% collagen mat and it clearly indicated the presence of collagen. TGA results are illustrated in the Appendix E, Figures E.1-E.6. By integrating the weight loss rate with temperature,

the TGA composition calibration curve was determined. The curve is illustrated in Appendix E, Figure E.7.

4.1.6 Dispersion of Collagen and PLLA

In order to evaluate electrospinning from a heterogeneous fluid, thermal analysis of the dispersion of collagen in TFA and PLLA in methylene chloride was performed. The DSC thermogram is illustrated in Figure 4.18. The DSC result of the dispersion indicates a glass transition temperature of about 51°C and a sharp cold crystallization at 78 °C followed by melting of the crystals at about 173 °C. These results are very similar to the DSC of electrospun PLLA which shows a glass transition of 50 °C, cold crystallization at 81 °C and melting at 171 °C.

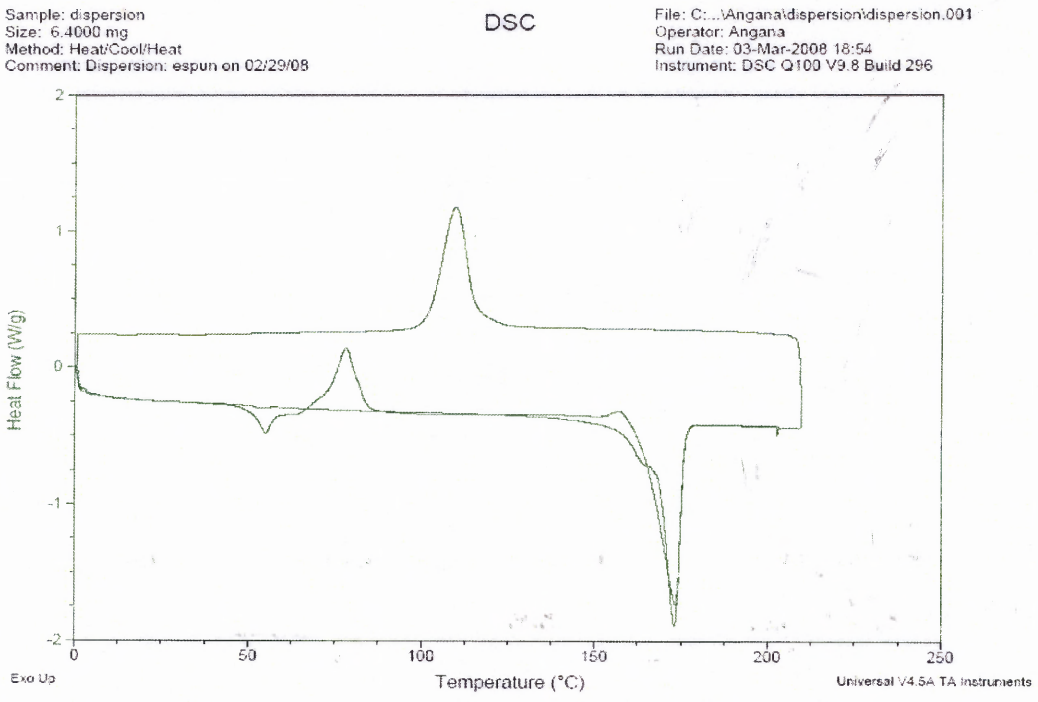

Figure 4.18 DSC thermogram of collagen-PLLA dispersion.

4.2 Morphological Analysis

Blended nanofibers of sizes varying between 100-800nm were obtained by electrospinning the solutions of different compositions like 1%, 5%, 8% by weight of collagen. Also, pure collagen nanofibers and pure PLLA nanofibers were observed to have larger diameters (in the range of 500nm to a micron) than the blended nanofibers as illustrated in Figures F.1 and F.2.

Following on the thought that polymers are immiscible and they would phase separate from a solution during electrospinning, it was important to understand the morphology of these polymer blends and describe the spatial arrangement of collagen and PLLA phases in the filaments. S.Wang [20] leeched out PLLA from the blended electrospun mats to determine the location of collagen in the fibers. Under optical microscope, she observed that the collagen was able to retain the structural integrity of the mat.

In order to gain a better understanding of the morphology of these fibers, in this work, methylene chloride was used to extract the PLLA. This step was followed by overnight vacuum drying and then observation under the SEM. The diameters of the fibers before and after extraction were compared. It was found that the diameters of the extracted mat were at least a 100 to 200 nm lower than that of the unextracted mat. This suggested that the PLLA must be somewhere on the outside of the filament, which when extracted, reduces the diameter of the filament. This process was repeated with different compositions of fibers and the diameters are stated in Appendix G, Tables G.1, G.2 and G.3. The consistency of the results led to the formation of a hypothesis that, the collagen

and PLLA exist in sheath core morphology, where PLLA forms the outer sheath and the collagen forms the core.

The exception to this appears to be the morphology of the 1% nanofiber blend after extraction of PLLA. The long and extended interface of the fibers could no longer be observed under the SEM. The fibers seem to have taken the shape of sharp shard like structures and were about 300-500nm in diameter. This experiment was repeated and the same morphology was observed. Figures 4.2.1 and 4.2.2 are the SEM images of 1% unextracted and extracted mats. Figures 4.2.3 and 4.2.4 are the SEM images of 5% extracted and unextracted mats. Figures 4.2.5 and 4.2.6 are the SEM images of 8% extracted and unextracted mats and Figures 4.2.7 and 4.2.8 are the SEM images of 10% extracted and unextracted mats.

Scanning Electron Microscopy was also performed with Energy Dispersive X-ray Spectroscopy. It confirmed the presence of the element nitrogen in electrospun collagen mats and absence of nitrogen on the surface of the 5% electrospun blend. The details of this analysis are in Appendix H, Tables H.1 and H.2. While the lack of detection of nitrogen in the electrospun blends is consistent with the sheath-core morphology of the nanofibers, the accuracy of the EDS may be questioned because the depth of penetration of the X rays was unknown. In order to further demonstrate the sheath core morphology of the nanofibers, TEM experiments were attempted. The nanofibers used for the TEM analysis were electrospun from a solution composed of 5% by weight of collagen. The TEM copper grids were used as the collecting device during electrospinning. Care was taken such that there were less than ten fibers deposited on each grid. TEM images of the fibers clearly demonstrate the sheath core morphology of the collagen-PLLA nanofibers.

In addition, the images also show the existence of two distinct shades of fibers- a darker shade and a lighter shade. The sheath core morphology is also not uniformly seen in the fibers. Figures 4.27 and 4.28 are the TEM images of the fibers that demonstrate the sheath core morphology.

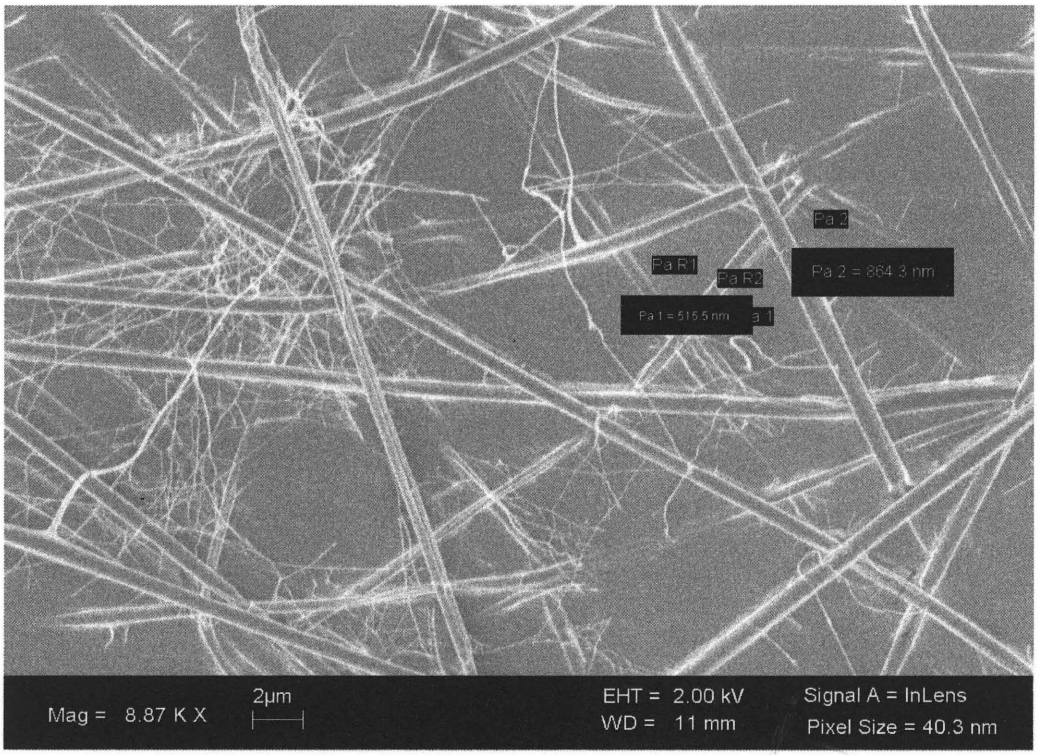

Figure 4.19 SEM image of 1% collagen-PLLA electrospun blend.

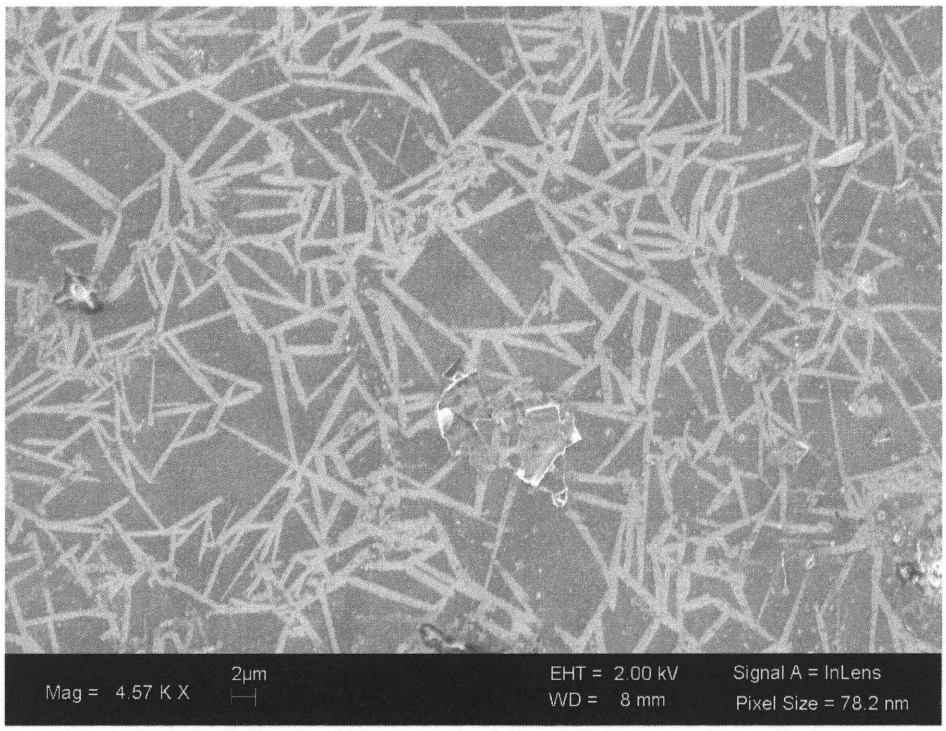

Figure 4.20 SEM image of 1% collagen-PLLA electrospun blend after extraction of PLLA with methylene chloride.

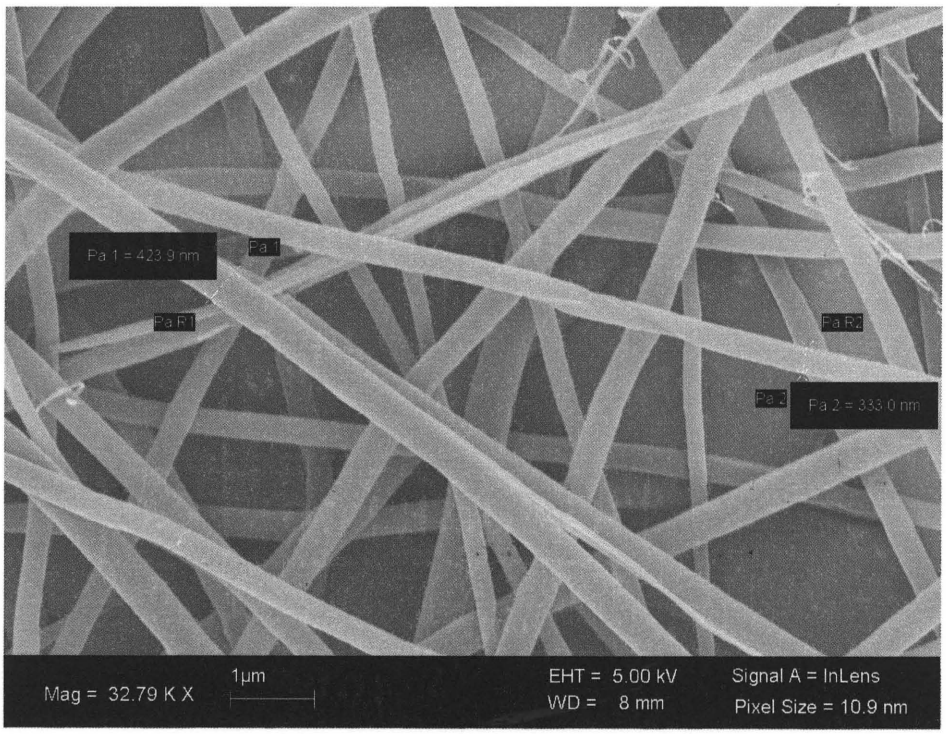

Figure 4.21 SEM image of 5% collagen-PLLA electrospun blend.

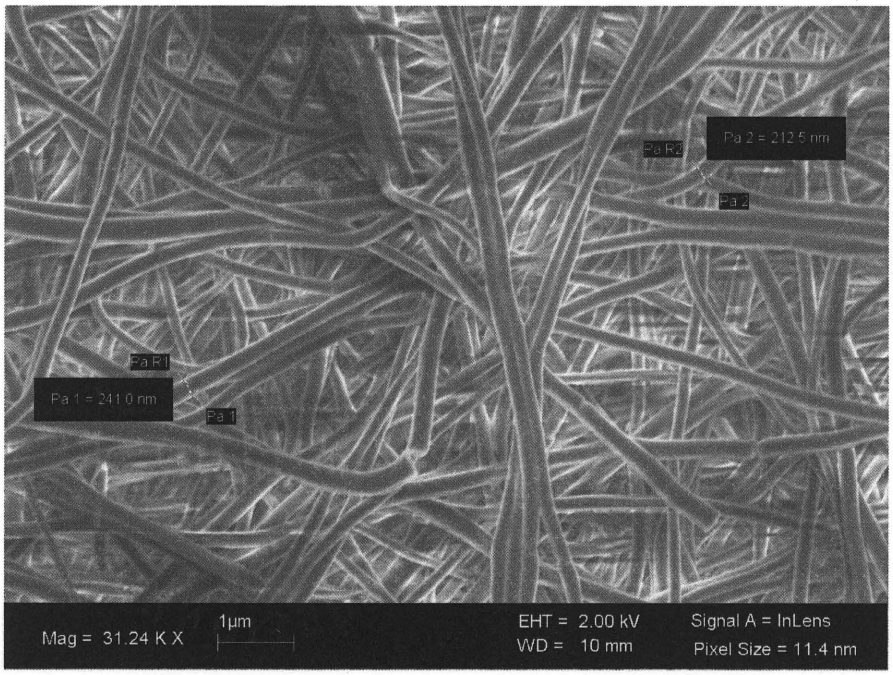

Figure 4.22 SEM image of 5% collagen-PLLA electrospun blend after extraction of PLLA with methylene chloride.

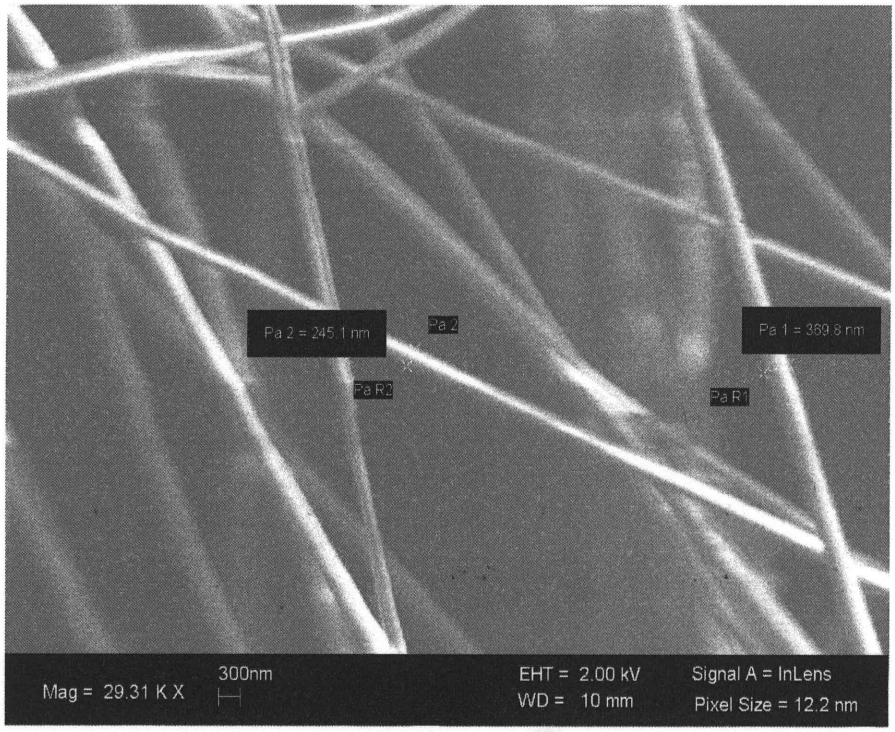

Figure 4.23 SEM image of 8% collagen-PLLA electrospun blend.

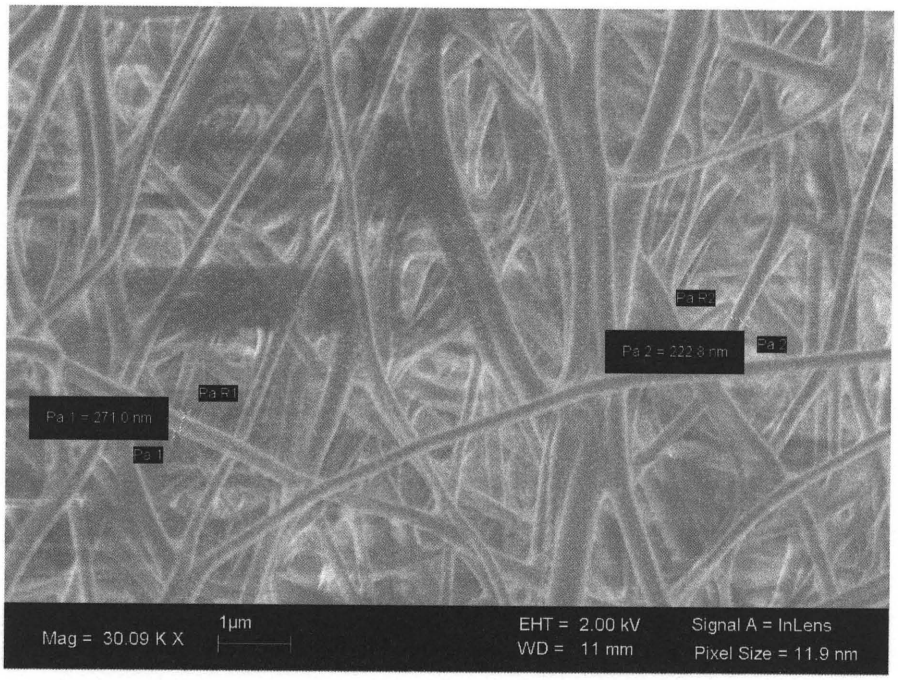

Figure 4.24 SEM image of 8% collagen-PLLA electrospun blend after extraction of PLLA with methylene chloride.

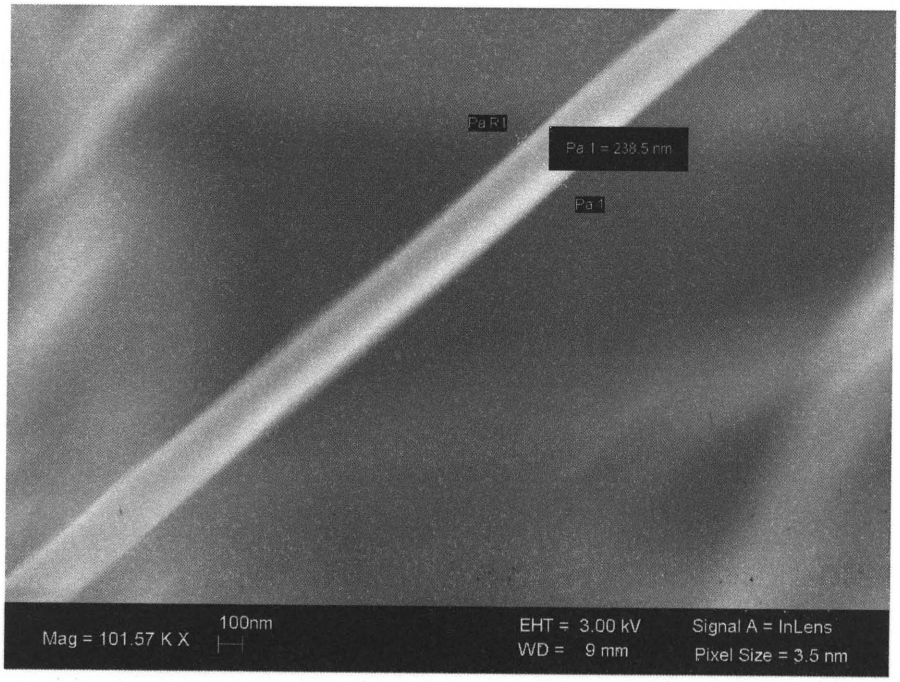

Figure 4.25 SEM image of 10% collagen-PLLA electrospun blend.

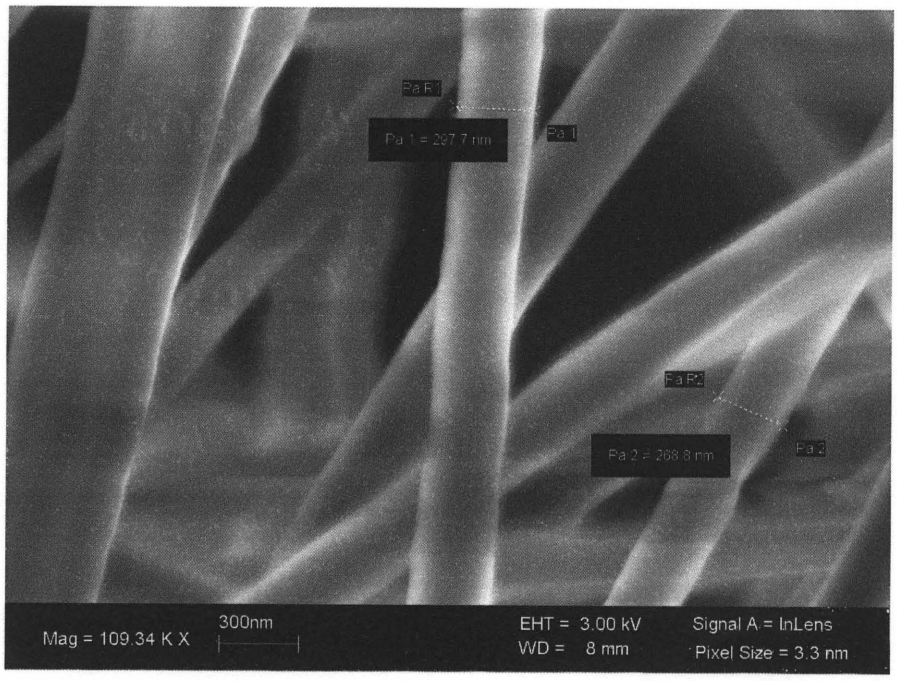

Figure 4.26 SEM image of 10% collagen-PLLA electrospun blend after extraction of PLLA with methylene chloride.

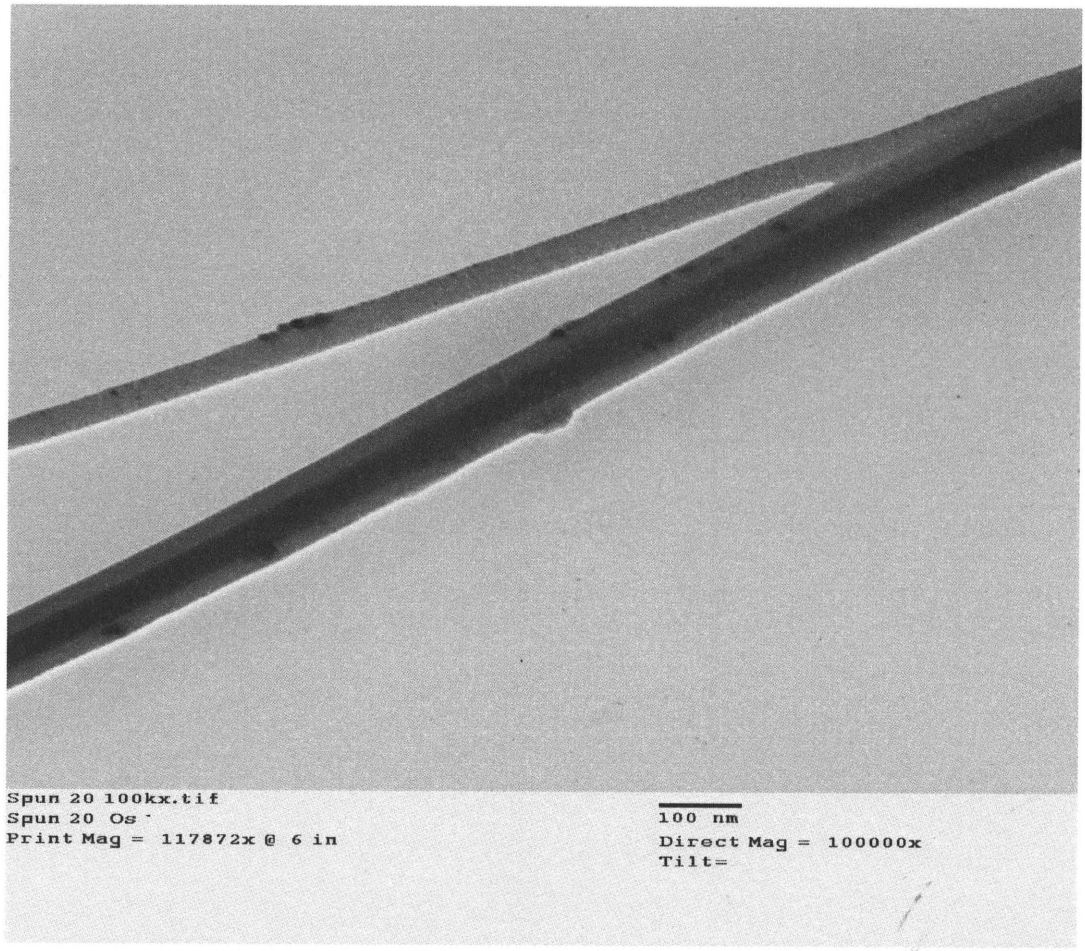

Figure 4.27 TEM image of a 5% electrospun collagen-PLLA nanofiber.

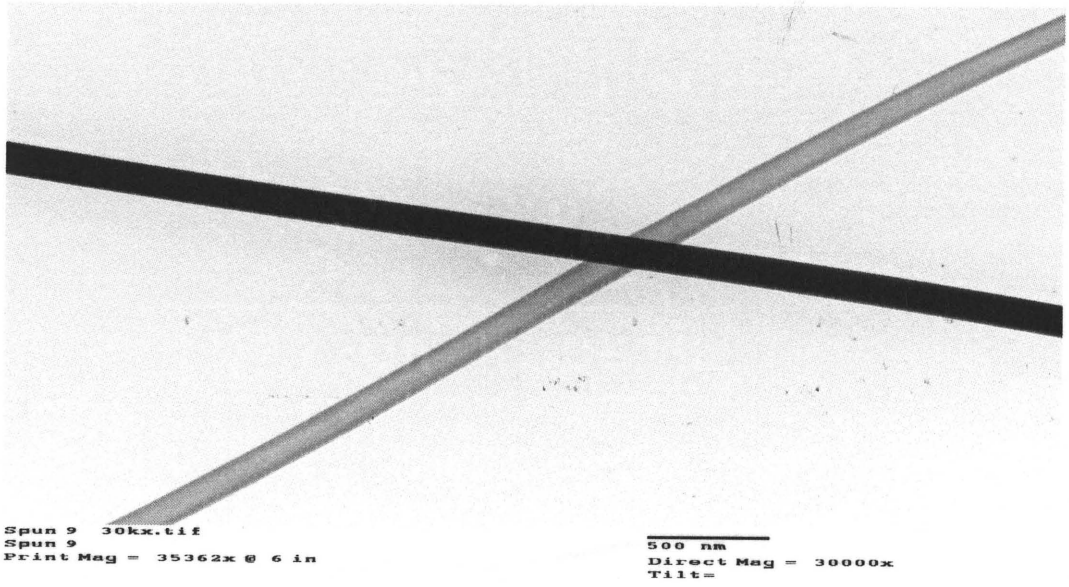

Figure 4.28 TEM image of a 5% electrospun collagen-PLLA nanofiber.

SEM analysis of the mat produced from electrospinning the heterogeneous dispersion was performed. It was prepared by adding collagen in TFA, followed by Methylene chloride and finally addition of PLLA. It was observed that the fibers produced were beaded and were evenly spread through out the mat. The fibers had an average diameter of less than 100-200nm and the beads were of the range of a micron. Such small diameters of fibers led to the hypothesis that the beads were collagen lumps and the fibers were formed of PLLA. In order to demonstrate this, the dispersion was dissolved in methylene chloride and then viewed under the SEM after overnight drying of the mat. The Figures 4.29 and 4.30 illustrates the images of the dispersion, before and after extraction. It was distinctly visible after extraction that, the fibers were no longer present, what remained were only the beads of collagen.

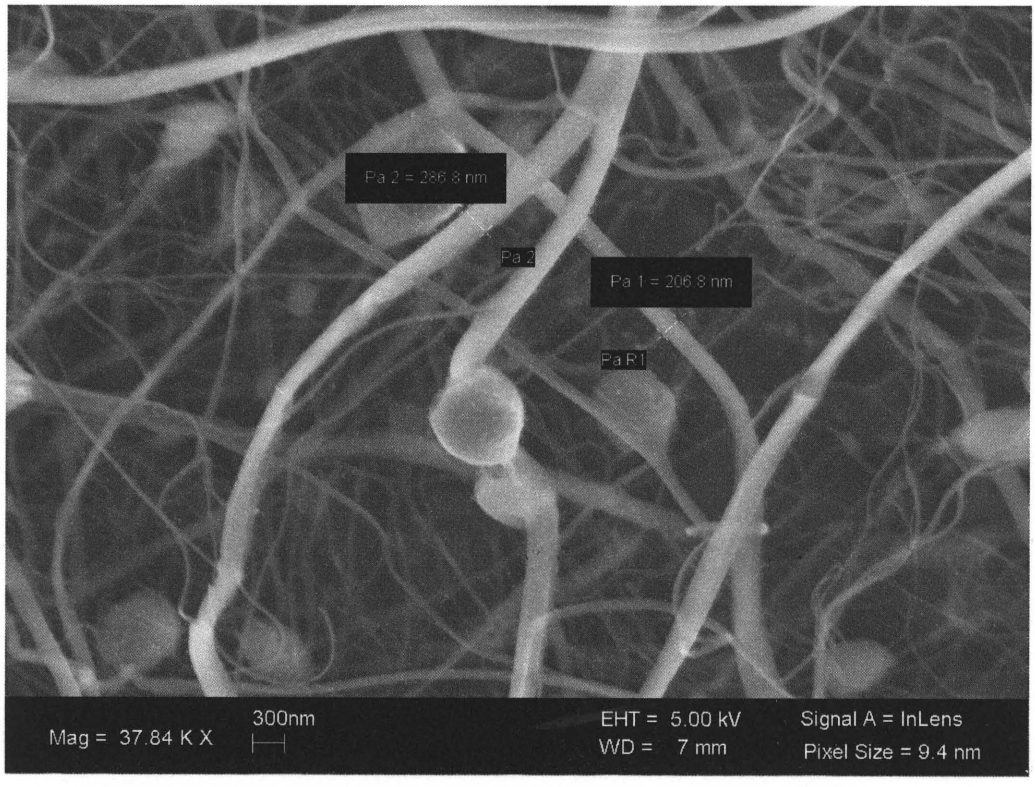

Figure 4.29 SEM image of dispersion mat.

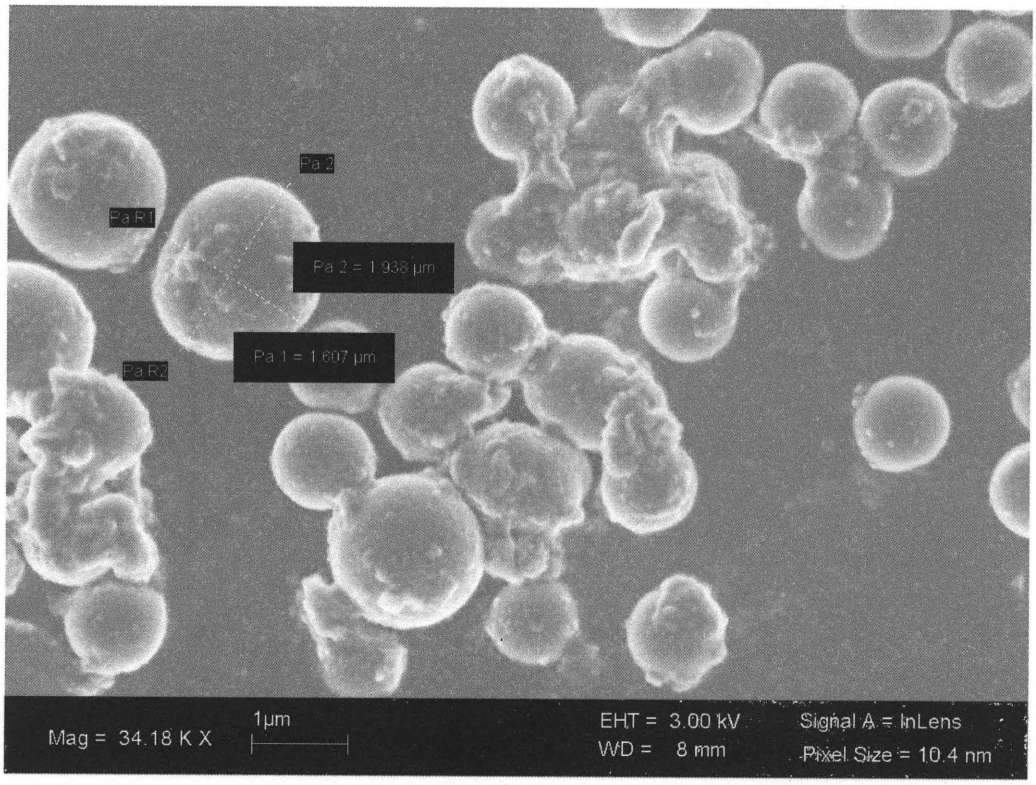

Figure 4.30 SEM image of PLLA extracted dispersion mat.

CHAPTER 5

DISCUSSION

The idea of electrospinning a solution containing a synthetic polymer and a protein has opened new avenues for future biopolymer and synthetic polymer blends. Such blends can be successfully used as scaffolds in tissue engineering applications with the appropriate choice of polymers.

The sharp endothermic peak at the glass transition of PLLA, as observed by S. Wang [20] is a phenomenon that is typically seen to occur only after annealing the polymer for long periods of time below its glass transition temperature. In order to evaluate the occurrence of this phenomena at such a short time scale, in depth analysis of the behavior of PLLA has been carried out. In this research, the thermal behavior of PLLA pellets, PLLA electrospun mats and collagen-PLLA electrospun blends have been examined individually and then compared. Thermal analysis using DSC has been performed on the pellets and the electrospun mats after they were aged at a temperature below the glass transition of PLLA, as well as, after aging them at room temperature for about 45-60 days.

The DSC thermograms of the PLLA pellets before and after aging at 40°C overnight (Figures 4.1 and 4.2), has indicated no evidence of structural relaxation near the glass transition of PLLA. There were hardly any significant changes in the thermal behavior of the aged pellets. The first heat cycle in both the cases (before and after aging) only indicated a melting peak around 170°C. This indicates that the pellets were essentially crystalline. During the cooling cycle of the pellet, a Tg was observed for both

the pellets. Also, the second heat cycle showed a broad cold crystallization (Tc) at about 132°C which is a lot higher than the Tc observed in the case of S.Wang's electrospun 5% collagen-PLLA blend. Also, the Tg for both cases (before and after aging) in the second heat cycle were observed at 59°C. The absence of the structural relaxation demonstrates that there was no apparent densification of the polymer chains taking place in the aged PLLA pellets. But, the structural relaxation peak was observed when the pellets were aged at 40°C overnight after a heat-cool cycle in the DSC (Figure 4.3). During the heat-cool cycle, the pellets were heated to 210°C and then cooled to 0°C. There was no crystallization observed on cooling and thus, the pellets were considered to be in the form of an amorphous film. On performing DSC on the aged heat-cooled pellets, the thermogram clearly indicated the presence of a sharp endothermic peak. This suggests that during the aging process after the heat-cool cycle, the polymer chains attempted to relax to a thermodynamically stable configuration, which is indicated by the presence of the sharper endothermic peak at the Tg of PLLA in the thermogram.

Once the pellets were studied, focus of the research was shifted to the electrospun PLLA mats. PLLA was dissolved in TFA and electrospun to produce PLLA nanofiber mat. The DSC of the electrospun PLLA mat indicated a striking feature when compared to the PLLA pellets. The cold crystallization peak (Figures 4.4 and 4.5) in the electrospun PLLA mats had shifted to a much lower temperature (60°C) than the Tc observed in PLLA pellets (130°C). This gives direction to the thought that there must be some conditions prevailing in electrospinning that facilitates crystallization. During electrospinning, the polymer chains are subjected to very high elongational forces. The ratio of the fluid velocities at the capillary exit and the collection point has been derived

to be 1:27,000 [51]. Thus, such high elongational flow must be facilitating the formation of extended chain structures in PLLA. As a result, the molecules may be already arranged in a way that facilitates crystallization. The illustration in Figure 5.1 A demonstrates the oriented but non-crystalline disposition of the polymer chains due to electrospinning. Figure 5.1B illustrates the ability of chains to crystallize with minimum segmental diffusion. It is also important to note here, that a crystallization peak appeared in the DSC of the electrospun mats during the cooling cycle. The reason for this may be degradation in the molecular weight of PLLA during electrospinning. Degradation experiments have been discussed later in this thesis.

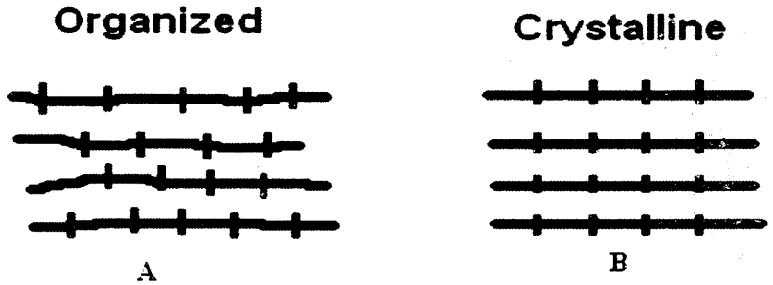

Figure 5.1 Illustrates the polymer chains in an oriented (A) and crystalline (B) state.

The next set of experiments that followed involved comparison of the aged and the non-aged electrospun PLLA mats. The electrospun PLLA mats when aged at 40°C overnight, developed a distinct structural relaxation (Figure 4.5). Unlike the DSC of the aged pellets where no structural relaxation appeared, the appearance of structural relaxation in the electrospun mats indicate that, the electrospun mats possess more amorphous phase than the pellets. In addition, a sharper structural relaxation was observed when the original electrospun mats were aged for 45-60 days at room temperature. This demonstrates the facile tendency of the polymer chains in the

electrospun mats to undergo a relaxation to a lower free energy state with aging. A brief description of the structural relaxation has been provided in the following passage.

Consider that a material has been immobilized at its glass transition (Tg) and it is in a glassy state X at a temperature, T < Tg. Let the thermodynamically stable lowest free energy state of this material be a state A. In such a situation, the material tries to attain the lowest free energy state by approaching the state A. In order to do this, the system absorbs heat and the final enthalpy of the system increases. This transition from the non-equilibrium state X to the thermodynamically more stable state A is called enthalpy recovery. In contrast, on cooling the polymer, when the soft and rubbery state moves to a glassy state, heat is liberated and the final enthalpy of the system decreases. This decrease in enthalpy of the system to reach a lower free energy state is called as enthalpy relaxation. It must be borne in mind that the non-equilibrium state X and the final state A possess two different thermokinetic structures, thus the process X→A is also called structural relaxation. This phenomenon takes place only after annealing the material below its Tg over long periods of time and thus, observation of the structural relaxation in such short time scale definitely suggests the effect of electrospinning. The high speed elongational flow during electrospinning may lead to the formation of an oriented and non-crystalline microstructure which is at non-equilibrium. This oriented non-crystalline microstructure facilitates a rapid densification. Thus, on aging, the polymer segments start to relax to a thermodynamically favorable state indicated by the sharp endothermic peak.

Similar comparison of DSC thermograms of the non-aged and aged electrospun mats have been performed for collagen-PLLA electrospun blends. Different concentrations of collagen-PLLA blended electrospun mats were aged at 40°C overnight (Figures 4.7 to 4.16). Aging of 1%, 3%, 5% and 7% mats at 40°C overnight indicated the appearance of structural relaxation in the DSC. Sharper structural relaxation peaks were obtained when DSC was repeated on the electrospun mats which were aged for 45-60 days at room temperature. In order to evaluate the presence of collagen in the electrospun mats, TGA of the mats were performed. A composition calibration curve was also plotted which clearly indicated the increase in the weight loss of the mats as the concentration of collagen increased. Another interesting aspect was the shift of the cold crystallization peak. Not only did the cold crystallization peak shift to higher temperatures with increase in concentration of collagen but a shift was also noticed on aging the electrospun mats of the same composition. The shift of Tc with the increase in collagen percentage suggests the probable interaction between collagen and PLLA. At this juncture, it is important to understand that, polymers chains which have been extended due to the elongational forces as a result of electrospinning are in a state of non-equilibrium. These chains are able to relax to a lower free energy state by two possible modes of relaxation. They are entropic relaxation and enthalpy or structural relaxation. Entropic relaxation takes place when the polymer chains are less restricted in their motion and they are able to curl up individually, thus taking up a more statistical configuration. Structural or enthalpy relaxation is the type of relaxation in which the entire system of chains moves to a denser state, thus attaining a lower free energy state.

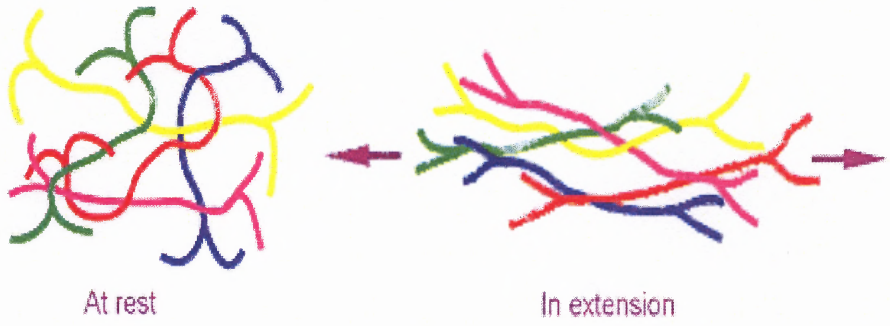

Figure 5.2 Illustrates the polymer chains before and after electrospinning.

As previously mentioned, even though electrospinning aligns the chains in such a way that they facilitate crystallization, it may so happen that, on aging the chains may undergo entropic relaxation and thus, they become misaligned. As a result, it takes more time for the chains to attain a crystalline configuration and thus, the cold crystallization peak rises to a higher temperature.

In order to evaluate whether it is the process of electrospinning that facilitates structural relaxation, DSC of the cast films of 1%, 3%, 5% and 8% were performed. The DSC thermograms of the cast films did not indicate the presence of any structural relaxation peaks (Appendix A in Figures C.1-C.4). Thus, it reinforces the concept that the appearance of the structural relaxation peak at much shorter time scales than usual is the result of the process of electrospinning.

In order to qualitatively understand the effect of a lower molecular weight on the appearance of the structural relaxation peak, the degradation experiments were performed. This was a purely qualitative analysis as the molecular weight was not assessed quantitatively. TFA being a highly corrosive solvent was known to degrade both collagen and PLLA if they were left in solution over a period of time. This could be easily observed as the solution appeared to reduce in viscosity when it was left for more

than a couple of days. Thus, the experiments were framed such that for collagen degradation, collagen was allowed to remain in solution for 4, 10 and 20 hours longer before the addition of PLLA. Similarly, for analyzing the effect of a lower molecular weight of PLLA, PLLA was allowed to remain in solution for 4, 10 and 20 hours longer before the addition of collagen. In a different set of experiments, about 10 microliters of water was added to facilitate hydrolytic degradation. In all the experiments involving degradation of collagen, there appeared no evidence of a distinct structural relaxation peak and thus it can be inferred that the development of the peak is not the result of collagen or PLLA degradation in the solution. However, when PLLA was degraded for 20 hours longer than collagen in solution and 10 microliters of water was added to it, the DSC thermogram showed the presence of a small endothermic peak. But, when the experiment was repeated after degrading PLLA for 40 hours in solution before the addition of collagen, no peak was observed. Thus, no strong evidence for the development of structural relaxation due to the degradation of either PLLA or collagen in the solution could be obtained. Thus, the possibility of a lower molecular weight facilitating structural relaxation may be ruled out.

In order to evaluate electrospinning from a heterogeneous solution with the aim of creating a different morphology, a dispersion of PLLA and collagen was produced. The DSC thermogram of the dispersion indicated a thermal behavior which closely resembled the thermal behavior of electrospun PLLA.

In all the DSC results obtained so far, the structural relaxation peaks on aging the electrospun mats have never appeared as sharp as S.Wang observed in her study. It is of importance to mention that the experiments in this research work have been performed

with the PLLA which was purchased about six years ago. We have to consider that the molecular weight of the PLLA may have reduced over time. It is likely that S.Wang [20] who electrospun the blends about four years back was using a higher molecular weight of PLLA. The change in the molecular weight of the polymer may have an influence on this result. It is important to understand that the presence of entanglements in polymer chains restricts the flexibility in the movement of the chains. Polymers with a higher molecular weight are more probable to contain entanglements rather than polymers with a lower molecular weight where the chains will be shorter with fewer entanglements. It has been found out that the estimated fluid velocities at the capillary exit and at the collection point are in the ratio of 1:27,000 [51]. This suggests that even before the whipping phenomenon occurs, the molecular orientation processes will be dominated by elongational forces. Figure 5.2 illustrates the polymer chains before and after electrospinning. The reason for the appearance of a sharper structural relaxation at higher molecular weight has been illustrated in Figure 5.3.

In general, polymers with higher molecular weight contain entanglements due to the overlapping between their chains. Due to the greater number of entanglements, the chains become more restricted in their motion. As a consequence of the elongational forces experienced by the polymer electrospinning, the polymer chains are in a state of non equilibrium and they possess an aligned and oriented microstructure. On aging, these chains are able to undergo relaxation to a thermodynamically stable state. The constrained motion in the polymer chains favors enthalpy relaxation rather than entropic relaxation. Thus it is likely that a much sharper enthalpy recovery peak could be observed for the high molecular weight than in the case of low molecular weight polymers.

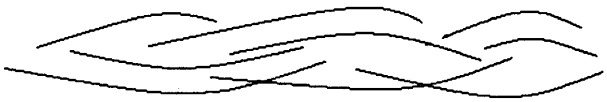

Polymers with low molecular weights will possess fewer entanglements in their chains. Due to the presence of a smaller number of entanglements or absence of entanglements, the chains are not restricted in motion. The process of electrospinning helps to align and orient the polymer chains as explained previously. On aging, these chains undergo relaxation by the process of entropic relaxation when the chains curl up and move to a more relaxed and stable thermodynamic state. Thus, the enthalpy recovery peak is less distinct and it becomes more prominent only after it is allowed to age for a significantly long time.

Figure 5.3 Illustrates the effect of higher and lower molecular weight between entanglements.

The morphological analysis of the collagen-PLLA nanofibers showed the formation of fibers in the diameter range of 100nm to a few microns. It was also noted that only PLLA or only collagen nanofibers had larger diameters than the collagen-PLLA blends. During the initial SEM analysis, it was very difficult to establish any morphological differences between collagen nanofibers, PLLA nanofibers and collagen-PLLA blended nanofibers. All of them appeared very similar and had smooth surfaces. There was no distinct phase separation observed in the blends. This was quite unusual as the theory related to the thermodynamics of polymer blends mention that polymers are immiscible in the solid state. Flory Huggins lattice theory states that the Flory Huggins binary interaction parameter has to be negative in order to form a single phase. In this research, methylene chloride is known to dissolve PLLA and it has no effect on collagen. Thus, there would be no possibility of collagen and PLLA forming a single phase.

Bearing the theories in mind, the experiments involving extraction of PLLA by methylene chloride were attempted to analyze the phase separation. SEM analysis indicated reduction in diameter of the fibers as compared to the unextracted mats as indicated in Appendix G, Tables G.1, G.2 and G.3. This was the first step in the hypothesis of the sheath core morphology. This clearly indicated that there was something on the outer side of the fiber which, when removed, brought about a reduction in the diameter of the filaments. Since methylene chloride dissolves PLLA only and has no effect on collagen, PLLA was thought to be on the outside. This finding led to the other experiments involving EDS and TEM. PLLA being an aliphatic polyester would not contain the element nitrogen and collagen on the other hand, being a protein would contain nitrogen. Thus, the goal was to evaluate if nitrogen was present on the surface of

the electrospun blends or not. The results of the EDS on collagen-PLLA blends did not indicate the presence of nitrogen whereas the collagen mats confirmed the presence of nitrogen. Thus, the concept was reinforced that collagen may not be located on the outside of the fiber. Finally, in order to look through each individual filament, TEM experiments were performed with the collagen-PLLA nanofibers. The TEM image (Figure 4.2.9) clearly demonstrated the presence of two separate phases. It showed that one component was ensheathed in the other. According to the previous results obtained from the PLLA extraction experiments, it could be confirmed that the outer sheath must be PLLA and the inner core is composed of collagen. As a consequence of this type of morphology, there was reduction in the diameter of the blended nanofibers when PLLA was extracted with methylene chloride. A schematic representation of the sheath core morphology is shown in Figure 5.4 (A).

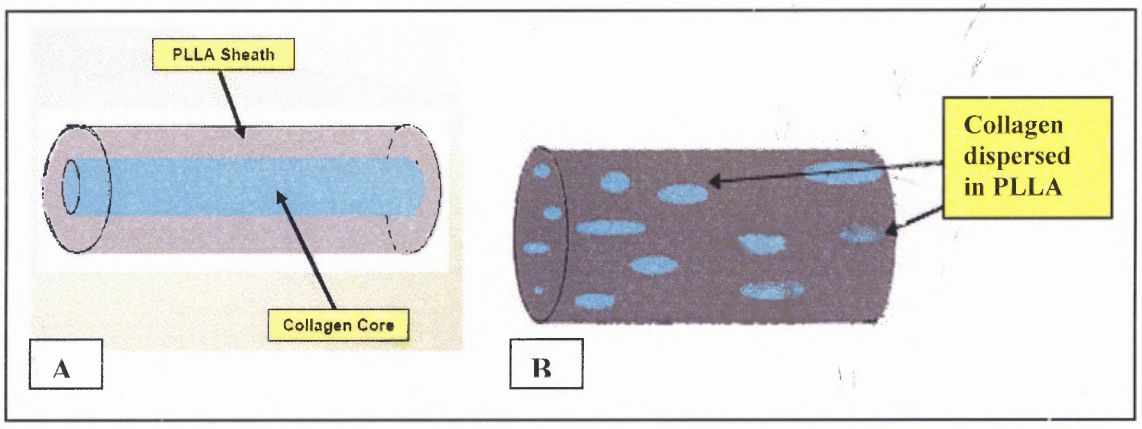

Figure 5.4 Illustration of morphology of collagen-PLLA nanofiber blends.

It is also of importance to note that during the TEM study, all fibers did not reveal the same type of morphology. Thus, it cannot be certainly said that all fibers are in this form. In addition, the TEM images (Figures 4.2.9 and 4.2.10) showed the presence of three types of morphological features in the fibers. One was the sheath-core type; another

had a darker shade while the third category of fibers demonstrated a much lighter shade. So, it may be such that some were only PLLA fibers or only collagen fibers and the others were the blended fibers that demonstrated the sheath core morphology. It is of significance to understand that the TEM analysis required the presence of only a few fibers on each grid. Thus, the solution was electrospun each time for the first ten seconds only. As this is a very short time, the flow may not have been stabilized to give rise to fibers with uniform morphology.

The reason for the formation of sheath-core morphology may be related to the differences in solubility of the two components in the solvent. While making solutions, it was noted that collagen takes slightly a longer time to get completely dissolved in TFA than PLLA. Following on the same thought, the least soluble component is expected to come out first. Thus, collagen comes out first forming the core of the structure and PLLA comes out soon after, enveloping the collagen core, forming the outer sheath of the fiber. The other possibility is the existence of another type of phase separation called spinodal decomposition. This type of decomposition is known to take place in rapid processes and a mixture of two or more materials separate into two distinct regions with different material concentrations. It may so happen that, the rapid elongational flow during electrospinning leads to the formation of linearized co-continuous spinodal decomposition.

Another interesting feature appeared at low concentrations of collagen in the PLLA-collagen blend. In stead of the sheath-core morphology, the fibers showed domains that when extracted appeared to be extended and fibrullar, shard like structures.

This behavior demonstrates the change in morphology with concentration of collagen in the blend. Such dispersed phase morphology has been demonstrated in Figure 5.4 (B).

Electrospinning of a heterogeneous dispersion of collagen-PLLA nanofibers led to the formation of collagen beads in the PLLA filaments. The size of the PLLA filaments is in the range of 100nm. On extraction of the PLLA by using methylene chloride, only collagen beads could be obtained. Hence, this is a process for obtaining collagen beads which may have potent applications in the tissue engineering industry. Previously, research has been performed by other scientists to produce bead shaped articles by using biopolymers which have been used as bead foods and as supports for immobilizing physiologically active substances.

CHAPTER 6

CONCLUSION

On the basis of the experiments performed and analysis of the results obtained, the following conclusions have been reached.

- It has been demonstrated that electrospinning leads to the formation of an oriented and organized microstructure of the chains but not a crystalline arrangement. This suggests as general phenomena that on electrospinning a polymer with sufficiently high molecular weight, the microstructure of the resulting nanofiber will contain highly aligned chains. As a consequence of this, amorphous polymers are likely to show structural relaxation and high molecular weight crystallizable polymers would be subject to an extended chain crystals configuration. This is likely to be true for all polymer experiments and operative in all electrospun polymer fibers.
- The thermal analysis of the electrospun collagen-PLLA nanofiber blends have resulted in the unusual appearance of an endothermic peak which signifies the occurrence of structural relaxation in the polymer chains. It is speculated that the occurrence of this thermal event is more prominent in PLLA with higher molecular weight due to the presence of entanglements. It is more favorable for polymers with higher molecular weights to undergo structural or enthalpy relaxation than entropic relaxation.
- Electrospinning of collagen-PLLA blends have resulted in the formation of nanofibers which possess sheath core morphology directly observed by using

TEM for a 5% by weight of collagen mat. PLLA extraction experiments, EDS results and SEM images reinforce the concept of PLLA forming the outer sheath of the filament and collagen forming the inner core. This is true for collagen concentrations up to 8%.

- It has also been demonstrated that, at lower concentrations of collagen, the filaments no longer possess an extended interface and they become shard like structures which suggests that collagen filamentous domain remain dispersed in PLLA.
- Electrospinning a heterogeneous dispersion of collagen-PLLA blends have resulted in the formation of distinct collagen beads on 100nm PLLA extended interface fibers. This opens a new avenue to create collagen beads in the size range of microns by extracting the PLLA.

CHAPTER 7

FUTURE WORK

The results of this research suggest several other areas for further investigation.

- Similar research should be performed on high molecular weight PLLA, followed by thermal analysis using DSC to be able to confirm the possibility of a sharper structural relaxation.
- A more detailed imaging analysis of the sheath-core morphology of the nanofibers is required to be performed in order to analyze the appearance of this type of morphology at the higher concentrations of collagen (above 8% by weight of collagen) in the collagen-PLLA blend.
- The possibility of obtaining hollow PLLA fibers by dissolving the collagen that forms the core of the nanofiber blends should be explored.
- Morphological analysis of the cast films produced from the blends should be carried out in order to understand the structural differences between the films and electrospun mats.
- More research should be carried out to understand the mechanism of sheath-core structures in order to facilitate the application of such structures in other polymer blends that can be used in biomaterial applications.
- Further work should be done on the production of collagen beads which may be useful as supports for immobilizing physiologically active substances.

APPENDIX A

DSC THERMOGRAMS

DSC thermograms of non-electrospun and electrospun collagen, 5% and 10% by weight of collagen-PLLA.

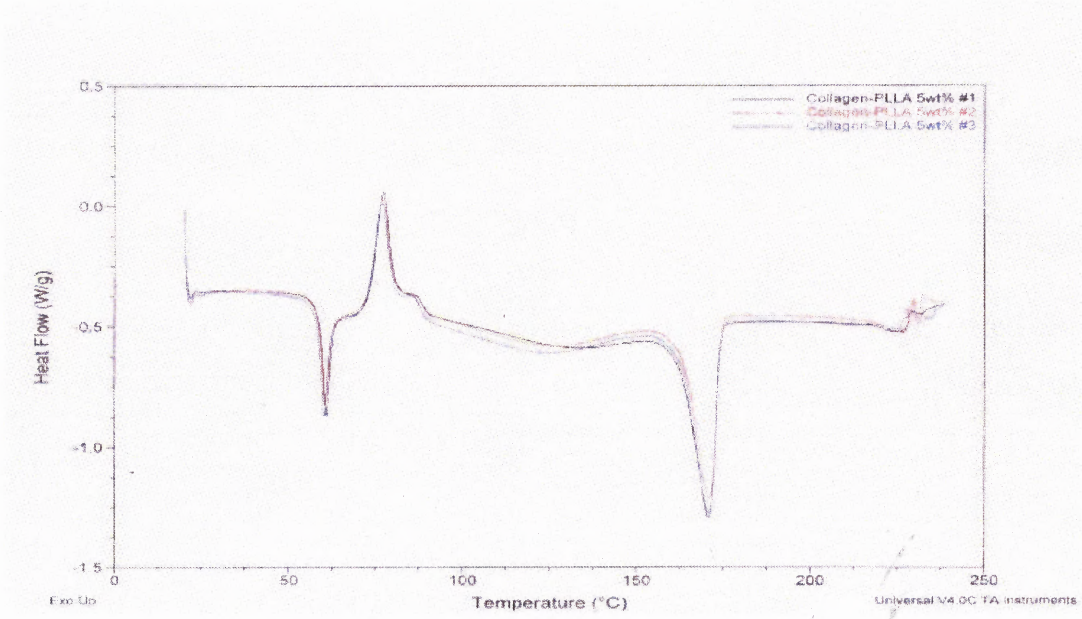

Figure A.1 DSC of 5% Collagen-PLLA Electrospun Mats [20].

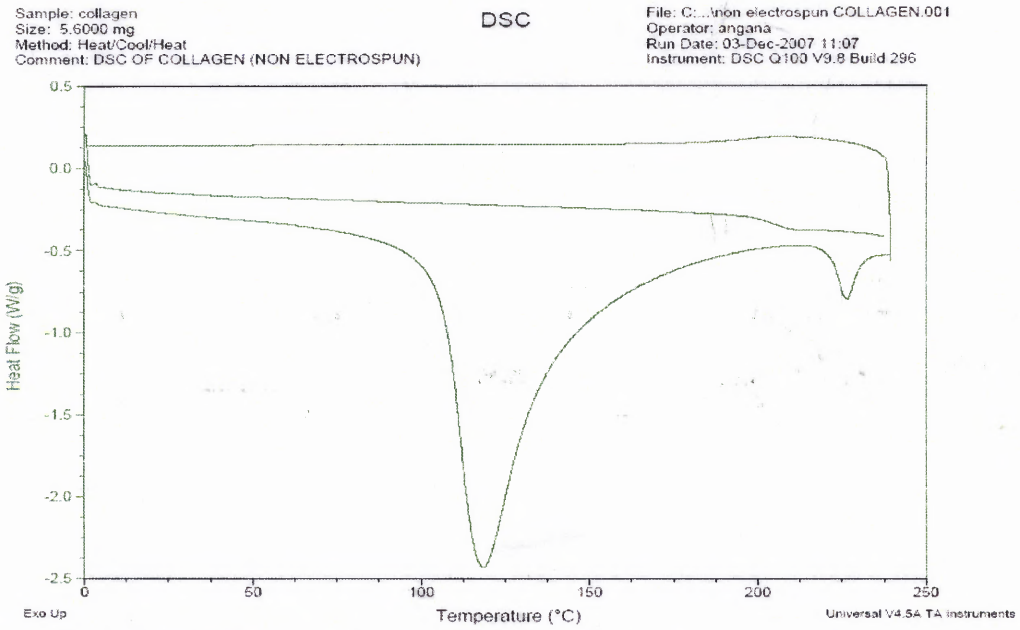

Figure A.2 DSC Thermogram of Non-electrospun Collagen.

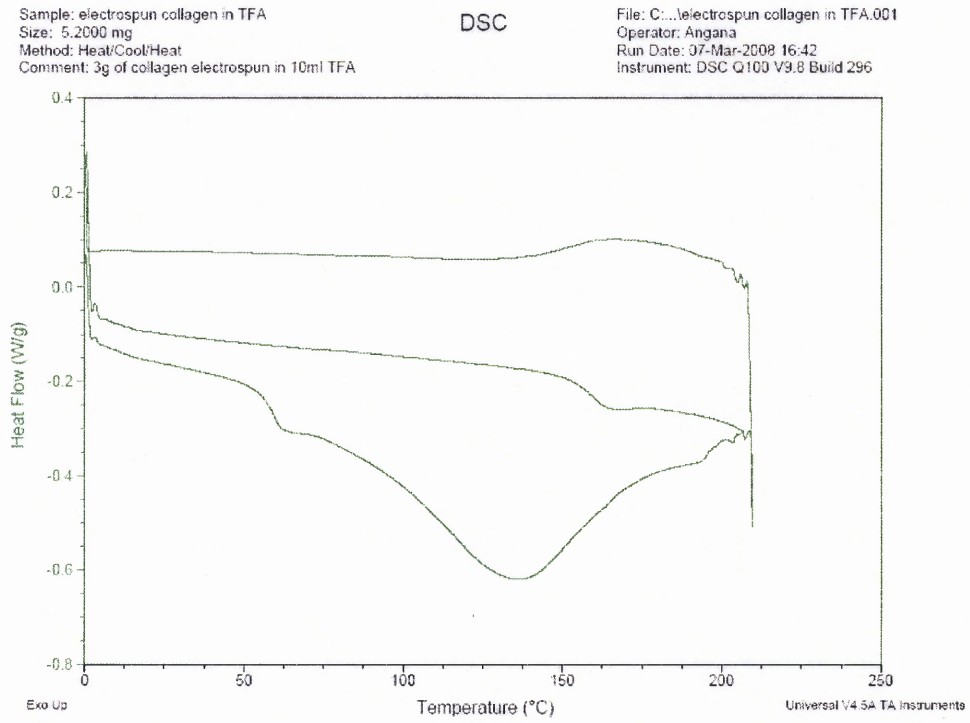

Figure A.3 DSC Thermogram of Electrospun Collagen in TFA.

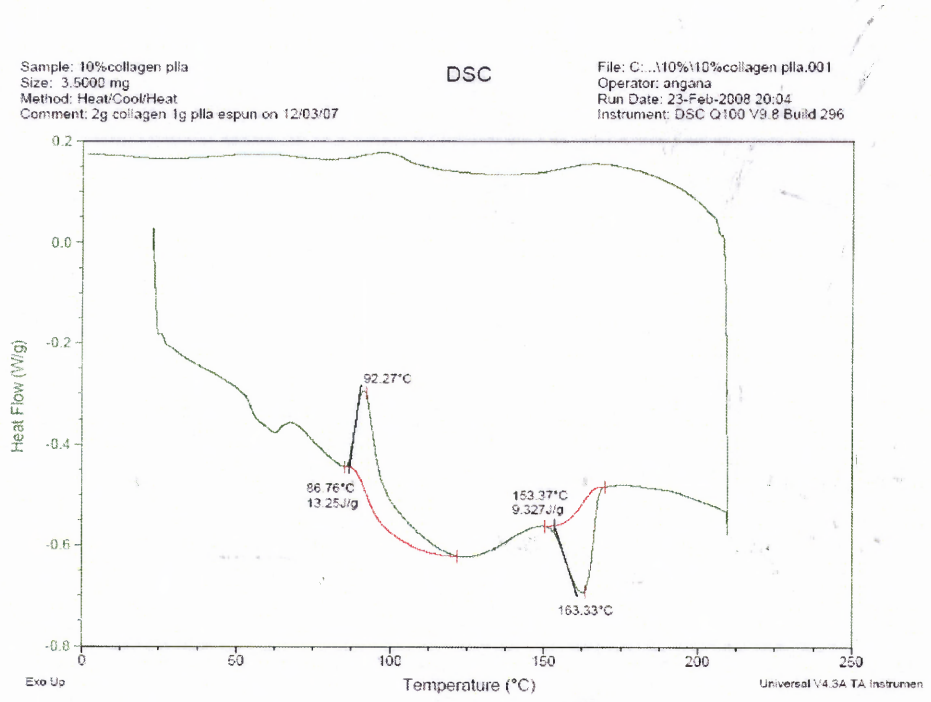

Figure A.4 DSC Thermogram of First Heat Cycle of Electrospun 10% Collagen-PLLA Mat.

APPENDIX B

MAGNITUDES OF THE PEAKS IN THE DSC THERMOGRAMS

The position and magnitude of the cold crystallization peak as well as melting peak, position of the glass transition, position of structural relaxation peak for PLLA pellets, aged PLLA pellets, aged PLLA pellets after a heat-cool cycle, electrospun PLLA and aged electrospun PLLA are mentioned in Tables B.1 to B.6. The position and magnitude of the cold crystallization peak as well as melting peak, position of the glass transition, position of structural relaxation peak for 1%, 3%, 5%, 7%, and 8% collagen-PLLA electrospun mats, aged blended mats are mentioned in Tables B.7- to B.18. Tables B.7 to B.12 are the details for blended electrospun mats, Tables B.12-B.18 are for aged blended electrospun mats

Table B.1 Position of Cold Crystallization Peak.

Composition	Peak position (1^{st} Heat Cycle) (°C)	Peak Position (2^{nd} Heat Cycle) (°C)
PLLA pellets	N/A	131
Aged PLLA pellets	N/A	132
PLLA pellets aged after heat-cool cycle	130	131
Electrospun PLLA (3g of PLLA in 10ml of TFA)	81	98
Aged electrospun PLLA	80	N/A

Table B.2 Cold Crystallization Magnitude.

Composition	Peak in 1st Heat Cycle (°C)	Peak in 2nd Heat Cycle (J/g)
PLLA pellets	N/A	28
Aged PLLA pellets	N/A	33
PLLA pellets aged after heat-cool cycle	27	31
Electrospun PLLA (3g of PLLA in 10ml of TFA)	21	7
Aged electrospun PLLA	20	N/A

Table B.3 Position of Enthalpy Recovery Peak.

Composition	Peak position (1st Heat Cycle) (°C)	Peak Position (2nd Heat Cycle) (°C)
PLLA pellets	N/A	N/A
Aged PLLA pellets	N/A	N/A
PLLA pellets aged after heat-cool cycle	63	N/A
Electrospun PLLA (3g of PLLA in 10ml of TFA)	51	N/A
Aged electrospun PLLA	61	N/A

Table B.4 Position of Glass Transition.

Composition	Peak position (1^{st} Heat Cycle) (°C)	Peak Position (2^{nd} Heat Cycle) (°C)
PLLA pellets	N/A	59
Aged PLLA pellets	N/A	59
PLLA pellets aged after heat-cool cycle	60	61
Electrospun PLLA (3g of PLLA in 10ml of TFA)	50	N/A
Aged electrospun PLLA	57	N/A

Table B.5 Position of Melting Peak.

Composition	Peak position (1^{st} Heat Cycle) (°C)	Peak Position (2^{nd} Heat Cycle) (°C)
PLLA pellets	190	178
Aged PLLA pellets	190	170
PLLA pellets aged after heat-cool cycle	177	170
Electrospun PLLA (3g of PLLA in 10ml of TFA)	171	173
Aged electrospun PLLA	175	175

Table B.6 Melting Peak Magnitude.

Composition (% in solution, solid ratio)	Peak in 1st Heat Cycle (J/g)	Peak in 2nd Heat Cycle (J/g)
PLLA pellets	71	40
Aged PLLA pellets	79	40
PLLA pellets aged after heat-cool cycle	43	43
Electrospun PLLA (3g of PLLA in 10ml of TFA)	65	57
Aged electrospun PLLA	62	51

Table B.7 Position of Cold Crystallization Peak.

Composition (% collagen in TFA, % collagen in total solids)	Peak position (1st Heat Cycle)	Peak Position (2nd Heat Cycle)
(1,7)	80	N/A
(3,20)	85	N/A
(5,33)	88	N/A
(7,43)	84	82
(8,50)	89	89 (2 peaks)

Table B.8 Cold Crystallization Magnitude.

Composition (% in solution, solid ratio)	Peak in 1st Heat Cycle (J/g)	Peak in 2nd Heat Cycle (J/g)
(1,7)	13.7	N/A
(3,20)	15.5	N/A
(5,33)	17.8	N/A
(7,43)	10	4.3
(8,50)	8	5.5

Table B.9 Position of Enthalpy Recovery Peak.

Composition (% in solution, solid ratio)	Peak position (1st Heat Cycle)	Peak Position (2nd Heat Cycle)
(1,7)	N/A	N/A
(3,20)	N/A	N/A
(5,33)	51	N/A
(7,43)	46	N/A
(8,50)	48	N/A

Table B.10 Position of Glass Transition.

Composition (% in solution, solid ratio)	Peak position (1^{st} Heat Cycle)	Peak Position (2^{nd} Heat Cycle)
(1,7)	50	N/A
(3,20)	N/A	N/A
(5,33)	50	N/A
(7,43)	48	N/A
(8,50)	47	N/A

Table B.11 Position of Melting Peak.

Composition (% in solution, solid ratio)	Peak position (1^{st} Heat Cycle)	Peak Position (2^{nd} Heat Cycle)
(1,7)	174	175
(3,20)	172	175
(5,33)	169	170
(7,43)	162	156
(8,50)	162	160

Table B.12 Melting Peak Magnitude.

Composition (% in solution, solid ratio)	Peak in 1st Heat Cycle (J/g)	Peak in 2nd Heat Cycle (J/g)
(1,7)	62	55
(3,20)	49	37
(5,33)	37	39
(7,43)	29.5	22
(8,50)	22	21

Table B.13 Position of Cold Crystallization Peak.

Composition (% collagen in TFA, % collagen in total solids)	Peak position (1st Heat Cycle)	Peak Position (2nd Heat Cycle)
(1,7)	85	N/A
(3,20)	91	N/A
(5,33)	89	N/A
(7,43)	98	89
(8,50)	102	81

Table B.14 Cold Crystallization Magnitude.

Composition (% in solution, solid ratio)	Peak in 1st Heat Cycle (J/g)	Peak in 2nd Heat Cycle (J/g)
(1,7)	13.32	N/A
(3,20)	13	N/A
(5,33)	18	N/A
(7,43)	12	2.5
(8,50)	8	6

Table B.15 Position of Enthalpy Recovery Peak.

Composition (% in solution, solid ratio)	Peak position (1st Heat Cycle) (°C)	Peak Position (2nd Heat Cycle) (°C)
(1,7)	61	N/A
(3,20)	62	N/A
(5,33)	62.7	N/A
(7,43)	54	N/A
(8,50)	N/A	N/A

Table B.16 Position of Glass Transition.

Composition (% in solution, solid ratio)	Peak position (1^{st} Heat Cycle) (°C)	Peak Position (2^{nd} Heat Cycle) (°C)
(1,7)	56	N/A
(3,20)	57	N/A
(5,33)	59	N/A
(7,43)	54	N/A
(8,50)	55	N/A

Table B.17 Position of Melting Peak.

Composition (% in solution, solid ratio)	Peak position (1^{st} Heat Cycle) (°C)	Peak Position (2^{nd} Heat Cycle) (°C)
(1,7)	176	176
(3,20)	173	175
(5,33)	169	170
(7,43)	166	165
(8,50)	164	161

Table B.18 Melting Peak Magnitude.

Composition (% in solution, solid ratio)	Peak in 1st Heat Cycle (J/g)	Peak in 2nd Heat Cycle (J/g)
(1,7)	59	53
(3,20)	45	36
(5,33)	40	43
(7,43)	30	32
(8,50)	24	29

APPENDIX C

DSC THERMOGRAMS OF CAST FILMS AND DEGRADATION EXPERIMENTS

Figures C.1-C.4 illustrates the DSC thermograms for cast films with compositions of 1%, 3%, 5% and 8% by weight of collagen. Figures C.5-C.9 illustrates the DSC thermograms for time based degradation of 5% electrospun blend of collagen-PLLA mat at the 10^{th}, 14^{th}, 18^{th}, 34^{th} and 54^{th} hour in solution.

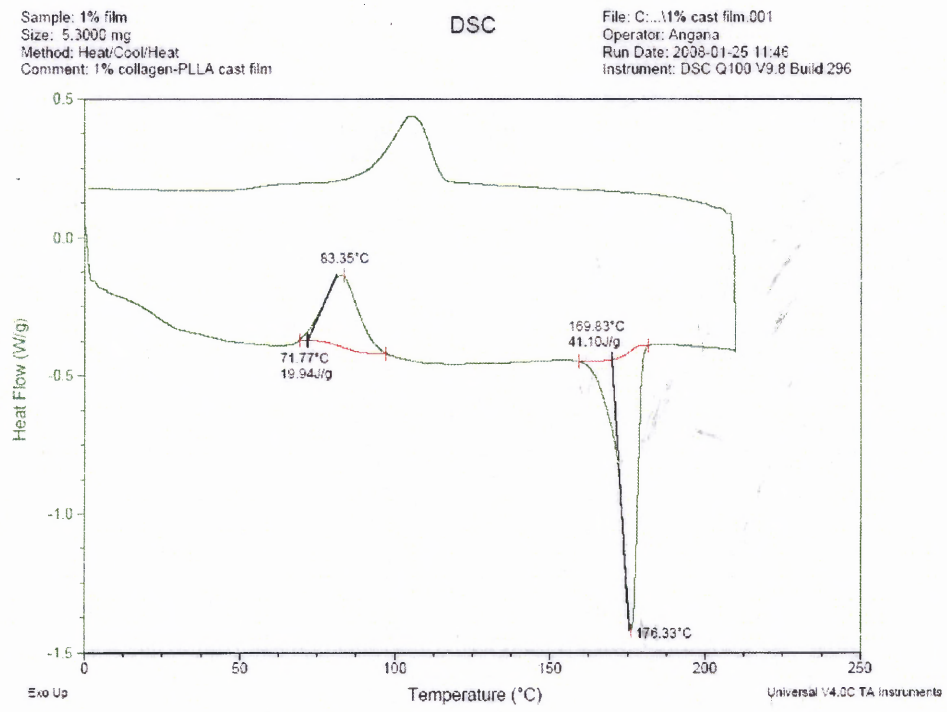

Figure C.1 DSC of First Heat Cycle of 1% Collagen-PLLA Cast Film.

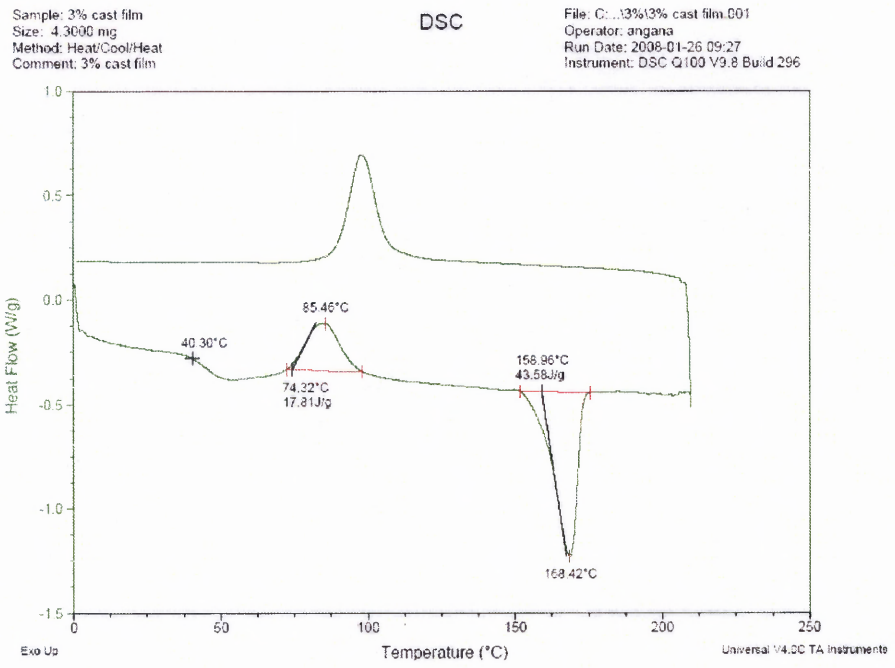

Figure C.2 DSC of First Heat Cycle of 3% Collagen-PLLA Cast Film.

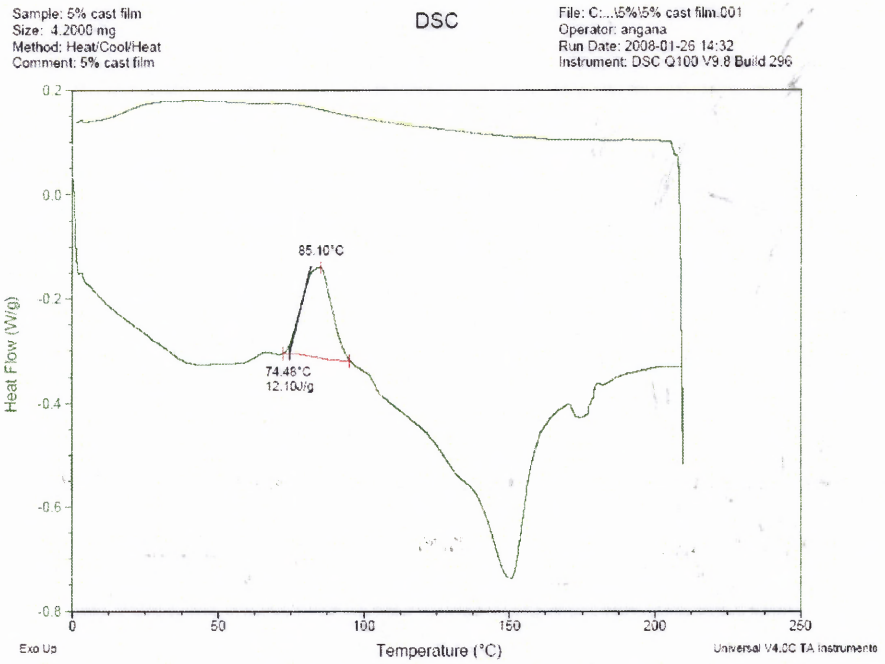

Figure C.3 DSC of First Heat Cycle of 5% Collagen-PLLA Cast Film.

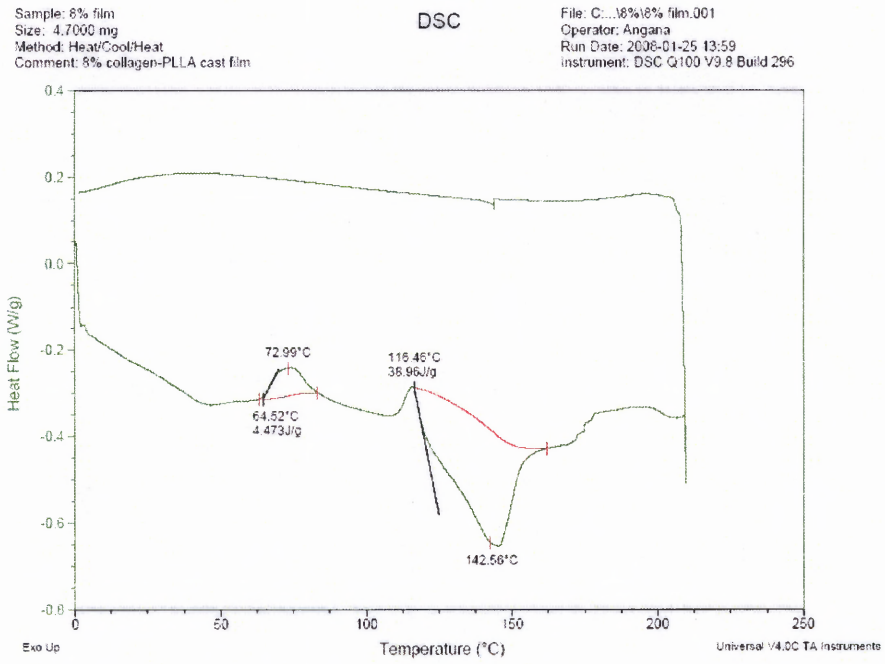

Figure C.4 DSC of First Heat Cycle of 8% Collagen-PLLA Cast Film.

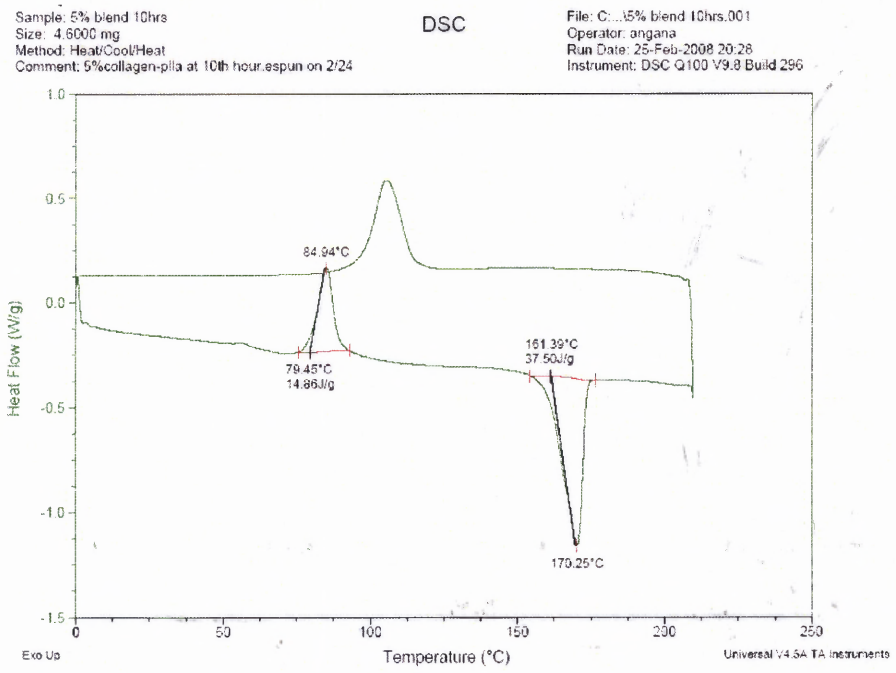

Figure C.5 DSC of First Heat Cycle of 5% Electrospun Blend After 10 Hours in Solution.

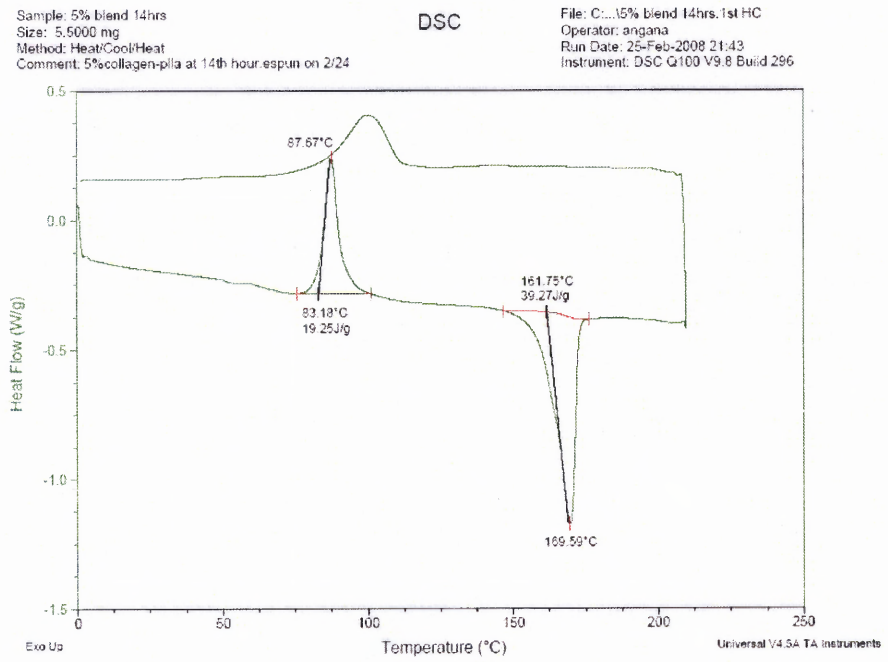

Figure C.6 DSC of First Heat Cycle of 5% Electrospun Blend After 14 Hours in Solution.

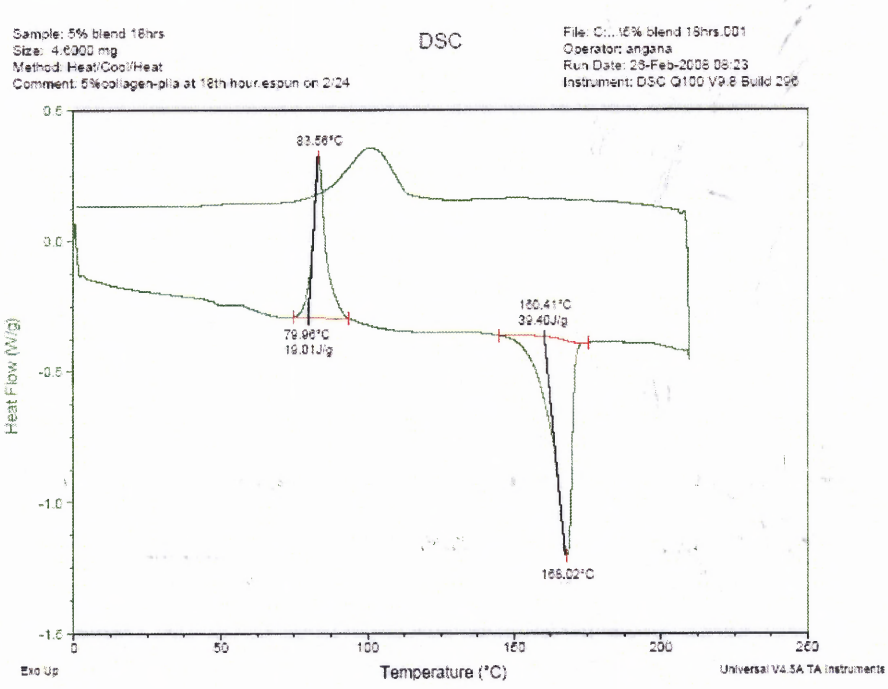

Figure C.7 DSC of First Heat Cycle of 5% Electrospun Blend After 18 Hours in Solution.

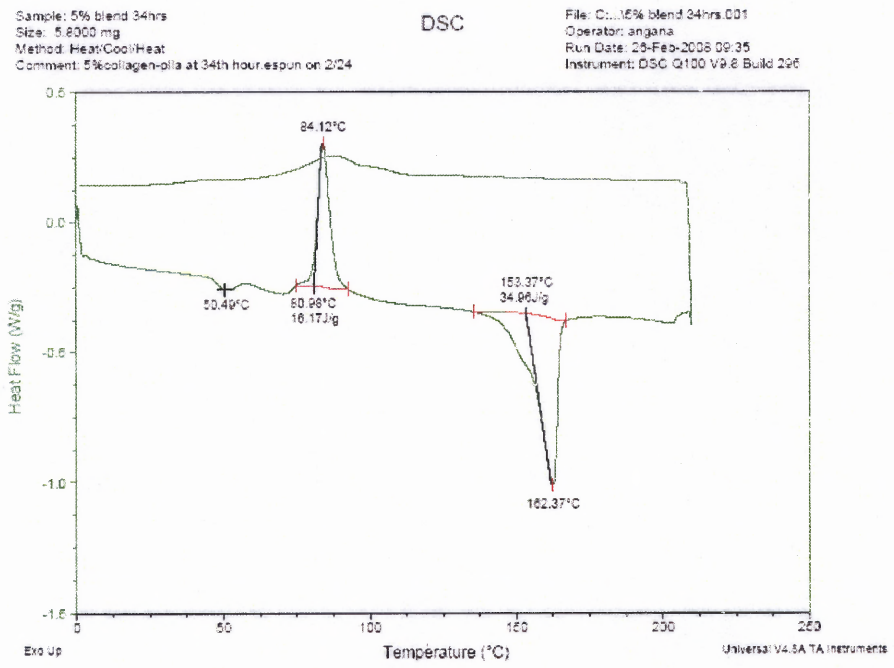

Figure C.8 DSC of First Heat Cycle of 5% Electrospun Blend After 34 Hours in Solution.

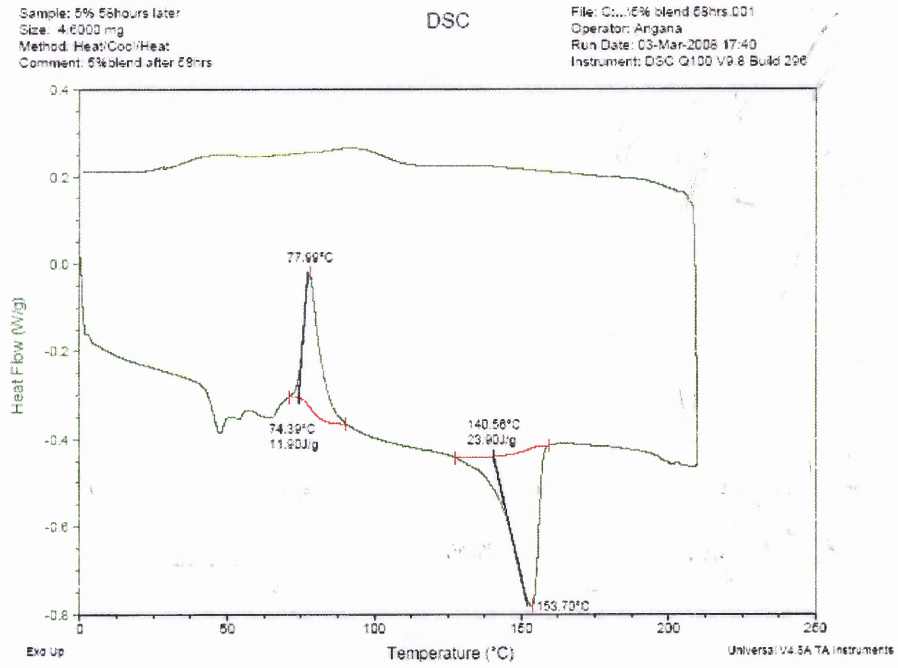

Figure C.9 DSC of First Heat Cycle of 5% Electrospun Blend After 54 Hours in Solution.

APPENDIX D

DSC THERMOGRAMS FOR PLLA AND COLLAGEN DEGRADATION EXPERIMENTS

Figures D.1 –D.6 illustrates DSC thermograms of electrospun mats when PLLA was added 4, 10 and 20 hours after the addition of collagen and also addition of water to the TFA. Figures D.7-D.13 illustrates DSC thermograms of electrospun mats when collagen was added 4, 10 and 20 hours after the addition of PLLA and also addition of water to the TFA. Figures D.14-D.17 illustrates the DSC thermograms performed on the electrospun mats, 45 to 60 days after electrospinning.

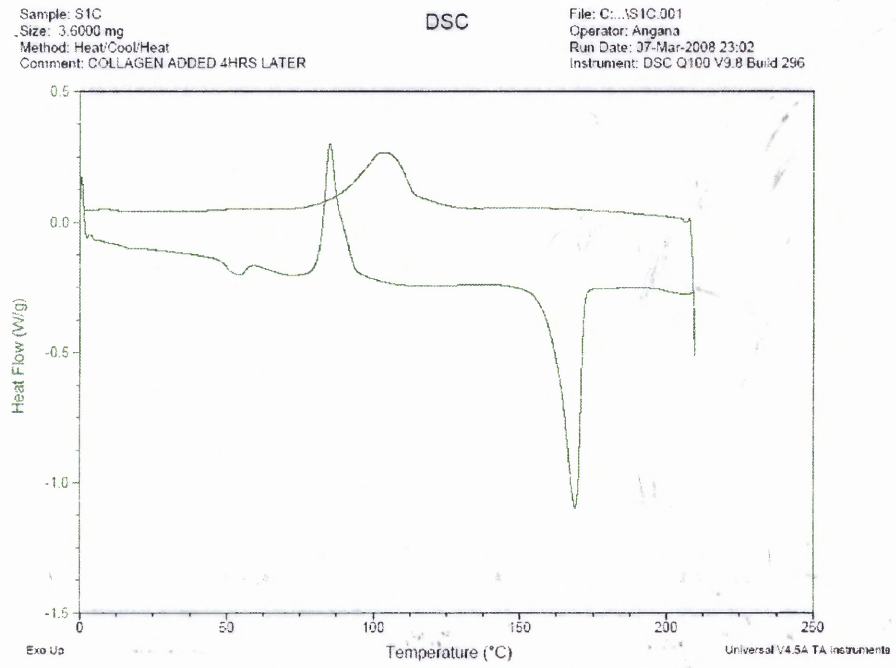

Figure D.1 DSC of 5% Electrospun Collagen-PLLA Mat When PLLA Was Added 4 Hours After the Addition of Collagen to TFA.

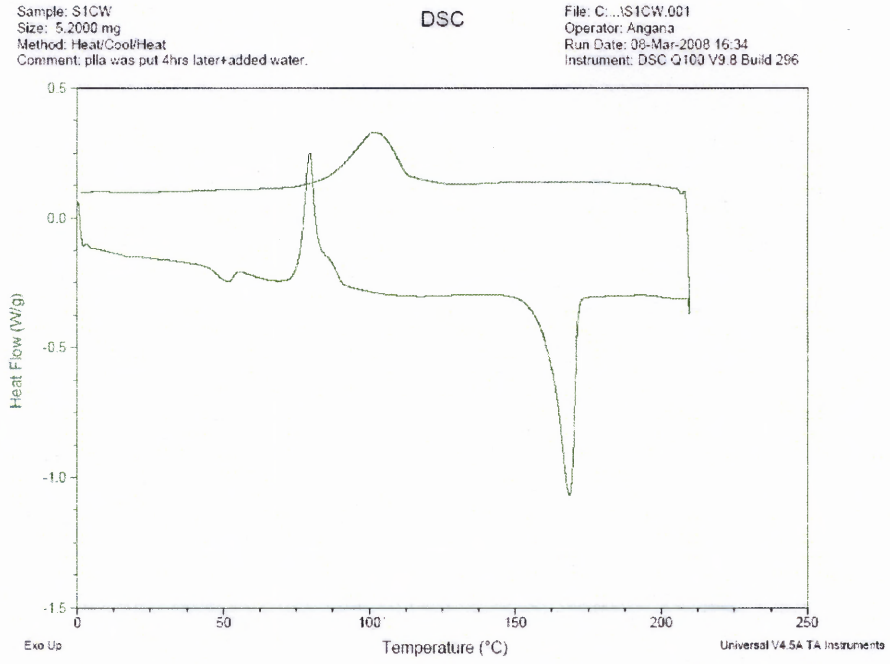

Figure D.2 DSC of 5% Electrospun Collagen-PLLA Mat When PLLA Was Added 4 Hours After the Addition of Collagen to TFA. 10microliters of Water Was Added to TFA.

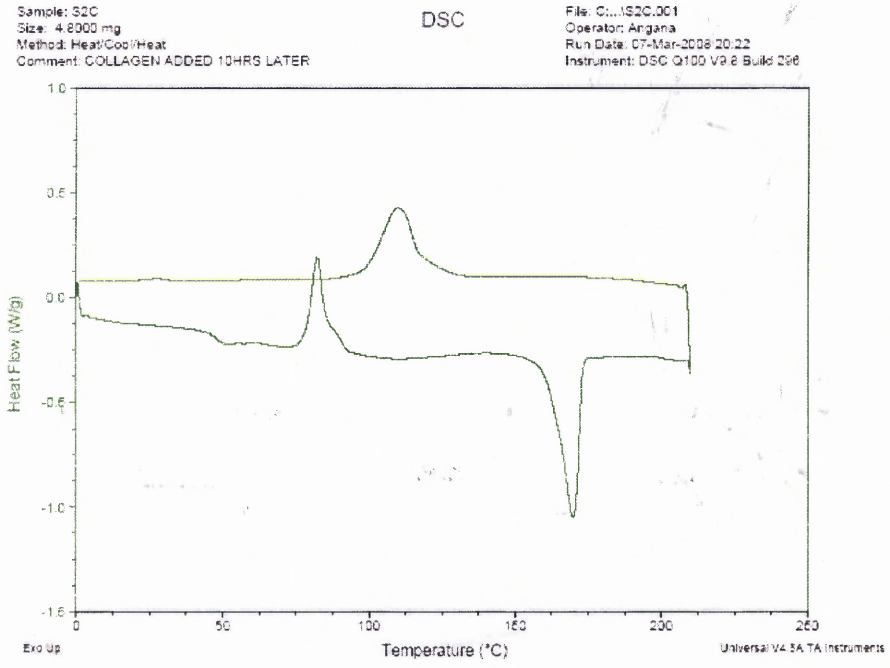

Figure D.3 DSC of 5% Electrospun Collagen-PLLA Mat When PLLA Was Added 10 Hours After the Addition of Collagen to TFA.

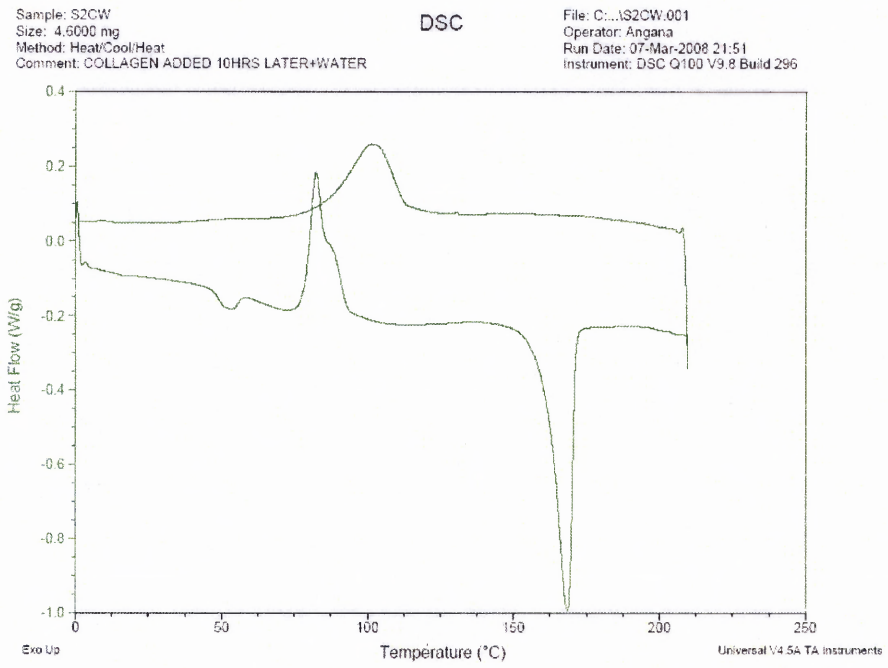

Figure D.4 DSC of 5% Electrospun Collagen-PLLA Mat When PLLA Was Added 10 Hours After the Addition of Collagen to TFA. 10microliters of Water Was Added to TFA.

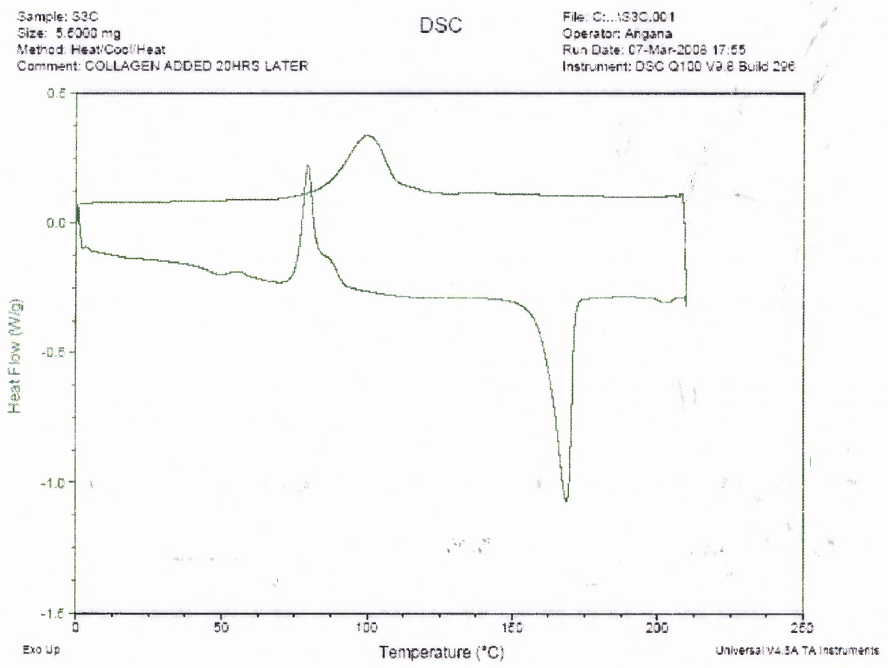

Figure D.5 DSC of 5% Electrospun Collagen-PLLA Mat When PLLA Was Added 20 Hours After the Addition Of Collagen to TFA.

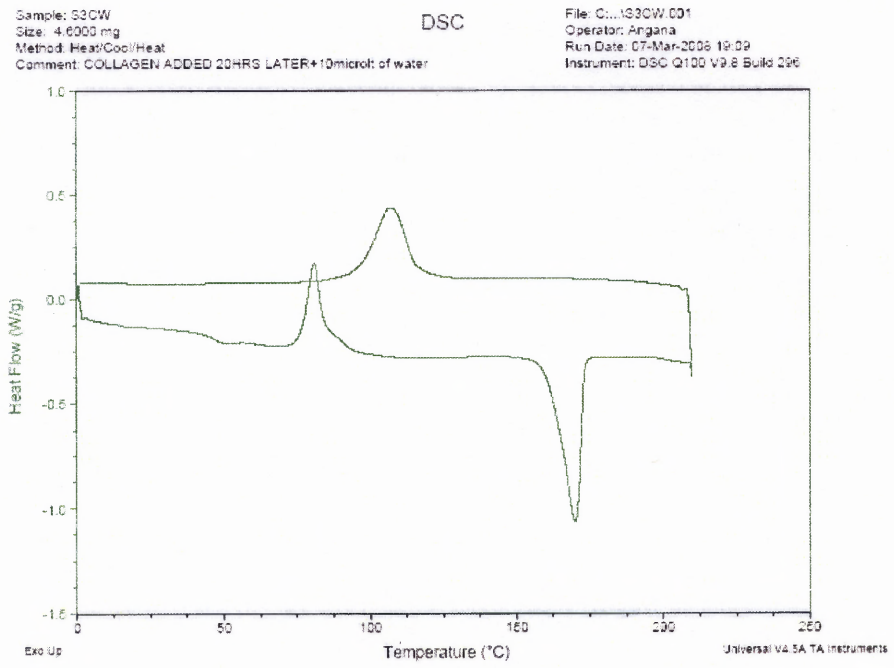

Figure D.6 DSC of 5% Electrospun Collagen-PLLA Mat When PLLA Was Added 10 Hours After the Addition of Collagen to TFA. 10microliters of Water Was Added to TFA.

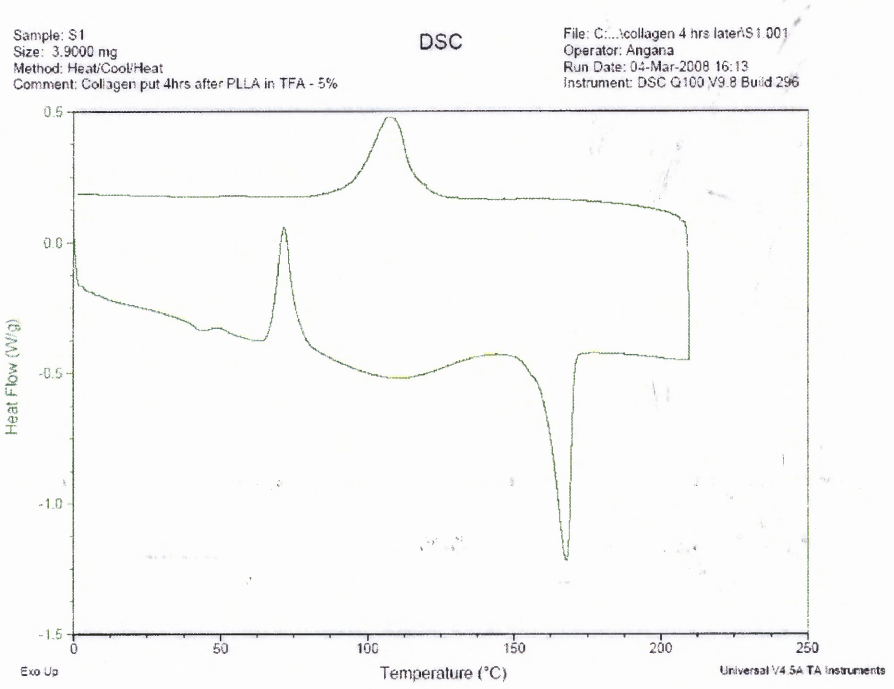

Figure D.7 DSC of 5% Electrospun Collagen-PLLA Mat When Collagen Was Added 4 Hours After the Addition of PLLA to TFA.

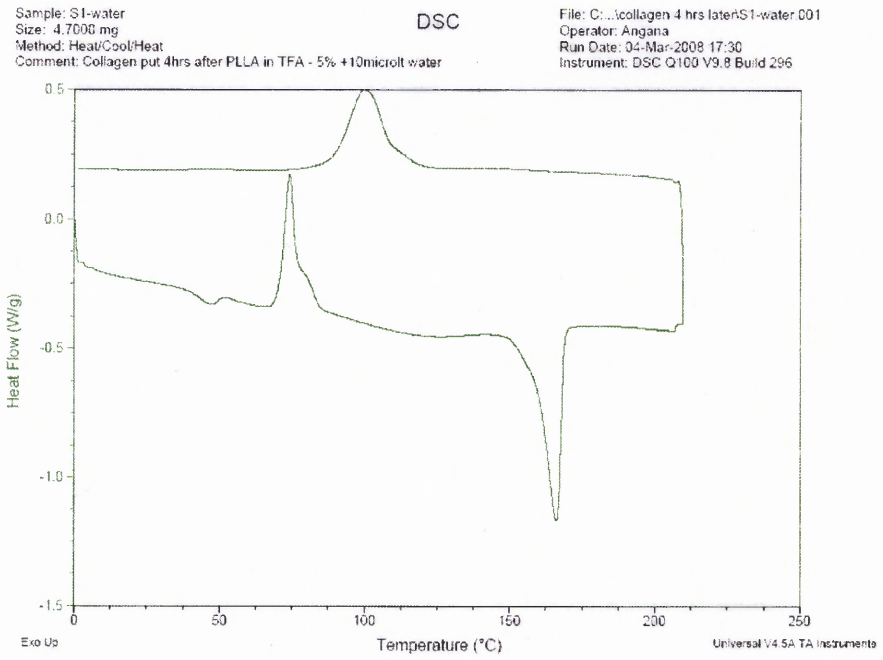

Figure D.8 DSC of 5% Electrospun Collagen-PLLA Mat When Collagen Was Added 4 Hours After the Addition of PLLA to TFA. 10 Microliters of Water Was Added to TFA.

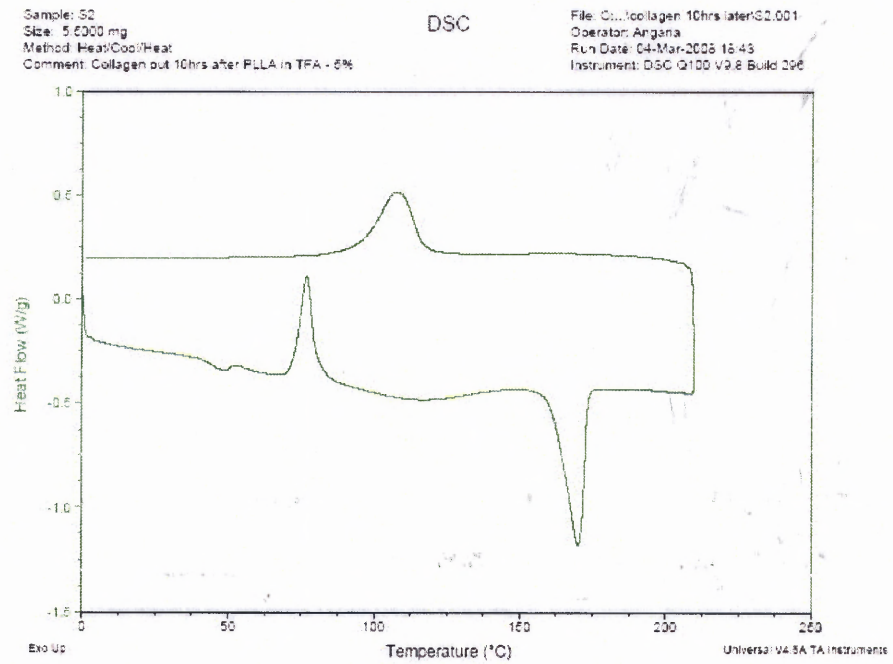

Figure D.9 DSC of 5% Electrospun Collagen-PLLA Mat When Collagen Was Added 10 Hours After the Addition of PLLA to TFA.

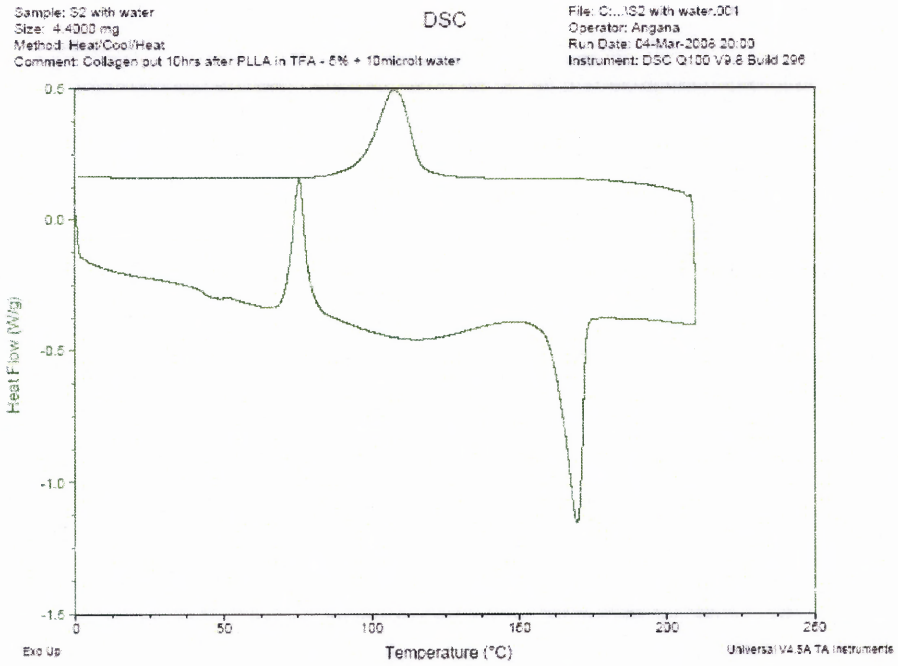

Figure D.10 DSC of 5% Electrospun Collagen-PLLA Mat When Collagen Was Added 10 Hours After the Addition of PLLA to TFA. 10 Microliters of Water Was Added to TFA.

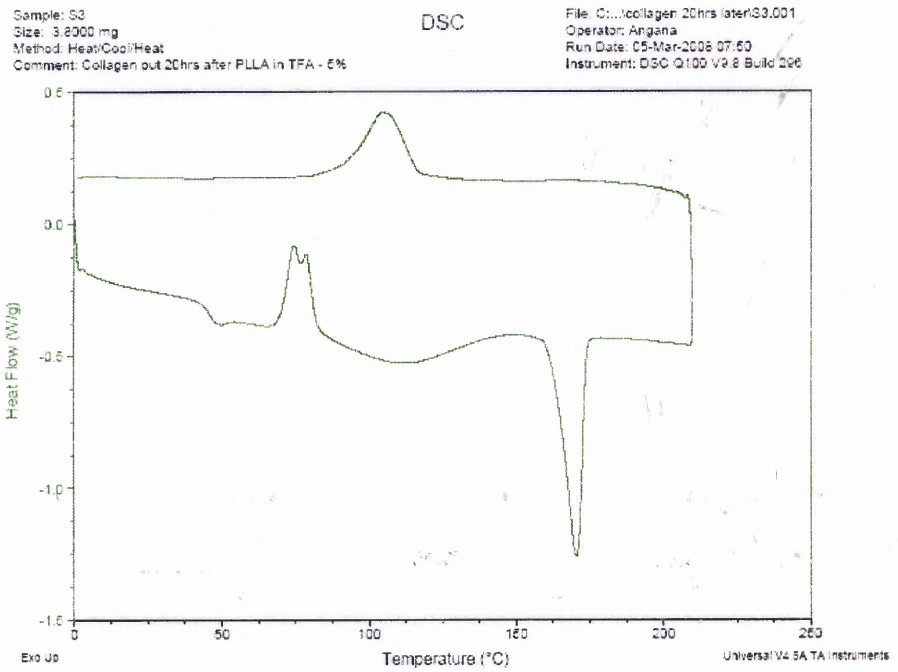

Figure D.11 DSC of 5% Electrospun Collagen-PLLA Mat When Collagen Was Added 20 Hours After the Addition of PLLA to TFA.

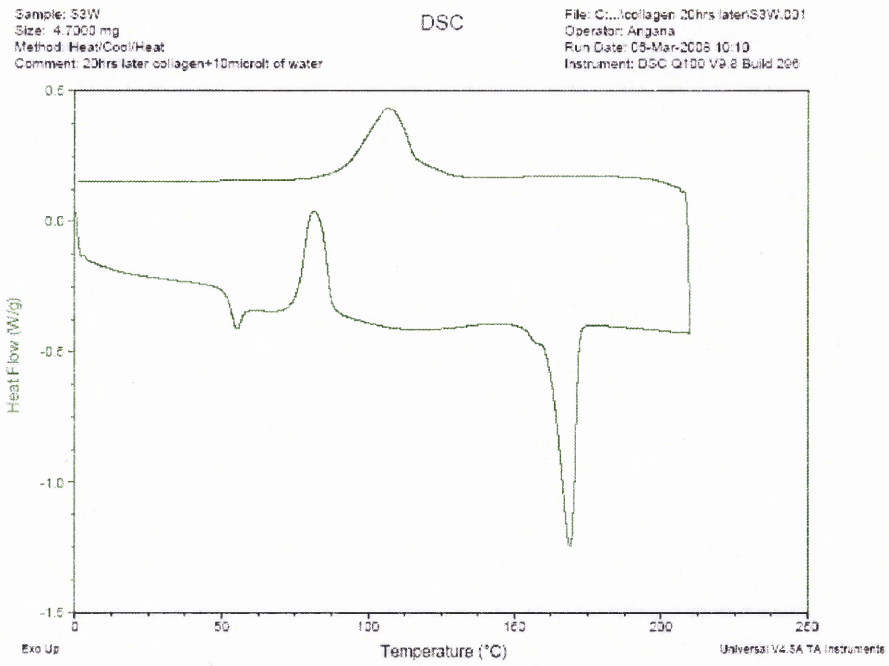

Figure D.12 DSC of 5% Electrospun Collagen-PLLA Mat When Collagen Was Added 20 Hours After the Addition of PLLA to TFA. 10 Microliters of Water Was Added to TFA.

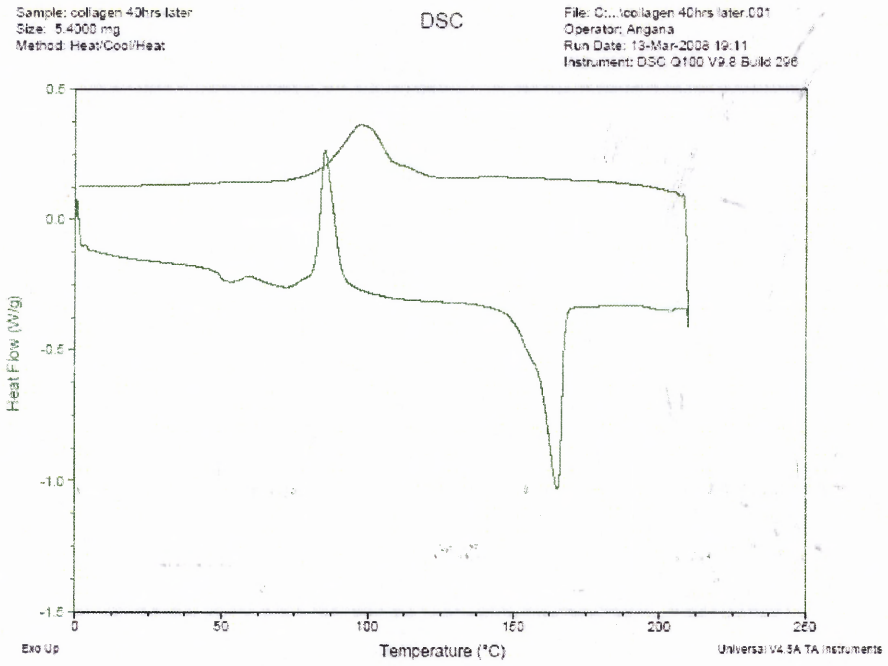

Figure D.13 DSC of 5% Electrospun Collagen-PLLA Mat When Collagen Was Added 40 Hours After the Addition of PLLA to TFA. 10 Microliters of Water Was Added to TFA.

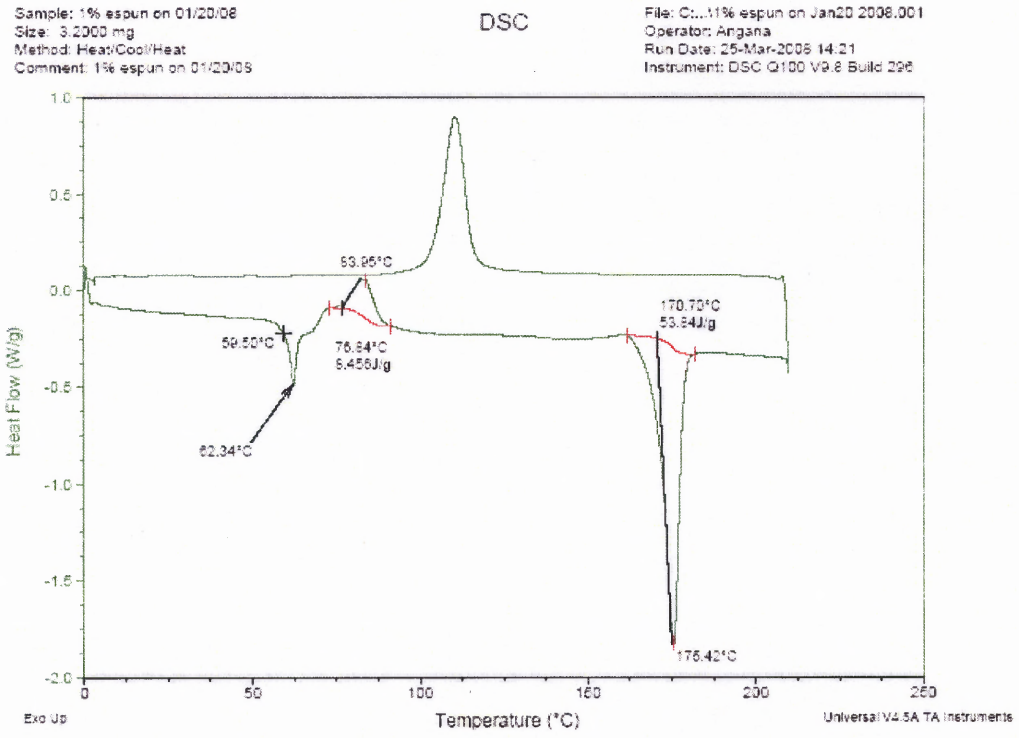

Figure D.14 DSC of First Heat Cycle of 1% Electrospun Collagen-PLLA Mat After 45 to 60 Days of Electrospinning.

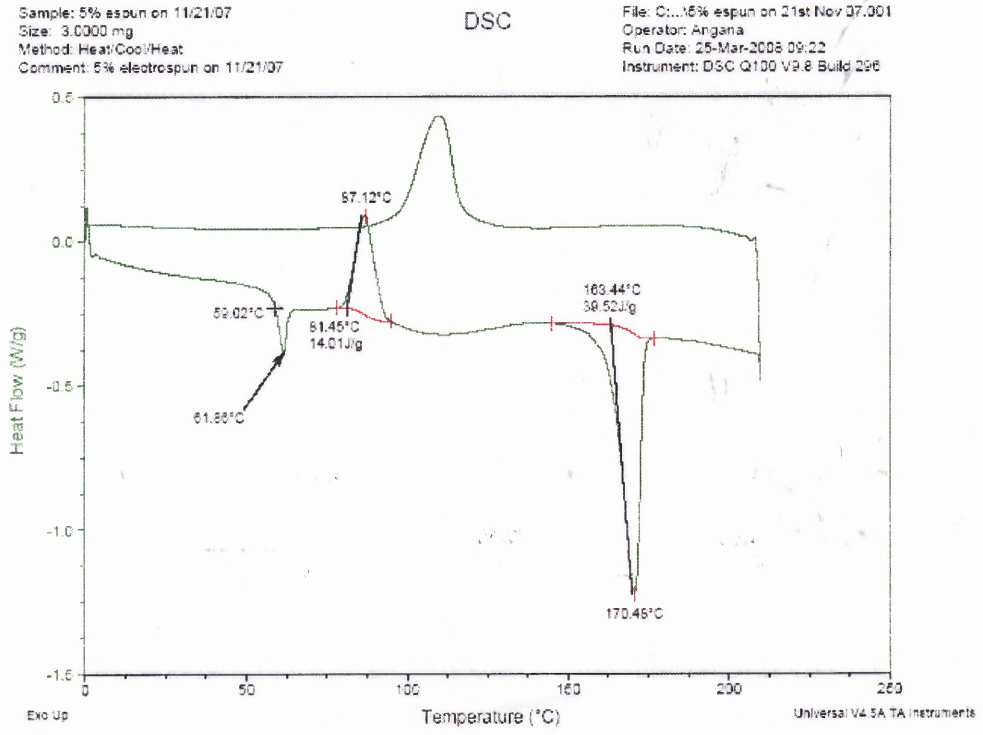

Figure D.15 DSC of First Heat Cycle of 5% Electrospun Collagen-PLLA Mat After 45 to 60 Days of Electrospinning.

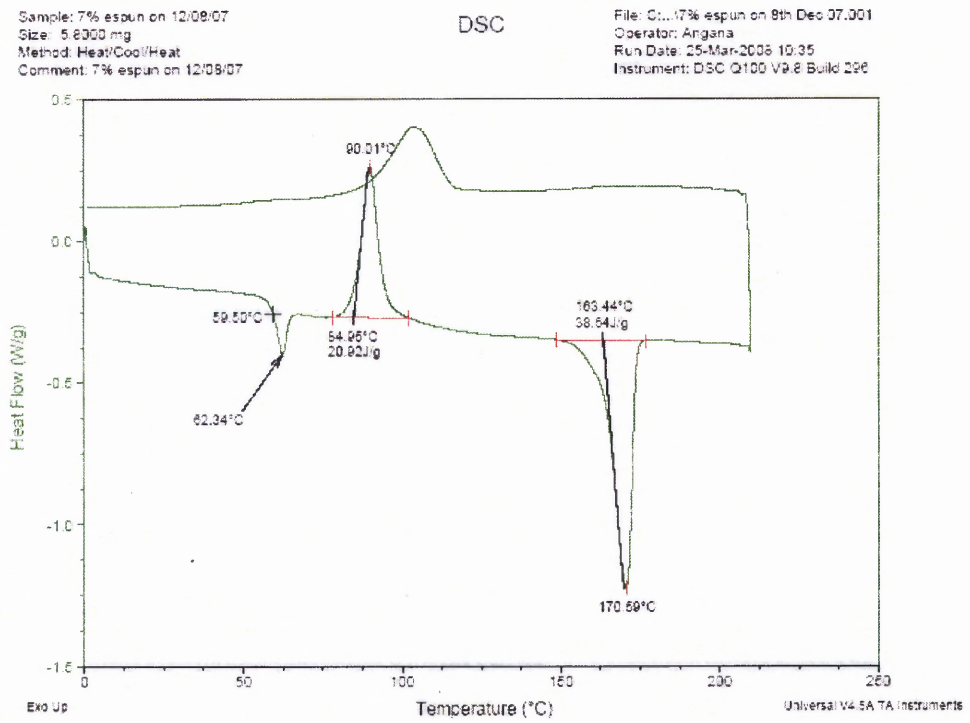

Figure D.16 DSC of First Heat Cycle of 7% Electrospun Collagen-PLLA Mat After 45 to 60 Days of Electrospinning.

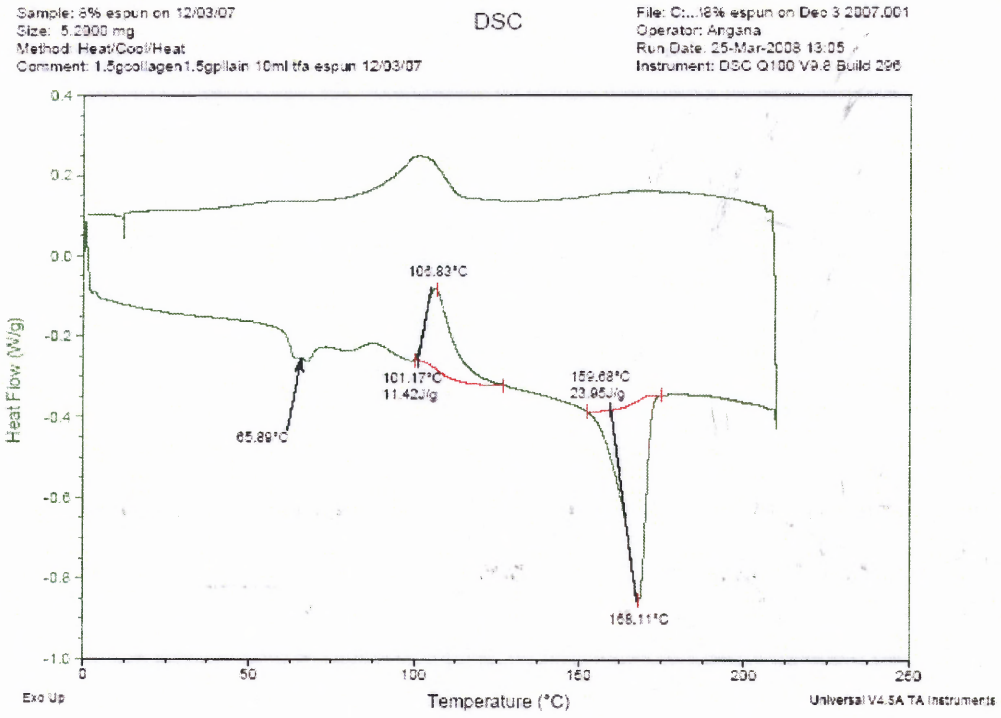

Figure D.17 DSC of First Heat Cycle of 8% Electrospun Collagen-PLLA Mat After 45 to 60 Days of Electrospinning.

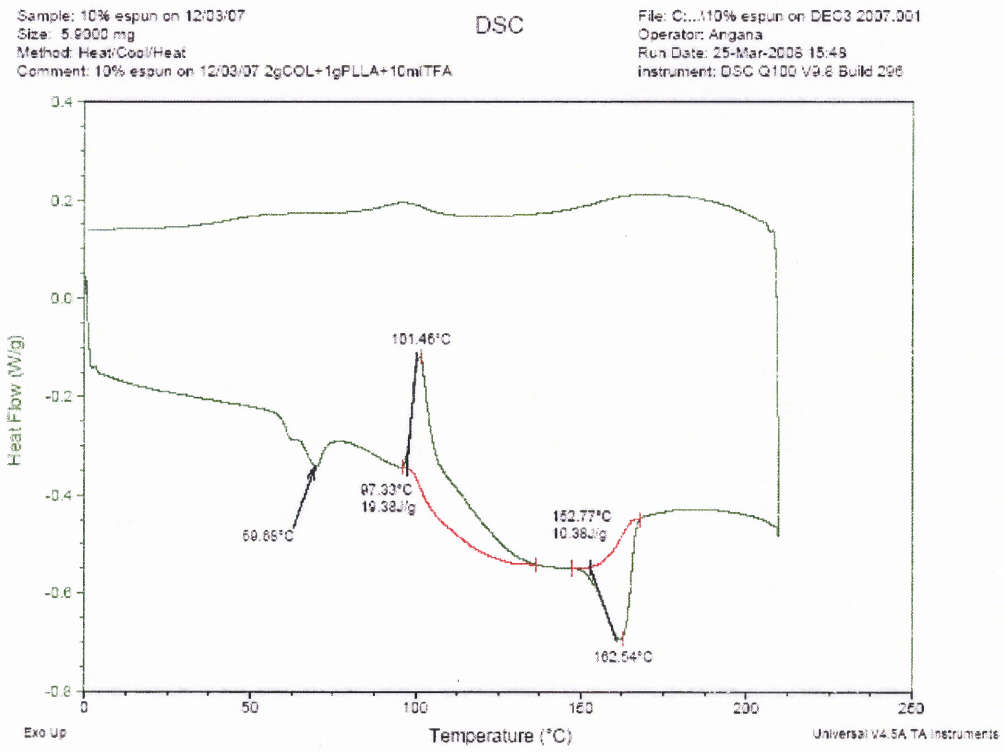

Figure D.18 DSC of First Heat Cycle of 10% Electrospun Collagen-PLLA Mat After 45 to 60 Days of Electrospinning.

APPENDIX E

TGA RESULTS

Following are the TGA results of electrospun mats.

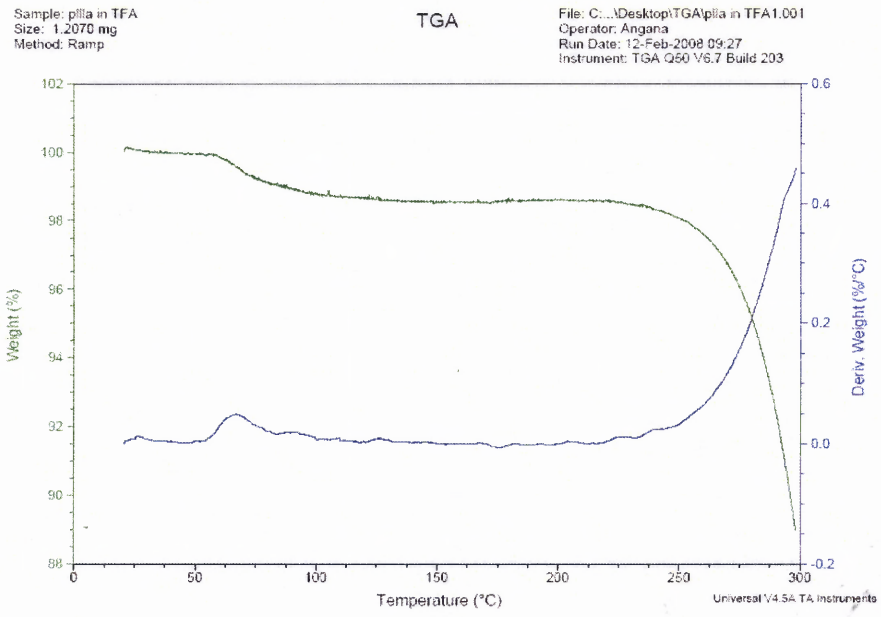

Figure E.1 TGA Analysis of Electrospun PLLA Mat.

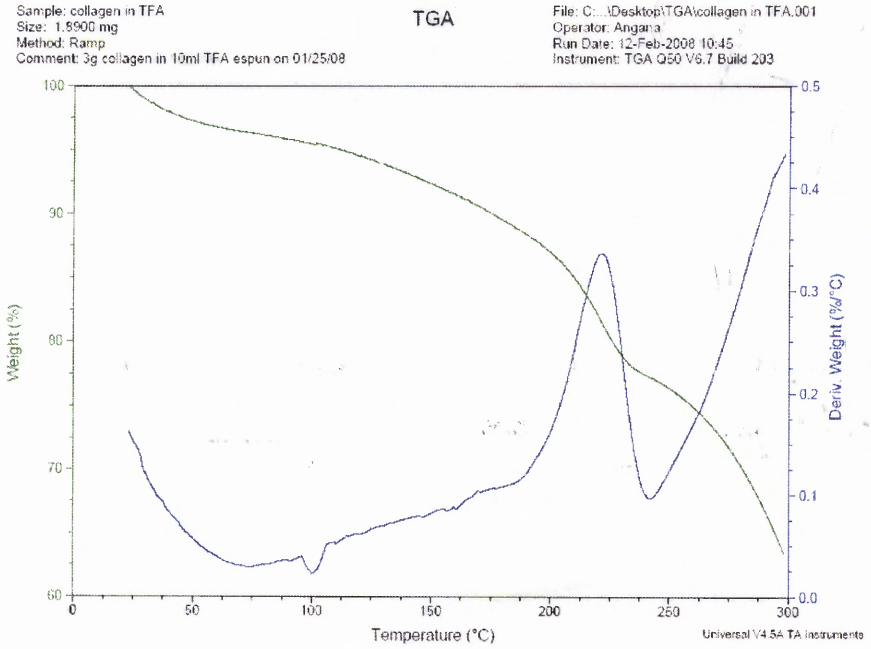

Figure E.2 TGA Analysis of Electrospun Collagen Mat.

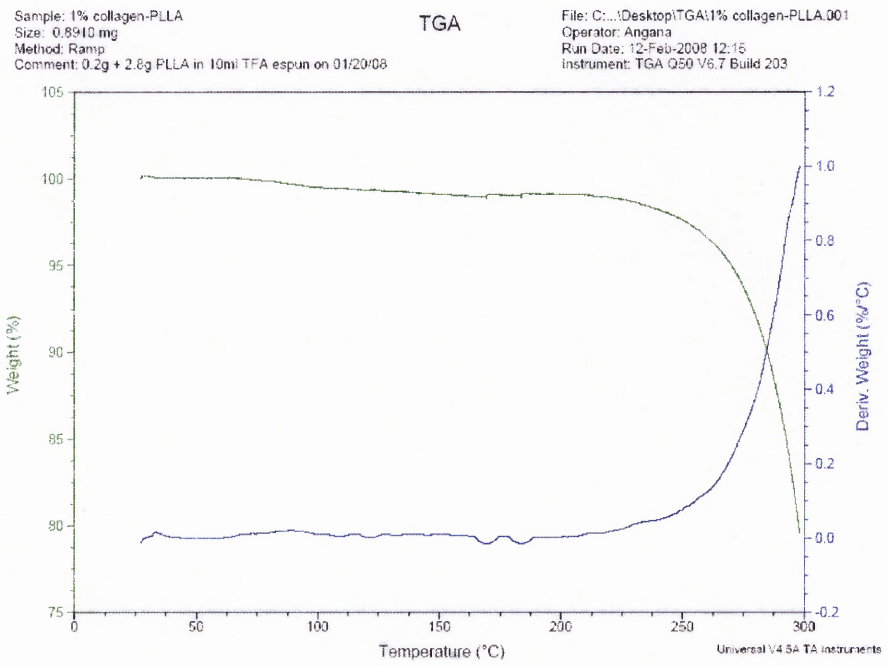

Figure E.3 TGA Analysis of 1% Electrospun Collagen-PLLA Mat.

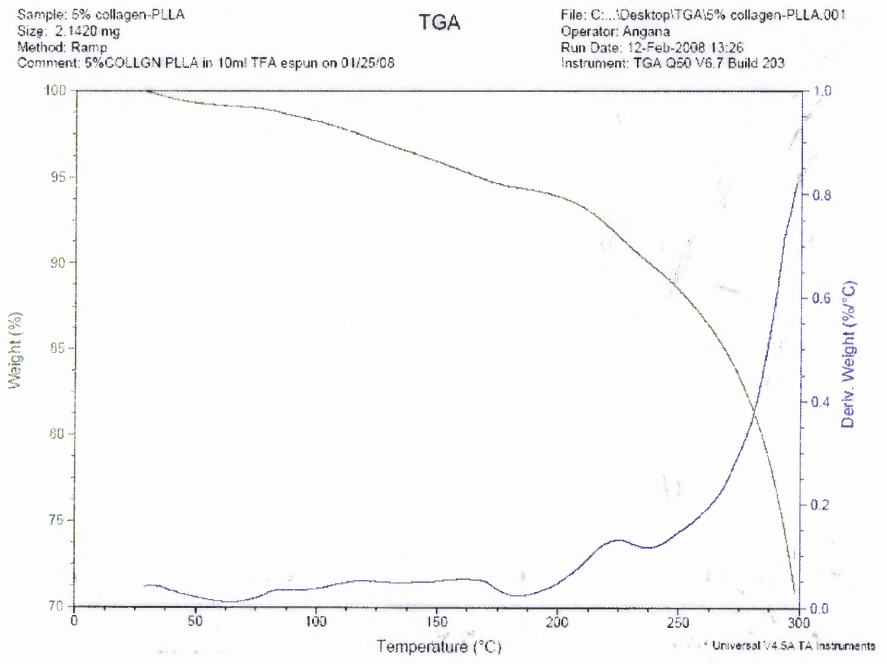

Figure E.4 TGA Analysis of 5% Electrospun Collagen-PLLA Mat.

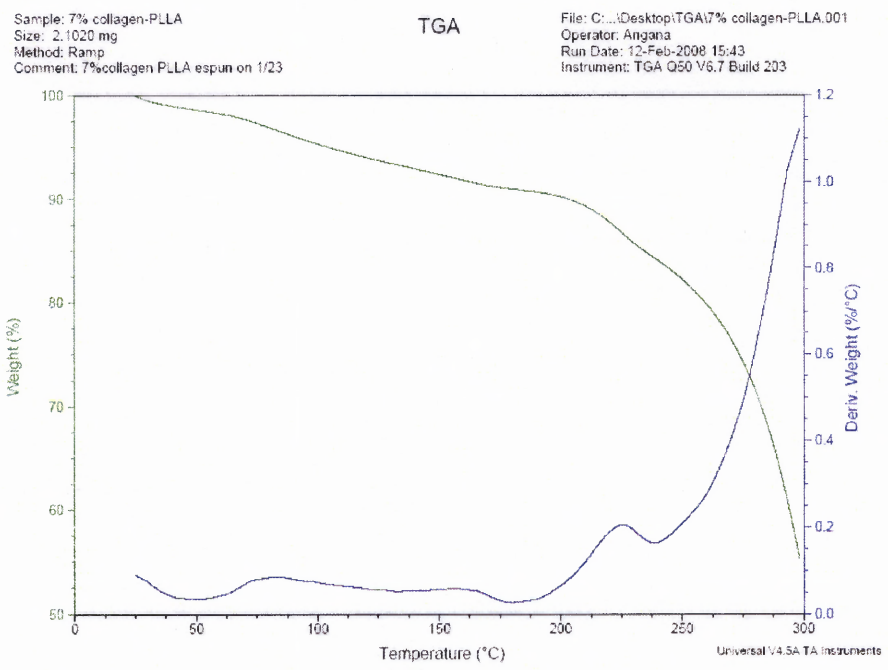

Figure E.5 TGA Analysis of 7% Electrospun Collagen-PLLA Mat.

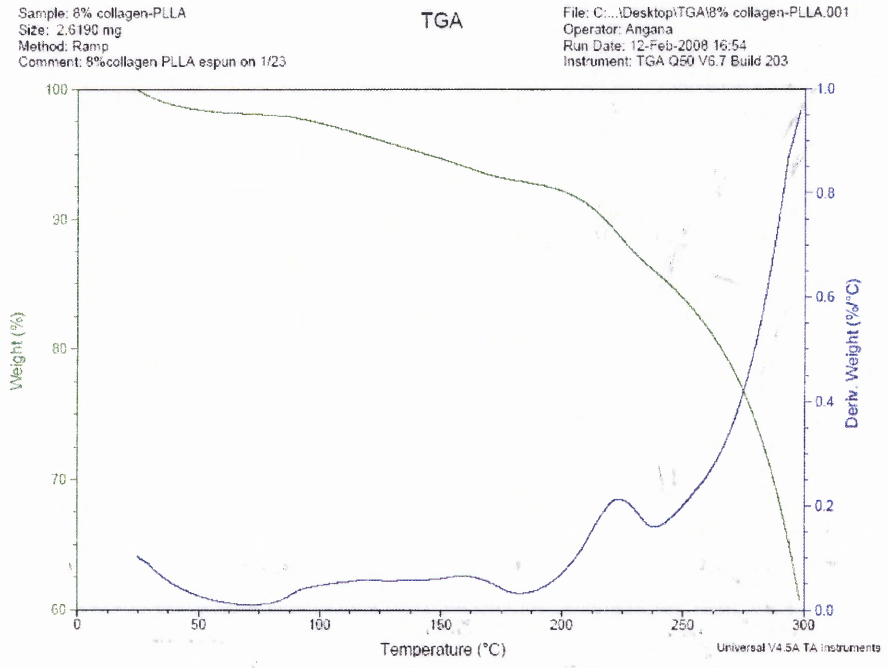

Figure E.6 TGA Analysis of 8% Electrospun Collagen-PLLA Mat.

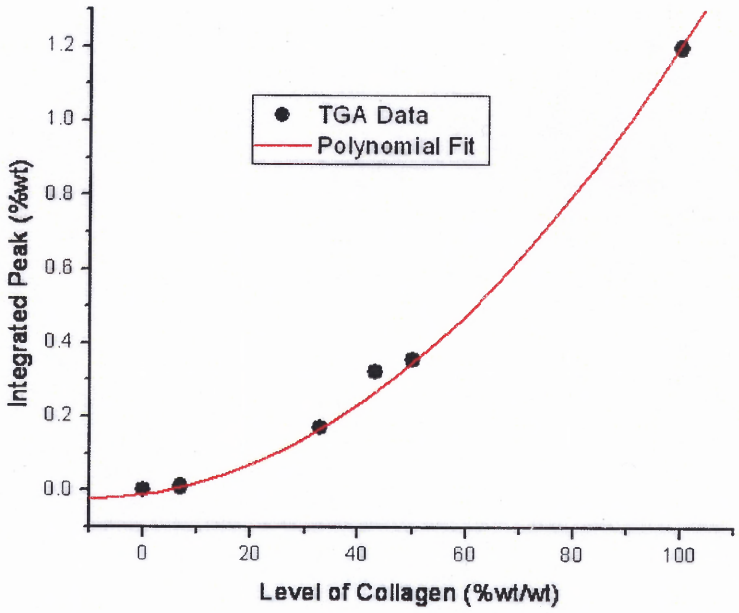

Figure E.7 TGA Composition Calibration Curve.

APPENDIX F

SEM MICROGRAPHS

Following are the SEM images of the electrospun mats.

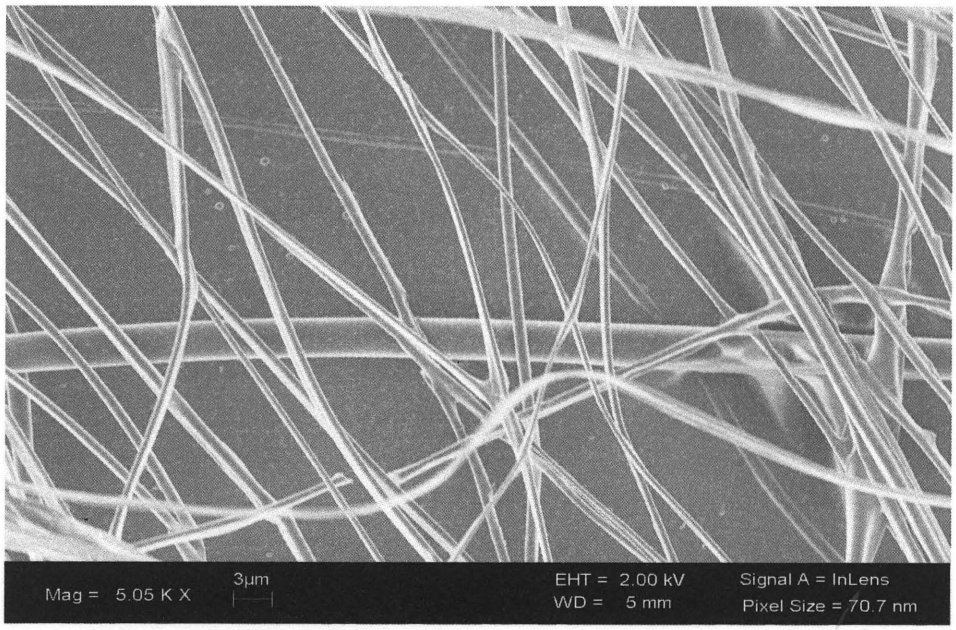

Figure F.1 PLLA Nanofibers Visualized Under the SEM.

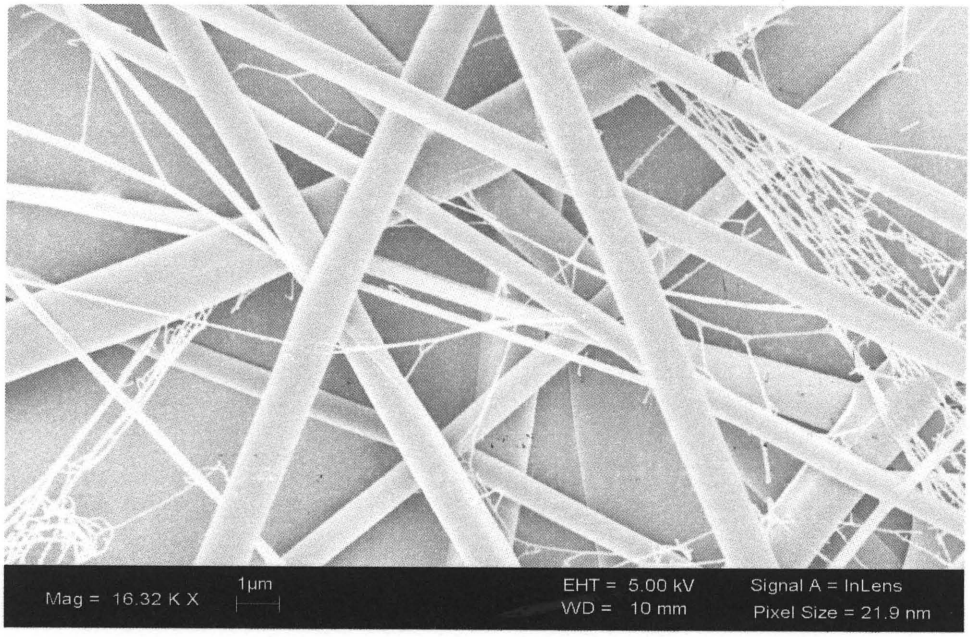

Figure F.2 Collagen Nanofibers Visualized Under the SEM.

APPENDIX G

EXTRACTION EXPERIMENTS

Table G.1 and G.2 indicates the diameters of electrospun collagen-PLLA nanofibers before and after extraction of PLLA by methylene chloride.

Table G.1 Diameters of 8% Collagen-PLLA Nanofibers Before and After Extraction.

8% collagen PLLA mat (nm)	8% dissolved collagen PLLA mat (nm)
448	256
461	201
466	269
423	221
363	270
301	216
332	271
350	310
281	223
245	181
369	222

Table G.2 Diameters of 5% Collagen-PLLA Nanofibers Before and After extraction.

5% collagen PLLA mat (nm)	5% dissolved collagen PLLA mat (nm)
272	200
465	171
281	172
271	155
377	156
182	180
402	176

Table G.3 Diameters of 5% Collagen-PLLA Nanofibers Before and After Extraction.

5% SW collagen PLLA mat (nm)	5% SW dissolved collagen PLLA mat (nm)
323	212
256	241
483	224
597	177
466	184
542	226
351	176
426	329
477	223
460	183
467	196

The nanofiber mat used for this experiment was produced by Sherry Wang in 2004

APPENDIX H

Energy Dispersive X-ray Spectroscopy (EDS) RESULTS I:

EDS results of collagen mat and collagen-PLLA blended electrospun mats are given.

Spectrum processing: No peaks omitted

Processing option: All elements analyzed (Normalized)

Number of iterations = 1

Standard :0

C CaCO3 1-Jun-1999 12:00 AM

O SiO2 1-Jun-1999 12:00 AM

Table H.1 EDS Results for 5% Electrospun Blend.

Element	Weight %	Atomic %
C K	103.34	102.49
O K	-3.34	-2.49
Totals	100.00	

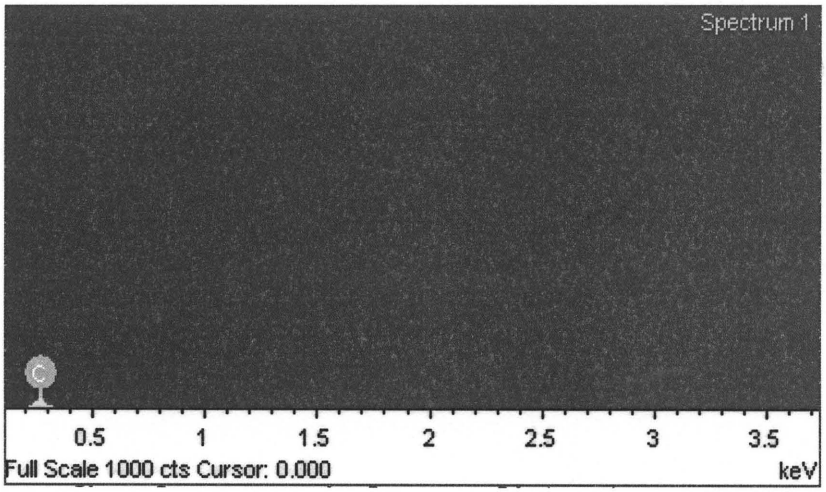

Spectrum processing: No peaks omitted

Processing option: All elements analyzed (Normalized)

Number of iterations = 5

Standard:

C CaCO3 1-Jun-1999 12:00 AM

N Not defined 1-Jun-1999 12:00 AM

O SiO2 1-Jun-1999 12:00 AM

Ti Ti 1-Jun-1999 12:00 AM

Table H.2 EDS Results for Electrospun Collagen.

Element	Weight %	Atomic%
C K	35.34	64.08
N K	2.59	4.03
O K	4.06	5.53
Ti L	58.00	26.37
Totals	100.00	

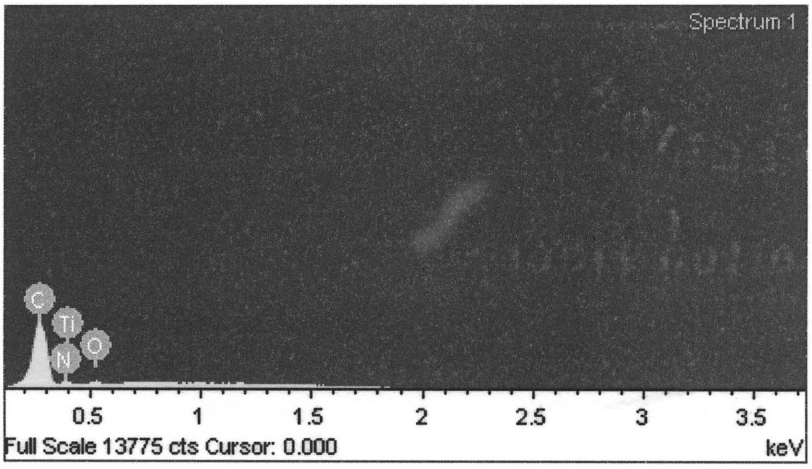

REFERENCES

1. Seeram Ramakrishna, K. F., Wee-Eong Teo, Thomas Yong, Zuwei Ma and Ramakrishna Ramaseshan. (2006). Electrospun nanofibers: solving global issues. *Materials Today 9*(3), 40-50.

2. Zufan, R. (2005). Electrospinning of Nanofibers. Retrieved February 28, 2008, from http://vienna.bioengr.uic.edu/RET/Reports/Final%20Reports/ZufanRETFinalReport.pdf.

3. Raghavendra R Hegde, A. D., M. G. Kamath. (2005, June 13). Nanofiber Nonwovens. Retrieved March 4, 2008, from http://www.engr.utk.edu/mse/Textiles/Nanofiber%20Nonwovens.htm.

4. Xu, C. Y., Inai, R., Kotaki, M., & Ramakrishna, S. (2004). Aligned biodegradable nanofibrous structure: A potential scaffold for blood vessel engineering. *Biomaterials, 25*(5), 877-886.

5. L. Koláčná, J. B., F. Varga, E. Košťáková, L. Plánka, A. Nečas, D. Lukáš, E. Amler, V. Pelouch. (2007). Biochemical and biophysical aspects of collagen nanostructure in the extracellular matrix. *Physiological Research, 56*(SUPPL. 1).

6. Kim, B. S., & Mooney, D. J. (1998). Development of biocompatible synthetic extracellular matrices for tissue engineering. *Trends in Biotechnology, 16*(5), 224-229.

7. Huang, Z. M., Zhang, Y. Z., Kotaki, M., & Ramakrishna, S. (2003). A review on polymer nanofibers by electrospinning and their applications in nanocomposites. *Composites Science and Technology, 63*(15), 2223-2253.

8. Ramakrishna, W. E. T. a. S. (2006). A review on electrospinning design and nanofibre assemblies. *Nanotechnology, 17*, R89-R106.

9. Doshi, J., & Reneker, D. H. (1995). Electrospinning process and applications of electrospun fibers. *Journal of Electrostatics, 35*(2-3), 151-160.

10. Subbiah, T., Bhat, G. S., Tock, R. W., Parameswaran, S., & Ramkumar, S. S. (2005). Electrospinning of nanofibers. *Journal of Applied Polymer Science, 96*(2), 557-569.

11. Gray, S. (1731). A letter concerning the electricity of water, from Mr. Stephen Gray to Cromwell Mortimer, M.D.Secr.R.S. *Phil. Trans., 37*, 227.

12. Larmor, J. (1898). Note on the complete scheme of electrodynamic equations of a moving material medium, and on electrostriction. *Proc. R. Soc., 63*, 365.

13. Young, D. S. (2006). *Hyaluronic Acid-based Nanofibers via Electrospinning.* Unpublished Master Thesis, North Carolina State University.

14. Formhals, A. (1940). *US Patent, 2,187,306.*

15. Formhals, A. (1934). Process and apparatus for preparing artificial threads. *US Patent 1,975,504.*

16. Shobana Shanmugasundaram, Y. I., Michael Jaffe. (2008). *Tissue Engineering: Roles, Materials and Applications*: Nova Science Publisher.

17. Catalani, L. H., Collins, G., & Jaffe, M. (2007). Evidence for molecular orientation and residual charge in the electrospinning of poly(butylene terephthalate) nanofibers. *Macromolecules, 40*(5), 1693-1697.

18. Electrospinning of nanofibers. Retrieved March 26, 2008, from http://www.ifp.se/Content.aspx?PageID=1231&PageTypeID=3.

19. Retrieved February 28, 2008, from http://www.centropede.com/UKSB2006/ePoster/images/background/ElectrospinFigure.jpg.

20. Wang, S. Unpublished Master's Thesis, New Jersey Institute of Technology, Newark.

21. Ma, P. X., & Zhang, R. (1999). Synthetic nano-scale fibrous extracellular matrix. *Journal of Biomedical Materials Research, 46*(1), 60-72.

22. Gouma, P. I. (2003). Nanostructured polymorphic oxides for advanced chemosensors. *Reviews on Advanced Materials Science, 5*(2), 147-154.

23. (March 26, 2008). Collagen. Retrieved March 27, 2008, from http://en.wikipedia.org/wiki/Collagenous_fibers#cite_note-2.

24. Walker, A. A. (1998). Oldest Glue Discovered Retrieved March 21, 2008, from http://www.archaeology.org/online/news/glue.html.

25. Di Lullo, G. A., Sweeney, S. M., Ko?rkko, J., Ala-Kokko, L., & San Antonio, J. D. (2002). Mapping the ligand-binding sites and disease-associated mutations on the most abundant protein in the human, type I collagen. *Journal of Biological Chemistry, 277*(6), 4223-4231.

26. Bruce Alberts, A. J., Julian Lewis, Martin Raff, Keith Roberts, and Peter Walter. *Molecular Biology of the Cell* (4 ed.): Garland Science.

27. Matthews, J. A., Boland, E. D., Wnek, G. E., Simpson, D. G., & Bowlin, G. L. (2003). Electrospinning of collagen type II: A feasibility study. *Journal of Bioactive and Compatible Polymers, 18*(2), 125-134.

28. Holmgren, S. K., Taylor, K. M., Bretscher, L. E., & Raines, R. T. (1998). Code for collagen's stability deciphered [9]. *Nature, 392*(6677), 666-667.

29. Raines, M. J. W. a. R. T. (2000). *Theoretical Analysis of the Basis of Collagen Stability.* Unpublished Senior undergraduate, University of Wisconsin

30. Buehler, M. J. (2006). Nature designs tough collagen: Explaining the nanostructure of collagen fibrils. *Proceedings of the National Academy of Sciences of the United States of America, 103*(33), 12285-12290.

31. Collagen and Natural Gut Strings. Retrieved March 27, 2008, from http://web.mit.edu/3.082/www/team1_f02/collagen.htm.

32. Matthews, J. A., Wnek, G. E., Simpson, D. G., & Bowlin, G. L. (2002). Electrospinning of collagen nanofibers. *Biomacromolecules, 3*(2), 232-238.

33. He, W., Ma, Z., Yong, T., Teo, W. E., & Ramakrishna, S. (2005). Fabrication of collagen-coated biodegradable polymer nanofiber mesh and its potential for endothelial cells growth. *Biomaterials, 26*(36), 7606-7615.

34. He, W., Yong, T., Teo, W. E., Ma, Z., & Ramakrishna, S. (2005). Fabrication and endothelialization of collagen-blended biodegradable polymer nanofibers: Potential vascular graft for blood vessel tissue engineering. *Tissue Engineering, 11*(9-10), 1574-1588.

35. Yasuniwa, M., Tsubakihara, S., Sugimoto, Y., & Nakafuku, C. (2004). Thermal analysis of the double-melting behavior of poly(L-lactic acid). *Journal of Polymer Science, Part B: Polymer Physics, 42*(1), 25-32.

36. Sodergard A., S. M. (2002). Properties of lactic acid based polymers and their correlation with composition. *Progress in Polymer Science (Oxford), 27*(6), 1123-1163.

37. Polylactic acid. Retrieved April 2, 2008, from http://en.wikipedia.org/wiki/Polylactic_acid.

38. Gupta, M. C., & Deshmukh, V. G. (1982). Thermal oxidative degradation of poly-lactic acid - Part I: Activation energy of thermal degradation in air. *Colloid & Polymer Science, 260*(3), 308-311.

39. Gupta, M. C., & Deshmukh, V. G. (1982). Thermal oxidative degradation of poly-lactic acid - Part II: Molecular weight and electronic spectra during isothermal heating. *Colloid & Polymer Science, 260*(5), 514-517.

40. Fischer, E. W., Sterzel, H. J., & Wegner, G. (1973). Investigation of the structure of solution grown crystals of lactide copolymers by means of chemical reactions. *Kolloid-Zeitschrift & Zeitschrift fu?r Polymere, 251*(11), 980-990.

41. Di Lorenzo, M. L. (2006). The crystallization and melting processes of poly(L-lactic acid). *Macromolecular Symposia, 234*, 176-183.

42. Crystallisation Kinetics Retrieved April 2, 2008, from www.dur.ac.uk/.../cryskinetics/handoutsalla.html.

43. Wang, Y., Ribelles, J. L. G., Sanchez, M. S., & Mano, J. F. (2005). Morphological contributions to glass transition in poly(L-lactic acid). *Macromolecules, 38*(11), 4712-4718.

44. Joziasse, C. A. P., Veenstra, H., Grijpma, D. W., & Pennings, A. J. (1996). On the chain stiffness of poly(lactide)s. *Macromolecular Chemistry and Physics, 197*(7), 2219-2229.

45. Grijpma, D. W., Penning, J. P., & Pennings, A. J. (1994). Chain entanglement, mechanical properties and drawability of poly(lactide). *Colloid & Polymer Science, 272*(9), 1068-1081.

46. Wei, M., Kang, B., Sung, C., & Mead, J. (2006). Core-sheath structure in electrospun nanofibers from polymer blends. *Macromolecular Materials and Engineering, 291*(11), 1307-1314.

47. Retrieved February 28, 2008, from http://www.centropede.com/UKSB2006/ePoster/images/background/ElectrospinFigure.jpg.

48. Differential scanning calorimetry. Retrieved February 28, 2008, from http://en.wikipedia.org/wiki/Differential_scanning_calorimetry.

49. Scanning electron microscope. Retrieved March 3 2008, from http://en.wikipedia.org/wiki/Scanning_electron_microscope#_ref-0.

50. Scanning electron microscope. Retrieved March 3, 2008, from www.purdue.edu/REM/rs/sem.htm.

51. Imura, Y. (Private Communication, Medical Device Concept Laboratory, NJIT, April 2008).

52. Retrieved April 2, 2008, from http://sundoc.bibliothek.uni-halle.de/diss-online/04/04H140/t5.pdf.